

**EXPERIMENTAL AND NUMERICAL INVESTIGATION  
ON WAVE INTERACTION WITH HORIZONTAL  
SLOTTED SUBMERGED POROUS BREAKWATER**

**M.Sc. Engineering Thesis**

**by**

**Rounak Afroz**



**Department of Water Resources Engineering  
Bangladesh University of Engineering and Technology (BUET)  
Dhaka**

**January 2015**

**EXPERIMENTAL AND NUMERICAL INVESTIGATION  
ON WAVE INTERACTION WITH HORIZONTAL  
SLOTTED SUBMERGED POROUS BREAKWATER**

**M.Sc. Engineering Thesis**

by

**Rounak Afroz  
Roll No. 0412162014P**

Submitted to

Department of Water Resources Engineering,  
Bangladesh University of Engineering and Technology, Dhaka  
in partial fulfillment of the requirement for the degree of  
Master of Science in Water Resources Engineering



**Department of Water Resources Engineering  
Bangladesh University of Engineering and Technology (BUET)  
Dhaka**

**January 2015**

**Bangladesh University of Engineering and Technology, Dhaka**

**Department of Water Resources Engineering**

**Certification of Thesis**

The thesis titled “**Experimental and Numerical Investigation on Wave Interaction with Horizontal Slotted Submerged Porous Breakwater**”, submitted by Rounak Afroz, Roll No. 0412162014P, Session April 2012, to the Department of Water Resources Engineering, Bangladesh University of Engineering and Technology, has been accepted as satisfactory in partial fulfillment of the requirements for the degree of Master of Science in Water Resources Engineering and approved as to its style and content. Examination held on January 31, 2015.

---

Dr. Md. Ataur Rahman  
Professor

Department of Water Resources Engineering  
Bangladesh University of Engineering and Technology  
Dhaka

Chairman  
(Supervisor)

---

Dr. Md. Sabbir Mostafa Khan  
Professor and Head

Department of Water Resources Engineering  
Bangladesh University of Engineering and Technology  
Dhaka

Member  
(Ex-officio)

---

Dr. A. T. M. Hasan Zobeyer  
Assistant Professor

Department of Water Resources Engineering  
Bangladesh University of Engineering and Technology  
Dhaka

Member

---

Dr. G. M. Jahid Hasan  
Professor

Department of Civil Engineering  
Military Institute of Science and Technology (MIST)  
Dhaka

Member  
(External)

## **Candidate's Declaration**

It is hereby declared that this thesis or any part of it has not been submitted elsewhere for the award of any degree or diploma.

Supervisor

Candidate

---

Dr. Md. Ataur Rahman  
Professor  
Department of Water Resources Engineering  
Bangladesh University of Engineering and Technology,  
Dhaka.

---

Rounak Afroz  
Roll No. 0412162014P

## ACKNOWLEDGEMENT

I express my gratitude and homage to the Almighty Allah for providing me the knowledge and capability to successfully complete the thesis work.

I would like to take this opportunity to express my sincere gratitude to Dr. Md. Ataur Rahman, Professor, Department of Water Resources Engineering, Bangladesh University of Engineering and Technology, for his advice and guidance throughout this study as well as his constant encouragement and productive criticism in my endeavors. I consider myself fortunate for getting the opportunity to work under his supervision.

My sincere appreciation is due to Dr. Md. Sabbir Mostafa Khan, Professor and Head, Department of Water Resources Engineering, BUET, for his timely co-operation and guidance.

I also intend to express my gratitude to Dr. A.T.M Hasan Zobeyer, Assistant Professor, Department of Water Resources Engineering, BUET, for his valuable comments, careful review and suggestions. I am also grateful to Dr. G.M. Jahid Hasan, Professor, Department of Civil Engineering, MIST, for his kind consent to be a member of the examination board. His precious comments, constructive criticism and suggestions in this study are duly appreciated.

I am very much grateful to Md. Sadiul Alam, undergraduate student, Department of WRE, BUET, for his sincere assistance in the collection of data during the laboratory experiments. I also acknowledge the great help and support provided by all laboratory staff of Hydraulics and River Engineering Laboratory, DWRE, BUET.

Last but not the least; I would like to express my gratitude to my mother and mother-in-law for their incessant inspiration and encouragement. The sacrifices, patience, moral support and help from my husband Kazi Atikuzzaman, Finance Manager, Coats Bangladesh, are really invaluable and I am really thankful to him for always being there for me.

**Rounak Afroz**

## ABSTRACT

In this research work the interaction between waves and horizontal slotted submerged porous breakwater has been investigated experimentally as well as using numerical model. To investigate the performance of proposed horizontal slotted submerged breakwater, experimental studies are carried out in a two-dimensional wave flume (21.3 m long, 0.76 m wide and 0.74 m deep) at the Hydraulics and River Engineering Laboratory of the Bangladesh University of Engineering and Technology. A set of experiments are carried out at 50 cm still water depth with fixed horizontal slotted submerged breakwaters of three different porosities ( $n = 0.4, 0.5$  and  $0.6$ ) for interaction with regular waves of four different wave periods ( $T = 1.6$  sec,  $1.7$  sec,  $1.8$  sec and  $2.0$  sec) in the wave flume. For 12 run conditions, data of water surface at different locations are collected manually by providing a vertical scale on the flume side made of glass. Six different locations both in front of and behind the breakwater are selected for data collection. At each measuring location, water surface data were recorded for 1 min, at 5 sec time interval. Also the position of wave breaking is simultaneously recorded with a digital video camera.

Different hydrodynamic co-efficient such as transmission co-efficient ( $K_t$ ), reflection co-efficient ( $K_r$ ) and wave energy loss co-efficient ( $K_L$ ) are determined from the measured water surface data for various run conditions. These co-efficient values were then, analyzed with respect to relative breakwater width ( $k.B$ ), [where,  $k =$  wave number ( $2\pi/L$ ),  $B =$  breakwater width] and porosity of breakwater. Experimental results reveal that, for transmitting smaller part of wave energy through the breakwater, minimum transmission co-efficient,  $K_t = 0.526$  was obtained for breakwater with the lowest porosity ( $n=0.4$ ) for the shortest wave, i.e.  $T = 1.6$  sec. Minimum reflection co-efficient,  $K_r = 0.03448$  was obtained for breakwater with the highest porosity ( $n=0.6$ ) for the longest wave, i.e.  $T = 2$  sec. It is also seen that wave energy loss co-efficient ( $K_L$ ) decreases from 0.68 to 0.47 with increasing porosity.

Two-dimensional numerical model based on the SOLA-VOF (SOLution Algorithm-Volume Of Fluid) method developed for wave interaction with fixed submerged breakwater has been updated in this research to study the wave interaction with horizontal slotted submerged porous breakwater. The SOLA scheme is employed to

calculate the pressure and velocities in each time step and the added dissipation zone method is adopted to treat the open boundary. The developed numerical model is verified by comparing the model generated wave with the wave as per Stokes 3<sup>rd</sup> order wave theory. The time series water surface profiles, water particle velocity field, VOF function F, pressure around a breakwater of different porosities ( $n=0.4, 0.5$  and  $0.6$ ) are simulated using the numerical model. The water surface profiles and breaking positions simulated by the developed numerical model show good agreement with the experimentally measured data. This study is expected to serve as a useful model to analyze wave deformation due to horizontal slotted submerged porous breakwater and will be important for designing submerged porous breakwater as a coastal protection measure.

# Table of Contents

Acknowledgement		i
Abstract		ii
Table of Contents		iv
List of Figures		vi
List of Tables		viii
List of Symbols		ix
<b>Chapter 1</b>	<b>Introduction</b>	<b>1</b>
1.1	General	1
1.2	Study Objectives	2
1.3	Study Scope and Contents	3
<b>Chapter 2</b>	<b>Literature Review</b>	<b>5</b>
2.1	General	5
2.2	Different Types of Breakwater as Shore Protection Structure	5
2.2.1	Floating breakwater	6
2.2.2	Fixed breakwater	8
2.2.3	Porous or permeable breakwater	10
2.3	Previous Studies on Breakwater	11
2.4	Numerical Model Based On SOLA-VOF	14
2.4.1	Basic equations	14
2.4.2	Parameters used in numerical model	16
2.4.3	Computational procedure	17
2.4.4	Boundary conditions	18
2.4.5	Numerical stability considerations	21
2.5	SOLA-VOF Used for Modeling Breakwaters	22
2.6	Present Study	23
<b>Chapter 3</b>	<b>Laboratory Experiment</b>	<b>24</b>
3.1	General	24
3.2	Laboratory Equipments	24
3.2.1	Two-dimensional wave flume	24
3.2.2	Wave generator	25
3.2.3	Wire screens to reduce wave reflections	26
3.2.4	Water reservoir	27
3.2.5	Horizontal slotted submerged porous breakwater	27
3.2.6	Wave absorber	28
3.2.7	Experimental setup	29
3.3	Measurement Techniques and Test Scenarios	30
3.4	Data Acquisition	32



3.5	Experimental Results	35
3.5.1	Water surface profile	35
3.5.2	Variation of $\eta/H_i$ with $t/T$	40
3.5.3	Variation of $\eta/H_i$ with $x/L$	43
3.5.4	Determination of hydrodynamic co-efficient	50
3.5.5	Effect of porosity on the wave reflection coefficient ( $K_r$ )	51
3.5.6	Effect of Porosity on the wave transmission coefficient ( $K_t$ )	52
3.5.7	Effect of Porosity on the wave energy loss coefficient ( $K_L$ )	53
<b>Chapter 4</b>	<b>Numerical Modeling</b>	<b>55</b>
4.1	General	55
4.2	Modification of SOLA-VOF for Horizontal Slotted Submerged Breakwater	55
4.3	Numerical Model Run Conditions	56
4.4	Verification of the Modified Numerical Model	58
4.5	Comparison between Numerical and Experimental Results	59
4.6	Numerical Model Simulation of Time Series Water Surface Profiles	66
4.7	Numerical Model Simulation of Point Velocity around the Horizontal Slotted Submerged Breakwater	71
4.8	VOF Function F around the Breakwater	76
4.9	Pressure Distribution around the Breakwater	79
<b>Chapter 5</b>	<b>Conclusions and Recommendations</b>	<b>82</b>
5.1	Conclusions	82
5.2	Recommendations	84
<b>References</b>		<b>85</b>

## List of Figures

<b>Figure No.</b>	<b>Title</b>	<b>Page No.</b>
Figure 2.1	Box - floating breakwater (Fezzano, SP-Italy)	7
Figure 2.2	Emerged breakwater (Portland Harbor)	8
Figure 2.3	Definition sketch for submerged breakwater	9
Figure 2.4	(a) Large accropode units are placed by a crane and (b) after placing accropode blocks on offshore roundhead breakwater (Oman)	11
Figure 2.5	Intensification factor of wave generation source function $q^*$	15
Figure 2.6	Staggered mesh and classification of cells	17
Figure 2.7(a)	Definition sketch for velocity distribution	19
Figure 2.7(b)	Definition sketch for pressure distribution	19
Figure 2.8	Open boundary treatment due to added dissipation zone	20
Figure 2.9	Treatment of the cells during the oscillation of the floating body	22
Figure 2.10	Free surface geometric model of VOF method for solid breakwater	23
Figure 3.1	Laboratory flume	25
Figure 3.2	Wave generator	25
Figure 3.3	Weir mesh (screen) to reduce wave reflections	26
Figure 3.4	Horizontal slotted submerged porous breakwater	27
Figure 3.5	Wave absorber to damp the transmitted wave	29
Figure 3.6	Detail of the experimental setup	29
Figure 3.7(a)	Measurement of wave paddle of wave generator	31
Figure 3.7(b)	Nomo gram to obtain the value of $e$ and $f$	31
Figure 3.8 (a)	Data collection of water surface elevation	33
Figure 3.8 (b)	Wave approaching the breakwater	33
Figure 3.8 (c)	Wave breaking near over the breakwater	34
Figure 3.8 (d)	Wave breaking at the onshore end of the breakwater	34
Figure 3.8 (e)	Wave breaking just behind the breakwater	34
Figure 3.8 (f)	Transmitted wave after passing the breakwater	35
Figure 3.9	Water surface profile for different wave periods and porosities	36
Figure 3.10	Variation of $\eta/H_i$ with $t/T$ for different wave periods	41
Figure 3.11	Variation of $\eta/H_i$ with $x/L$ for different wave periods and porosities	44
Figure 3.12	Effect of breakwater porosity on the reflection coefficient	51
Figure 3.13	Effect of breakwater porosity on the transmission coefficient	52
Figure 3.14	Effect of breakwater porosity on the wave energy loss coefficient	53
Figure 4.1	Free surface geometric model of VOF method for porous breakwater	55
Figure 4.2	Typical orientation of cells set in numerical model	57
Figure 4.3	Comparison of dimensionless water surface profiles by numerical computation and 3rd-order Stokes wave theory ( $H_i=12\text{cm}$ , $T=1.6$ )	59

	sec, h=50 cm)	
Figure 4.4	Comparisons between numerical and experimental results of water surface profile and wave breaking position for different Run conditions	60
Figure 4.5	Numerical model simulation of time series water surface profile for run 1	67
Figure 4.6	Numerical model simulation of time series water particle velocity around the horizontal slotted submerged breakwater for run 1	72
Figure 4.7	Numerical model results of VOF function value F around the breakwater for run 2	77
Figure 4.8	Numerical model results of VOF function value F around the breakwater for run 6	78
Figure 4.9	Numerical model results of VOF function value F around the breakwater for run 10	79
Figure 4.10	Numerical model results of pressure distribution around the breakwater for run 1	80
Figure 4.11	Numerical model results of pressure distribution around the breakwater for run 5	80
Figure 4.12	Numerical model results of pressure distribution around the breakwater for run 9	81

## List of Tables

<b>Table No.</b>	<b>Title</b>	<b>Page No.</b>
Table 2.1	List of parameters used in the numerical models and their values	16
Table 2.2	Classification of surface cell (i,k)	18
Table 3.1	Wave generator setup for experimental runs	30
Table 3.2	Test scenarios	32
Table 4.1	Typical inputs in the numerical model	56
Table 4.2	Incident wave property for different run conditions	57
Table 4.3	Input boundary conditions for velocity	58

## List of Symbols

$B$	=	Breakwater Width
$h_s$	=	Breakwater Height
$H$	=	Still Water Depth
$n$	=	Porosity
$k$	=	Wave Number
$K_r$	=	Reflection Coefficient
$K_t$	=	Transmission Coefficient
$K_L$	=	Energy Loss Coefficient
$H_i$	=	Incident Wave Height
$T$	=	Wave Period
$L$	=	Wave Length
$t$	=	Time
$\eta$	=	Instantaneous Water Surface

# CHAPTER 1

## INTRODUCTION

### 1.1 General

The coastal zone is the interface where the land meets the ocean, encompassing shoreline environments as well as adjacent coastal waters. The coastal zone includes river deltas, coastal plains, wetlands, beaches and dunes, reefs, mangrove forests, lagoons, other coastal features. Distinguished from the environmental properties of the land and the ocean, its natural condition is more complex and ecological environment is more tender and sensitive. Therefore, to take use of hydraulic structures for protecting the shoreline is necessary.

Recent developments in shore protection structures are offshore breakwaters. The primary objectives of an offshore breakwater system are to increase the longevity of a renourished beach, provide a wider beach for recreation and provide protection to upland areas from waves and flooding. Offshore breakwaters, also called bulkheads, reduce the intensity of wave action in nearshore waters and thereby reduce coastal erosion. They are constructed some distance away from the coast or built with one end linked to the coast. The breakwaters may be placed one to three hundred feet offshore in relatively shallow water, designed to protect a gently sloping beach. Breakwaters may be either fixed or floating; the choice depends on normal water depth and tidal range. Breakwater construction is usually parallel or perpendicular to the coast to maintain tranquility condition in the important coastal regions like a port.

Generally, many offshore breakwaters have been built with their crest above the water surface, that's to say, the emerge structures. Submerged breakwaters are a special type of breakwaters distinguished from other emerged offshore ones. They are built with their crests submerged in the water. With this advantage, they avoid the generation of significant reflected wave that affect the nearby shoreline. Although it might take some disadvantage for navigation, they may be used efficiently as a mean of erosion control as they provide an inexpensive measure of protecting beaches exposed to small or moderate waves and offer fast installation for temporary offshore works.

Porous structures protect lee-side wave attack by dissipating wave energy through the viscosity-induced resistance in the porous media. Submerged breakwaters, in addition, may trigger the early breaking of incident waves and dissipate most of the energy. This type is able to enhance water circulation and exchange of water between the open sea and sheltered areas. Because of the submergence of the breakwater, its application to protecting coastal areas may attract more attention due to environmental concerns.

Vertical porous breakwater is considered as a good and cost-effective substitute for the conventional type of breakwaters, especially for coastal works where the tranquility requirements are low. This type occupies small zone, not affecting the seabed creatures. The submerged types of this kind permit to exchange the water masses along the beaches, which minimize the pollution aspects. In addition, the landside of the emerged types of this breakwater can be used for berthing purposes.

The functional performance of the porous breakwater is evaluated by examining the wave reflection, transmission and wave energy dissipation caused by this breakwater. The reflected waves and the dissipated wave energy are strongly affected by water depth, wave properties such as period and height, and structure properties. The major structure properties are porosity, size distribution and shape of the components of the porous media, and geometry such as the clearance of the submerged breakwater.

## **1.2 Study Objectives**

In this research, the interaction between waves and horizontally slotted submerged porous breakwater has been investigated. To predict the interaction, a two-dimensional numerical model based on the SOLA-VOF (SOLution Algorithm–Volume Of Fluid) method is used here. Also a two-dimensional laboratory experiment has been carried out to investigate the performance of submerged breakwater in wave breaking as well as in dissipating the wave energy in terms of reduction of wave height.

The specific objectives of this study are:

- (1) To conduct experimental investigation of wave interaction with submerged porous breakwater and to analyze the effect of porosity on the wave reflection, wave transmission and wave energy loss coefficients.
- (2) To adapt a two-dimensional numerical model using the Volume of Fluid (VOF) technique to simulate interaction (wave breaking, deformation, energy dissipation etc) between wave and submerged porous breakwater.
- (3) To check the performance of the developed numerical model by comparing the model simulated results with the experimentally measured data.

### **1.3 Study Scope and Contents**

The interaction between a horizontally slotted submerged breakwater and waves is studied in this thesis. Both the numerical and experimental studies are carried out in a two-dimensional field. The numerical studies evaluate water surface profiles along the channel length, distribution of water particle velocity field, the value of VOF function  $F$  and pressure around the breakwater, etc. Laboratory experiments are carried out in a two-dimensional wave tank with different wave conditions and different porosities of the breakwater. All the theories, analyses, numerical estimations, experimental investigations are presented in the following chapters.

In Chapter 2, the details of the different types of breakwaters, their applications, advantages and disadvantages are described. Both experimental and numerical studies about breakwater are detailed out here. Then the modified governing equations and boundary conditions used in the model are described. The elaborated discussions of the computational procedures in numerical model are also given in this chapter. The numerical stability considerations are also presented. After that application of SOLA-VOF model for different types of breakwater is presented. And then the experimental and numerical investigations which are carried out in this research are described.

In Chapter 3, the details of laboratory experiment are described. Twelve experimental investigations were carried out. Experiments were carried out with three different



porosities of the breakwater and four different wave conditions. The details of the experimental setup, submerged porous body model, experimental conditions, instrumentation and data acquisition system etc are presented in this chapter. Based on experimentally measured data, water surface profiles along the channel length are developed.

The numerical analyses of horizontal slotted submerged porous breakwater under wave action are presented in Chapter 4. At first modification of SOLA-VOF model for the horizontal slotted submerged breakwater and the numerical run conditions are described. Then the verification of the numerical model based on SOLA-VOF scheme is done using the waves generated according to Stokes 3<sup>rd</sup> order wave theory. The comparisons between numerically simulated results with the experimentally measured data are presented in this chapter. Then the numerical analyses are done for horizontally slotted submerged breakwater of different porosities under different wave conditions. Time series water surface profiles, distribution of water particle velocity, VOF function  $F$  and pressure around breakwater of different porosities are analyzed under different wave conditions.

Finally, an overview of the main conclusions of this study and recommendations for further study are presented in Chapter 5.

# **CHAPTER 2**

## **LITERATURE REVIEW**

### **2.1 General**

Breakwaters are wave energy barriers designed to protect the land or near shore area behind them from the direct attack of waves. Breakwaters have traditionally been used only for harbor protection and navigational purposes; but in recent years, designs of shore-parallel segmented breakwaters have been used for shore protection purposes. Segmented breakwaters can be used to provide protection over longer sections of shoreline than is generally managed through the use of bulkheads or revetments. Wave energy is able to pass through the breakwater gaps, allowing for the maintenance of some level of longshore sediment transport, as well as mixing and flushing of the sheltered waters behind the structures.

The dissipation of wave energy allows drift material to be deposited behind the breakwater. This accumulation of material protects the shore and may also extend the beach. The amount of deposition depends on the site characteristics and the design of the breakwater.

### **2.2 Different Types of Breakwater as Shore Protection Structure**

A shoreline management breakwater serves two purposes such as to provide shelter from the waves and through this shelter, to manipulate the littoral transport conditions and thereby to trap some sand. According to different purposes there are several types of breakwaters as follows:

- Detached breakwater (Breakwaters can be completely isolated from the shore)
  1. Headland breakwaters
  2. Nearshore breakwaters
- Attached breakwater (Breakwater can be connected to the shoreline)
  1. Low crested structure
  2. High crested structure
  3. Rubble mound structure
  4. Composite structure

- Using mass (Caissons)
- Using a revetment slope (e.g. with rock or concrete armor units)
- Floating breakwater
- Rigid or impermeable breakwater
- Porous or permeable breakwater

### **2.2.1 Floating breakwater**

Floating breakwaters represent an alternative solution to protect an area from wave attack, compared to conventional fixed breakwaters. It can be effective in coastal areas with mild wave environment conditions. Therefore, they have been increasingly used aiming at protecting small craft harbors or marinas or, less frequently, the shoreline, aiming at erosion control. Some of the conditions that favor floating breakwaters are:

1. *Poor foundation:* Floating breakwaters might be a proper solution where poor foundations possibilities prohibit the application of bottom supported breakwaters.
2. *Deep water:* In water depths in excess of 6 m, bottom connected breakwaters are often more expensive than floating breakwaters.
3. *Water quality:* Floating breakwaters present a minimum interference with water circulation and fish migration.
4. *Ice problems:* Floating breakwaters can be removed and towed to protected areas if ice formation is a problem. They may be suitable for areas where summer anchorage or moorage is required.
5. *Visual impact:* Floating breakwaters have a low profile and present a minimum intrusion on the horizon, particularly for areas with high tide ranges.
6. *Breakwater layout:* Floating breakwaters can usually be rearranged into a new layout with minimum effort.

#### ***Types of floating breakwaters***

Floating breakwaters (Figure 2.1) are commonly divided into four general categories:

1. Box
2. Pontoon
3. Mat
4. Tethered float.



*Figure 2.1: Box - floating breakwater (Fezzano, SP-Italy)*

### ***Disadvantages of floating breakwater***

- Floating breakwaters are less effective in reducing wave heights for slow waves than fixed structures are; a practical upper limit for the design wave period is in the range of 4 to 6 seconds.
- Floating breakwaters are susceptible to structural failure during catastrophic storms.
- If the structure fails and is detached from its moorings, the breakwater may become a hazard.
- Relative to common fixed breakwaters (Figure 2.2), floating breakwaters require a high amount of maintenance.



*Figure 2.2: Emerged breakwater (Portland Harbor)*

### **2.2.2 Fixed breakwater**

Fixed breakwaters are most economical when the slope is gentle and the high water level at the proposed site is less than about four feet deep. If the water at high tide is deeper than four feet, the fixed breakwater would need to be built so high that its cost would be prohibitive. Floating breakwaters can adjust to higher tides, but they are effective only against waves of short length. The nature of the bottom material is also important. Stone rubble or sandbag breakwaters can rest on any type of bottom, but they may settle if placed on soft earth or sand. A filter layer between the structure and the bottom can relieve this problem.

Fixed breakwater can be divided into submerged and emerged breakwater. The height and porosity of a fixed breakwater determines the extent to which drift will be deposited behind the structure. It is generally desirable to allow some of the wave action to pass over or through the breakwater, because many people value the waves as part of the natural beauty of the shore and as an essential ingredient in their recreational experience. This wave energy also helps to keep the area between the breakwater and the shore from becoming overfilled with littoral drift. Breakwaters that are too porous are ineffective.

#### ***Submerged or low-crested breakwater***

Submerged or low-crested breakwaters (a definition sketch is shown in Figure 2.3) function by inducing wave-breaking and by allowing some wave transmission so that a milder wave climate is obtained in leeward of the submerged structure.

#### ***Advantages of submerged/low crested breakwater***

- The visual impact of a submerged/low structure is less damaging.
- A submerged or low-crested structure is less expensive.
- The impact on the sand accumulation is smoother.
- The overtopping water generates good water circulation behind breakwater.
- Submerged breakwaters are very similar to natural reefs. They attract fish and are therefore economically beneficial.

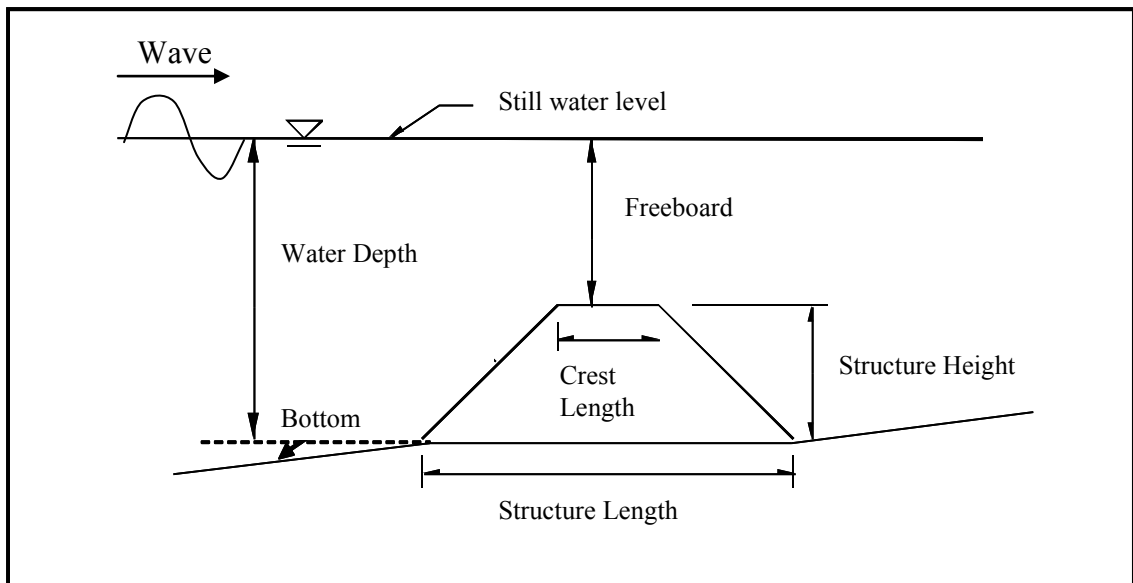


*Figure 2.3: Definition sketch for submerged breakwater*

### ***Disadvantages of submerged/low crested breakwater***

- A submerged structure can be dangerous for small craft navigation
- The overtopping water initiates local currents, which can be dangerous for swimmers
- A submerged or low-crested structure provides only partial attenuation of the wave action as well as partial shore protection.
- The efficiency of a submerged structure with respect to shore protection by the reduction of both waves and littoral transport very much depends on the crest freeboard of the design.
- The design is very difficult and challenging because the proper function of a submerged or low-crested structure depends on both water-level and wave conditions as well as on the specific structure.

### **2.2.3 Porous or permeable breakwater**

Rubble mound or porous breakwaters as shown in Figure 2.4 use structural voids to dissipate the wave energy. The core is made of rock and constitutes the main part of the breakwater. The porous flow inside the permeable core is caused by the waves and experiences high energy dissipation due to friction losses. The core material itself is not stable under wave attack and is protected by an armor layer of individual heavy

concrete blocks. These armor units withstand the waves. A toe at the sea bottom acts as a foundation for the armor layer. A filter layer between the core and the armor layer also acts as foundation layer for the armor layer, and prevents that the fine rock in the core is washed out in between the holes of the armor layer.

Waves propagate towards the breakwater and run-up and run-down the armor layer. Part of the wave energy is reflected back to the sea, part of the energy is dissipated in the armor and filter layer and in the core, the remaining part is transmitted through the breakwater. The porous flow inside the core has both laminar and turbulent flow characteristics and is connected to the wave attack via infiltration and seepage through the armor layer.



(a)

(b)

*Figure 2.4(a): Large accropode units are placed by a crane and (b) after placing accropode blocks on offshore roundhead breakwater (Oman)*

### **2.3 Previous Studies on Breakwater**

Various aspects of two and three dimensional problems of wave interaction with submerged, bottom founded, or floating surface-piercing structures have been studied both numerically and experimentally by many investigators. Liao et al (2013) studied on the wave breaking criteria and energy loss caused by a submerged porous breakwater on a horizontal bottom. Results show that almost all tested waves can be triggered to break when the ratio of the estimated equivalent deepwater wave height

to the freeboard of the submerged breakwater is greater than 1. Jin et al (2013) analyzed the horizontal and vertical velocities of each later interface in the process of solitary wave propagation through submerged breakwater. Wu et al (2012) studied the interactions between a non breaking solitary wave and a submerged permeable breakwater experimentally and numerically. To simulate the experiments they considered the 2D and 3D Volume of fluids (VOF) type model coupled with Large Eddy Simulation model. Wiryanto (2011) analyzed the wave propagation passing over the submerged breakwater for monochromatic and solitary waves. From the results it is seen that the amplitude decreases exponentially with respect to the space variable in the region above the breakwater. The reflected wave is also analyzed when the model is combined with the model using the shallow water equations.

Balaji (2012) studied the hydrodynamic performance of porous breakwater by numerical analysis to assess reflection and transmission characteristics. The finite difference method on BOUSS-2D was used to test the efficiency of porous breakwaters and it was found that the reflection coefficient increases, whereas the transmission coefficient decreases with the decrease in the porosity. Jhang et al (2011) developed the mechanism of the wave-permeable structure-porous sea bed interaction based on the Volume Averaged/ Reynolds-Averaged Navier-Stokes (VARANS) equation and Biot's poro-elastic theory. Numerical results indicated that after a full wave-structure interaction, the magnitude of pore pressure below the lee side of a breakwater decreases with an increasing structure porosity.

Hsu et al (2008) extended the parabolic equation for waves propagating over submerged permeable structures in the surf zone. The governing equation is a formulation of the breaking and energy dissipation effect of porous structures. Rageh (2009) presented the efficiency of the breakwater as a function of the transmission, the reflection and wave energy loss coefficients. It was found that both the transmission and the reflection coefficients decrease as the relative breakwater width ( $k.B$ ) increases, while the energy loss coefficient takes the opposite trend. Sidek and Wahab (2007) experimentally investigated the effects of porosity of submerged breakwater on non-breaking wave transformations. It was found that the transmission coefficient increases with the increased model porosity. Kobayashi et al (2007) developed a numerical model based on time averaged continuity, momentum and



energy equation to predict the mean and standard deviation of the free surface elevation and horizontal fluid velocities above and inside a porous submerged breakwater.

Al-Banna and Liu (2007) conducted a numerical study on the hydraulic performance of submerged porous breakwater under solitary wave attack based on solving the Reynolds-Averaged Navier-Stokes (RANS) equations. Lee et al. (2007) studied the transformation of irregular waves propagating over a submerged breakwater. By providing the incident irregular waves with repeatable amplitude and phase for each wave component, effects of the height and width of the breakwater on the wave transformation were studied systematically. Hieu and Tanimoto (2006) developed VOF based two phase flow model and applied to the simulations of wave interactions with a submerged breakwater as well as of wave breaking on a slope. Rahman et al (2006) developed a two-dimensional numerical model combining the SOLA-VOF(SOLution Algorithm – Volume Of Fluid) model and porous body model, to estimate the wave forces acting on a pontoon type submerged floating breakwater.

Lee C. et al. (2003) solved analytically the flow field of linear waves passing a submerged porous breakwater. The permeable breakwater was considered to be anisotropic but homogeneous. Hur and Mizutani (2003) have developed a numerical model, which combine the VOF model and porous body model, to estimate the wave forces acting on a three-dimensional body on a submerged breakwater. They examined wave induced deformation on the permeable submerged structure making use of the porous body model (Sakakiyama and Kajima (1992)) to express the governing equations of fluid motion. Huang et al (2003) solved the unsteady two dimensional Navier-Stokes equations and Navier-Stokes type model equations for porous flows to simulate the interaction between a solitary wave and a submerged porous breakwater. Mendez et al (2001) analyzed the influence of wave reflection and energy dissipation by breaking and by porous flow induced by a permeable submerged breakwater on second order mean quantities such as mass flux, energy flux, radiation stress and mean water level.

Rahman and Womera (2013) investigated the interaction between waves and rectangular submerged impermeable breakwater. To predict the investigation, a two-dimensional numerical model based on the SOLA-VOF method was proposed there.

Also a two- -dimensional laboratory experiment had been carried out and found that for any particular wave period the relative structure height and the relative structure width were the important parameters for the reduction of incident wave height. Rahman and Akter (2014) investigated the efficiency of the porous breakwaters governed by their porosity and their depth of submergence. In their study, experimental investigation has been carried out in a two-dimensional wave flume to investigate the effect of porosity on submerged and emerged porous breakwaters under various wave conditions.

## 2.4 Numerical Model Based On SOLA-VOF

The Volume of Fluid (VOF) method is powerful numerical computation technique for evaluating the free surface due to wave-structure interaction. The developed numerical model can simulate water surface profile, velocity distribution, pressure distribution along both axes of two-dimensional grid and also the value of fraction of volume occupied by fluid at any time.

### 2.4.1 Basic equations

The basic equations used for VOF method are the continuity equation, the Navier-Stokes equation for incompressible fluid and the advection equation that represents the behavior of the free surface. Because the wave generation source is placed within the computational domain, these equations involve the wave generation source. The continuity equation is,

$$\frac{\partial u}{\partial x} + \frac{\partial w}{\partial z} = q(x, z, t) \quad (2.1)$$

$$q(x, z, t) = \begin{cases} q^*(z, t); & x = x_s \\ 0; & x \neq x_s \end{cases} \quad (2.2)$$

where  $u$  and  $w$  are the flow velocity of  $x$  and  $z$  direction respectively,  $q$  is the wave generation source with  $q^*$  as the source strength which is only located at  $x = x_s$  and  $t$  is the time. The wave generation source  $q^*$  is defined as follows so that the vertically integrated quantity of  $q^*$  is equal to that in the non-reflection case (Ohyama and Nadaoka, 1991).

$q^*$  is also gradually intensified for the three wave periods (Figure 2.5) from the start of wave generation in order to guarantee a stable regular wave train, as mentioned by Brorsen and Larsen (1987), shown in Equation 2.3.

$$q^* = \begin{cases} \left\{ 1 - \exp\left(-\frac{2t}{T_i}\right) \right\} 2U_0 \frac{\eta_0 + h}{\eta_0 + h} / \Delta x_s & : t/T_i \leq 3 \\ 2U_0 \frac{\eta_0 + h}{\eta_0 + h} / \Delta x_s & : t/T_i > 3 \end{cases} \quad (2.3)$$

where  $t$  is the time from the start of wave generation,  $T_i$  is the incident wave period,  $h$  is the still water depth, and  $\eta_s$  is the water surface elevation at the source line ( $x = x_s = 0$ ).  $\Delta x_s$  is the mesh size in the  $x$ -direction at  $x = x_s$ , and is required in order to apply the non-reflective wave generator to the finite difference method.  $U_0$  and  $\eta_0$  are the time variation of horizontal velocity and water surface based on third-order Stokes wave theory, respectively. The coefficient "2" of  $U_0$  in the right hand side of Equation 2.3 corresponds to two propagating waves toward both the left and right sides of the wave generation source.

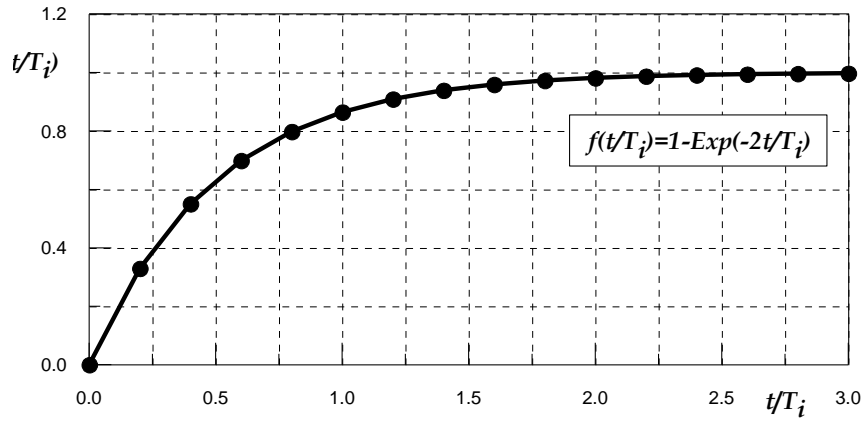


Figure 2.5: Intensification factor of wave generation source function  $q^*$  for  $t/T_i \leq 3$ .

The Navier-Stokes equation,

$$\frac{\partial u}{\partial t} + u \frac{\partial u}{\partial x} + w \frac{\partial u}{\partial z} = -\frac{1}{\rho} \frac{\partial p}{\partial x} + \nu \left( \frac{\partial^2 u}{\partial x^2} + \frac{\partial^2 u}{\partial z^2} \right) + uq \quad (2.4)$$

$$\frac{\partial w}{\partial t} + u \frac{\partial w}{\partial x} + w \frac{\partial w}{\partial z} = -\frac{1}{\rho} \frac{\partial p}{\partial z} + \nu \left( \frac{\partial^2 w}{\partial x^2} + \frac{\partial^2 w}{\partial z^2} \right) + wq + \frac{1}{3} \nu \frac{\partial q}{\partial z} - g - \beta w \quad (2.5)$$

where  $p$  is the pressure,  $\nu$  is the kinematic viscosity,  $\rho$  is the fluid density,  $g$  is the gravitational acceleration and  $\beta$  is the wave dissipation factor which equals 0 except for the added dissipation zone.

The advection equation of VOF function  $F$  is derived by considering conservation of mass of the fluid in each cell. The advection equation of VOF function  $F$ ,

$$\frac{\partial F}{\partial t} + \frac{\partial uF}{\partial x} + \frac{\partial wF}{\partial z} = Fq \quad (2.6)$$

The equations include the added terms different from the well-known continuity and Navier-Stokes equations because the wave generation source and the added dissipation zone exist within the computational domain.

#### 2.4.2 Parameters used in numerical model

List of parameters used in the 2-D numerical model based on SOLA-VOF is given in Table 2.1:

*Table 2.1: List of parameters used in the numerical models and their values  
(Rahman and Womera, 2013)*

Symbol	Name of the parameter	Value used in the 2-D numerical model
$\alpha$	Numerical stability factor	0.5
$\beta$	Wave dissipation factor	1.03(for added dissipation zone)
		0 (otherwise)
$\zeta$	Tolerance value for divergence term	$1 \times 10^{-3}$
$\nu$	Co-efficient of viscosity	$0.0101 \text{ cm}^2/\text{sec}$
$\omega$	Acceleration factor	$1.7 \text{ rad}/\text{sec}^2$
$\rho$	Fluid density	$1 \text{ gm}/\text{cm}^3$
$g$	Gravitational acceleration	$980 \text{ cm}/\text{sec}^2$

### 2.4.3 Computational procedure

On the staggered mesh, the flow velocities  $u$  and  $w$  are put on the cell boundary, and the pressure  $p$ , wave generation source  $q$  and VOF function  $F$  are set on the center of each cell as shown in Figure 2.6(a). Here  $\Delta x$  and  $\Delta z$ , in Figure 2.6(a), are the cell lengths in the respective directions of  $x$  and  $z$ , and each cell is identified by sub suffix  $(i, k)$ . The cell is classified into four types; a full cell filled with fluid, an empty cell occupied by air, a surface cell containing both fluid and air and an obstacle cell that represents the structure.

The SOLA scheme is employed to calculate the pressure and flow velocity in each time step. And a type of donor-acceptor flux approximation is used to calculate the advection of the VOF function  $F$  computing the free surface. The advections are calculated by velocities of the adjoining cell using a donor cell which transports a fluid and an acceptor cell which receives the advect fluid. The physical characteristics of the cell are defined by the values of VOF function  $F$ . The cell in air, in the surface and in the water are denoted with  $F=0$ ,  $0 < F < 1$ , and  $F=1$  respectively as displayed in Figure 2.6 (b).

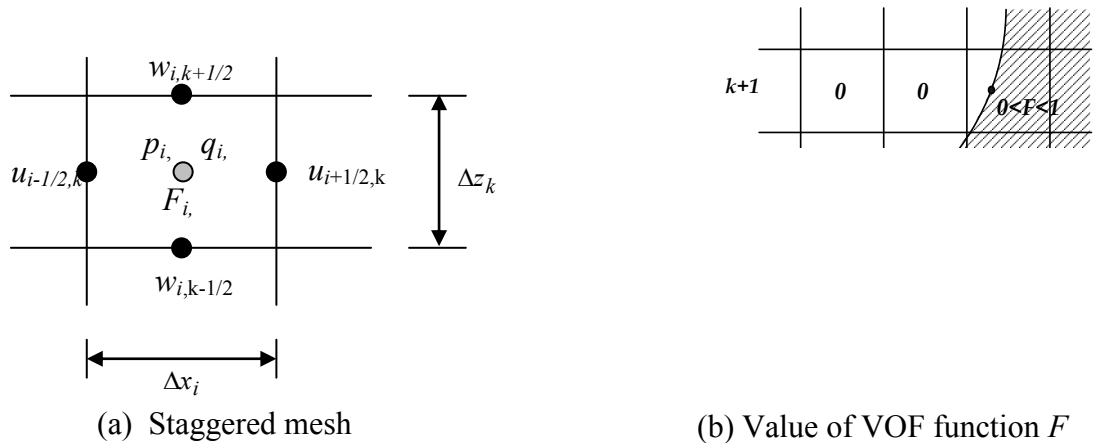


Figure 2.6: Staggered mesh and classification of cells

To determine accurately the location of the free surface at the next time step, it is therefore necessary to know the orientation of the free surface within the surface cell. Table 2.2 shows the classified orientation of the free surface.

Table 2.2: Classification of surface cell  $(i,k)$

$RF$	Contents
1	Surface normal to the x-axis and full cell at $(i-1,k)$
2	Surface normal to the x-axis and full cell at $(i+1,k)$
3	Surface normal to the z-axis and full cell at $(i,k-1)$
4	Surface normal to the z-axis and full cell at $(i,k+1)$

The basic procedure for the modified SOLA scheme is as follows:

- (i) Explicit scheme of the momentum equations (Equations (2.4) and (2.5)) are employed to calculate the first approximation of the velocity at the next time step using the velocity, pressure and the wave generation source at the present time step. The calculated velocities do not satisfy the continuity equation in general.
- (ii) To satisfy completely the continuity equation (Equation 2.1), the pressure and velocities are iteratively adjusted in the cell occupied by the fluid.

Stable numerical results can be obtained by repeating the above mentioned procedures under suitable boundary conditions at each time step. It should be noticed that the cell which can satisfy the continuity equation by means of the modified SOLA scheme is only the full one. The surface cell, however, can satisfy the continuity equation by employing the velocity boundary condition. The momentum equations are only used to calculate the velocity on the surface of full cell. Since the velocity on the interface between surface cells or between the surface cell and empty cell cannot be calculated with the momentum equations only, the boundary conditions are necessary to calculate the velocities.

#### 2.4.4 Boundary conditions

##### *Free-surface boundary conditions*

**Boundary conditions for velocity:**

There are two boundary conditions for water particle velocity, that is, (1) a boundary condition for the velocity parallel to the free-surface and (2) a boundary condition for the velocity normal to the free-surface.

In the first boundary condition, since an adjacent full cell exists in the direction indicated by the flag *RF*, the velocity on the surface cell is set equal to the velocity on the interface in contact with the adjacent full cell, which can be calculated by the governing equations (Equations (2.4) and (2.5)). In the 2<sup>nd</sup> boundary condition, the velocity is determined so that the continuity equation (Equation 2.1) is satisfied in surface cells. Even if a surface cell may change to a full cell at the next time step, the full cell is still able to satisfy the continuity equation.

**Boundary conditions for pressure:**

As mentioned before, the pressure in the full cell can be calculated by means of the SOLA scheme. However, in surface cells, different procedures are required because the locations of the pressure points in the staggered mesh generally differ from the actual locations on the free surface. Therefore, the linear interpolation or extrapolation between the pressure on the free surface (atmospheric pressure) and the pressure of the adjacent full cell in the direction indicated by flag *RF* is used to calculate the pressure of the surface cell as displayed in Figure 2.7 (b).

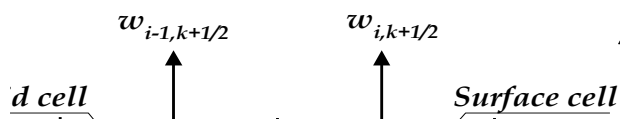


Figure 2.7(a): Definition sketch for velocity distribution

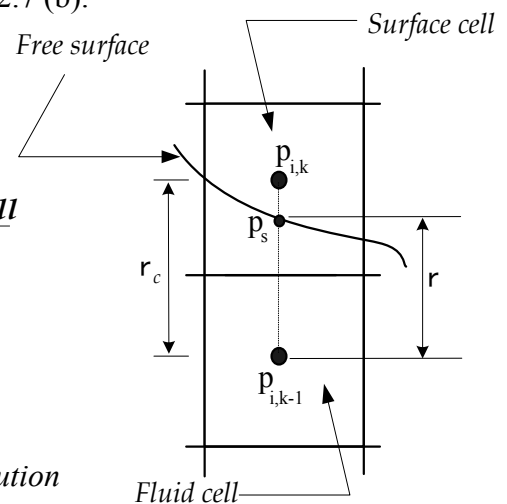
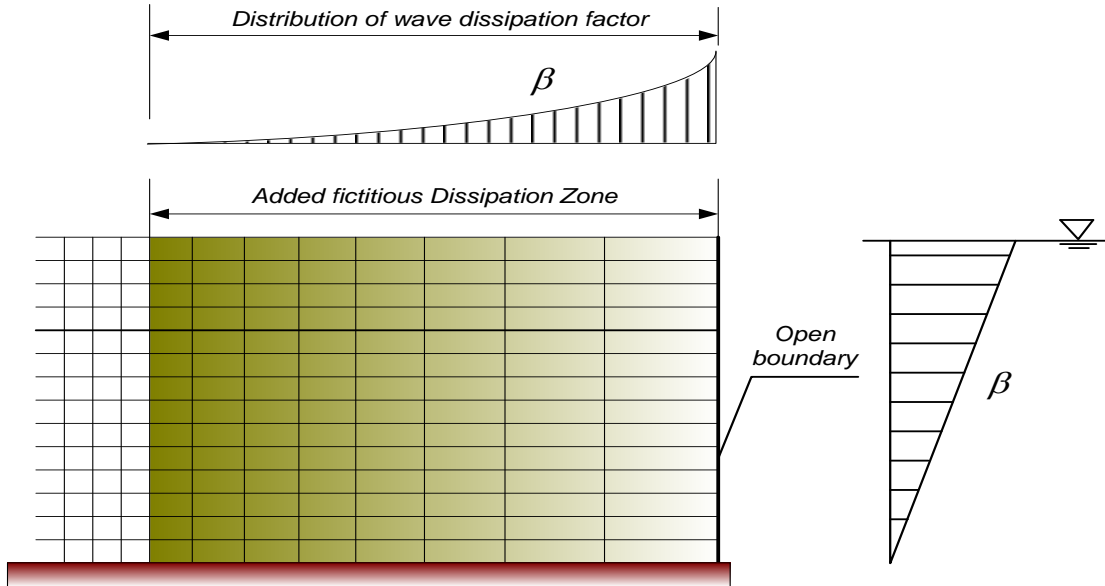


Figure 2.7(b): Definition sketch for pressure distribution

### ***Open boundary condition***

An added dissipation zone method (Hinatsu, 1992) is used to treat the open boundaries. As shown in Figure 2.8, the waves are damped by numerical dissipation effects due to the coarse grids and the fictitious damping forces based on the Stokes damping law.



*Figure 2.8: Open boundary treatment due to added dissipation zone*

The damping force in the  $x$ -direction is not taken into account to avoid the velocity damping in the uniform horizontal flow.

### ***Other boundary conditions***

Sommerfeld radiation condition (Equation 2.7) is applied for the open boundaries. And, non-slip condition is applied on the sea bed.

$$\frac{\partial Q}{\partial t} \pm C \frac{\partial Q}{\partial x} = 0 \quad (2.7)$$

where  $Q$  is the quantity representing the velocities  $u$  and  $w$ , and so on, and  $C$  is the wave celerity. The value of water particle velocity tends to zero at the sea bed because of non-slip condition. So the roughness parameter of the sea bed material has no influence in this model.



### 2.4.5 Numerical stability considerations

Numerical calculations often have computed quantities that develop large, high frequency oscillations in space, time, or both. This behavior is usually referred to as a numerical instability, especially if the physical problem being studied is known not to have unstable solutions. When the physical problem does have unstable solutions and if the calculated results exhibit significant variations over distances comparable to a cell width or over times comparable to the time increment, the accuracy of the results cannot be relied on. To prevent this type of numerical instability or inaccuracy certain restrictions must be observed in defining the mesh increments  $\Delta x_i$  and  $\Delta z_k$ , the time increment  $\Delta t$ , and the upstream differencing parameter  $\alpha$ .

For accuracy, the mesh increments must be chosen small enough to resolve the expected spatial variations in all dependent variables. When this is impossible because of limitations imposed by computing time or memory requirements, special care must be exercised in interpreting calculation results. For example, in computing the flow in a large chamber it is usually impossible to resolve thin boundary layers along the confining walls. In many applications, however the presence of thin boundary layers is unimportant and free-slip boundary conditions can be justified as a good approximation.

Once a mesh has been chosen, the choice of the time increment necessary for stability is governed by two restrictions. First, material cannot move through more than one cell in one time step because the difference equations assume fluxes only adjacent cells. Therefore, the time increment must satisfy the inequality

$$\Delta t < \min \left\{ \frac{\Delta x_i}{|u_{i,k}|}, \frac{\Delta z_k}{|w_{i,k}|} \right\} \quad (2.8)$$

where the minimum is with respect to every cell in the mesh. Typically,  $\Delta t$  is chosen equal to one-fourth to one-third of the minimum cell transit time. Second, when a nonzero value of kinematic viscosity is used, momentum must not diffuse more than approximately one cell in one time step. A linear stability analysis shows that this limitation implies

$$v\Delta t < \frac{1}{2} \left\{ \frac{\Delta x_i^2 \Delta z_k^2}{\Delta x_i^2 + \Delta z_k^2} \right\} \quad (2.9)$$

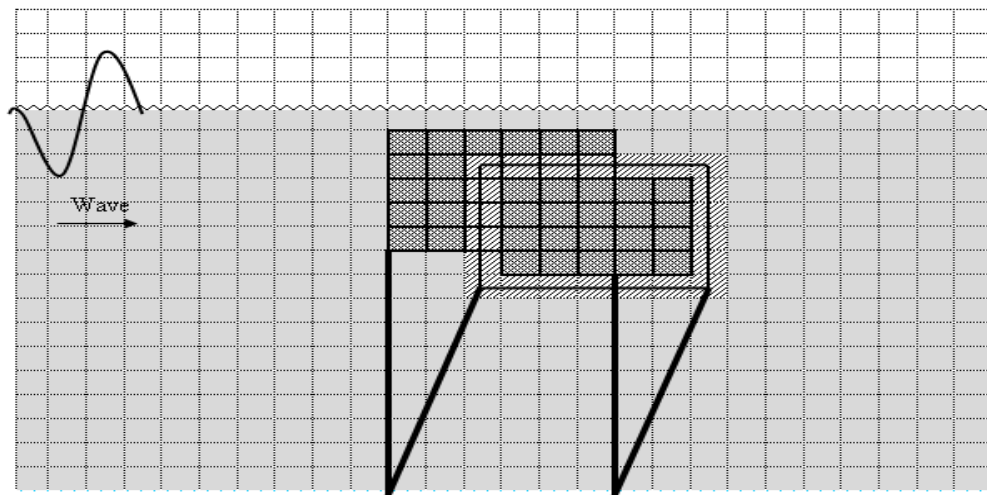
With  $\Delta t$  chosen to satisfy the above two inequalities, the last parameter need to ensure numerical stability is  $\alpha$ . The proper choice for  $\alpha$  is

$$1 \geq \alpha > \max \left\{ \left| \frac{u_{i,k} \Delta t}{\Delta x_i} \right|, \left| \frac{w_{i,k} \Delta t}{\Delta z_k} \right| \right\} \quad (2.10)$$

As a rule of thumb,  $\alpha$  approximately 1.2 to 1.5 times larger than the right-hand inequality is a good choice. If  $\alpha$  is too large an unnecessary smoothing (diffusion-like truncation errors) may be introduced.

## 2.5 SOLA-VOF Used for Modeling Breakwaters

Rahman et. al. (2006) developed a two-dimensional numerical model combining the SOLA-VOF model and porous body model, to estimate the wave forces acting on a pontoon type submerged floating breakwater. In Figure 2.9, the treatment of the cells during the oscillation of the floating body due to wave action is shown. Partially obstacle cells are obtained due to cutting the fluid or empty or surface cells by the surfaces of the floating body. These cells are partially filled by floating body material and partially by fluid and /or air.








- |   |   |               |   |   |                         |
|---|---|---------------|---|---|-------------------------|
|  | : | Empty cell    |    | : | Partially obstacle cell |
|  | : | Obstacle cell |    | : | Fluid cell              |
|   |   |               |  | : | Surface cell            |

Figure 2.9: Treatment of the cells during the oscillation of the floating body

Rahman and Womera (2013) developed a two-dimensional numerical model based on SOLA-VOF method to find the interaction between waves and fixed submerged breakwater.

A simplified geometric model of VOF method for solid breakwater is displayed in Figure 2.10. Four types of cells are shown in the figure, which are empty cell, surface cell, fluid cell and obstacle cell. The surface cell is the demarcation line in between fluid cells and empty cells. The empty cells are those filled with air and fluid cells are filled with water.

	E	E	E	E	E	E	E	E	E	E	E	E	E	E	
	E	E	E	E	E	S	S	S	S	S	S	S	E	E	
	S	S	E	E	S	S	F	F	F	F	F	F	S	S	
	F	S	S	S	S	F	F	F	F	F	F	F	F	F	
	F	F	F	F	F	F	F	F	F	F	F	F	F	F	
	F	F	F	F	F	F	OB	OB	OB	F	F	F	F	F	
	F	F	F	F	F	F	OB	OB	OB	F	F	F	F	F	
	F	F	F	F	F	F	OB	OB	OB	F	F	F	F	F	

*E = Empty cell, S = Surface cell, F = Fluid cell, OB= Obstacle cell*

*Figure 2.10: Free surface geometric model of VOF method for solid breakwater*

## 2.6 Present Study

In this study experimental investigations are carried out in a two-dimensional wave flume at the Hydraulics and River Engineering Laboratory of the Bangladesh University of Engineering and Technology to investigate the hydrodynamic performance of proposed rectangular type submerged porous breakwater. Twelve experimental runs are carried out with fixed porous rectangular breakwaters of different porosities for different wave periods in the same wave flume which is 21.3 m long, 0.76 m wide and 0.74 m deep.

Moreover, the two-dimensional model of wave interaction with fixed submerged breakwater developed by Rahman and Womera (2013) is updated to adapt it for simulating wave interaction with horizontal slotted submerged porous breakwater. The numerical model based on SOLA-VOF scheme simulates water surface profile; velocity components and magnitude of pressure along the computational domain. Also the experimentally measured data and model simulated results are analyzed.

# **CHAPTER 3**

## **LABORATORY EXPERIMENT**

### **3.1 General**

To investigate the hydrodynamic performance of proposed rectangular shaped horizontal slotted submerged porous breakwater, experimental studies are carried out in a two-dimensional wave flume at the Hydraulics and River Engineering Laboratory of the Bangladesh University of Engineering and Technology. A set of experiments are carried out with fixed porous rectangular breakwaters of different porosities for regular waves of different wave periods in the wave flume. The experimental setup and procedure of conducting the experimental works are described in this chapter.

### **3.2 Laboratory Equipments**

#### **3.2.1 Two-dimensional wave flume**

The experiment has been carried out in a 21.3 m long, 0.76 m wide and 0.74 m deep rectangular tilting flume in the Hydraulics and River Engineering Laboratory (Figure 3.1). The side walls of the flume are vertical, and made of clear glass for visual inspection. The bottom of wave flume is made of steel. In the wave flume artificial regular waves are generated by a wave generator. To damp the transmitted wave a wave absorber is installed at the end of the flume.

Flume bed has been kept horizontal and it is supported on an elevated steel truss. Rubber pads have been attached to prohibit the flush out of wave from the flume for the case of highest wave height generation. In the flume water was supplied by external pipes and water depth was kept to desired level. For avoiding any unnecessary leakage in the flume, necessary steps were taken.



*Figure 3.1: Laboratory flume (21.3 m long, 0.76 m wide and 0.74 m deep)*

### **3.2.2 Wave generator**

A wave generator is placed at one corner of upstream side of the wave flume. Wave generator consists of a motor and a wave making paddle, which is connected with two vertical limbs as displayed in Figure 3.2.



*Figure 3.2: Wave generator*

Waves are generated by rotating the wave paddle with different frequency as per the requirement. Displacement of wave paddle can be controlled by a crank which is connected to the wave paddle by a connecting rod. Radius of rotation of the crank can be controlled by screw adjustment. The wave paddle is allowed to move horizontally to a distance equal to the radius of rotation of the rotating crank. Therefore, the displacement of the wave paddle can be adjusted by changing the radius of rotation of



the crank. The wave period and wave height for different run conditions has been set by altering the rotational speed of the arm of paddle. Rotational speed can be altered between 20 rpm to 120 rpm and the paddle arm can be altered by 25 mm to 320 mm. Hence the required values can be set from the wave generator. Two displacements have been observed during the movement of wave paddle of the wave generator; firstly the rotational displacement and secondly the vertical displacement. These two types of adjustments can be adjusted by changing the vertical limbs of the wave generator.

### **3.2.3 Wire screens to reduce wave reflections**

In the flume several screens were set in front of the wave generator to reduce wave reflections. Screens were made of coarse wire mesh as can be seen from Figure 3.3.

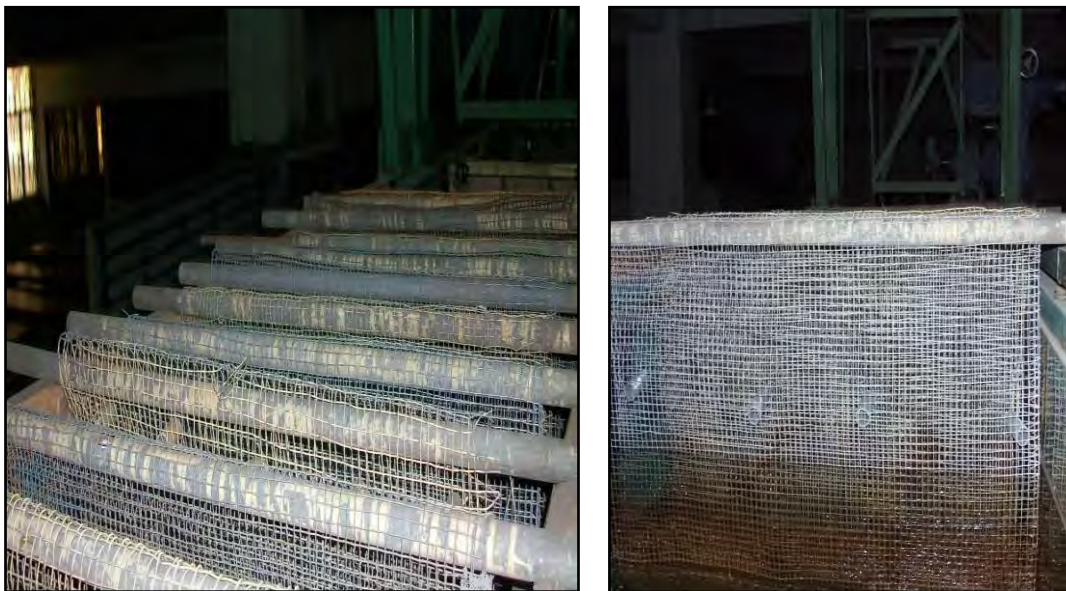


*Figure 3.3: Weir mesh (screen) to reduce wave reflections*

Screens were kept at approximately 6 inch apart from each other. In this study 15 screens have been used to reduce reflections.

### **3.2.4 Water reservoir**

The water reservoir used in the flume is a steel structure. Water is stored in the reservoir during the time of conducting the experiment. In the reservoir the water supply can be controlled by the existing facilities in the reservoir.

### 3.2.5 Horizontal slotted submerged porous breakwater

The breakwater was constructed by wooden planks in a steel frame as shown in Figure 3.4. Width of the breakwater along the wave direction was 100 cm and length of the breakwater was same as the width of the wave tank (76cm). The height of still water level which was maintained in the laboratory flume was 50 cm, whereas the porous breakwater height was 40 cm. Keeping the fixed dimensions of the breakwater width, length and height, three different breakwaters having different porosities ( $n= 0.4, 0.5, 0.6$ ) were constructed.



(a) Front View-along the wave direction

(b) Longitudinal View

Figure 3.4: Horizontal slotted submerged porous breakwater

To make porous breakwater, at first a rectangular framework was constructed by steel angles of desired dimensions. Then wooden planks of different thicknesses such as 8 cm, 6 cm and 4 cm are placed inside the steel frame (Figure 3.4) to create different porosities. 40% porosity ( $n=0.4$ ) is created using three wooden planks of 8 cm thickness and leaving two gaps of 8 cm each in the 40 cm high breakwater. 50% porosity ( $n=0.5$ ) is created using an 8 cm wooden plank at the bottom and two 6 cm wooden plank at middle and top leaving two gaps of 10 cm each. Hence, 60% porosity ( $n=0.6$ ) is created using a 8 cm wooden plank at the bottom and two 4 cm wooden planks at middle and top leaving two gaps of 12 cm each among them.

#### Basis of breakwater size selection

Dick and Brebner (1968) proved in their study on solid and permeable submerged breakwaters that for optimum reduction in transmitted wave height, breakwater width



B should be as large as possible in fact up to 2 wavelengths. This is unlikely to be an economical proposition, so that some narrower breakwater with greater height was investigated later. Kawasaki, K., Iwata, K. (2001) investigated the breaking limit, the breaker type and the breaking point due to various submerged trapezoidal breakwaters. In their study, they found for relative structure height  $h_s/h = 0.8$ , usually the waves break when the relative breakwater width  $B/L$  is in the range of 0.2 to 0.4.

In this study, the laboratory experiments are conducted for four different wave periods ranging from  $T = 1.6$  sec to 2.0 sec and corresponding wavelengths of 250 cm to 400 cm. For optimum reduction in transmitted wave height, the breakwater width along the wave direction was selected as 100 cm so that the relative structure width  $B/L$  ranges from 0.25 to 0.4. Breakwater lengths are usually selected so that they can cover the protection required length of the coastline. In this two-dimensional study, the breakwater length is selected as 76 cm which covers the full width of the two-dimensional wave flume.

### 3.2.6 Wave absorber

To damp the transmitted wave after passing the breakwater a wave absorber is installed at the end of the wave flume. It is a sloped surface (3.3H: 1V) made of wood. Its total horizontal length is 245 cm. The wave absorber dissipates the energy of the transmitted wave at the end of the flume to reduce the generation of reflecting wave. Figure 3.5 shows the photo views of wave absorber.



*Figure 3.5: Wave absorber to damp the transmitted wave*

### 3.2.7 Experimental setup

In 21.3 m long wave flume, the wave generator is placed at 190 cm downstream from the upstream end of the flume. The fixed submerged breakwater is installed at a distance of 800 cm from the wave generator. Six different positions are chosen to collect the data of water surface elevation.

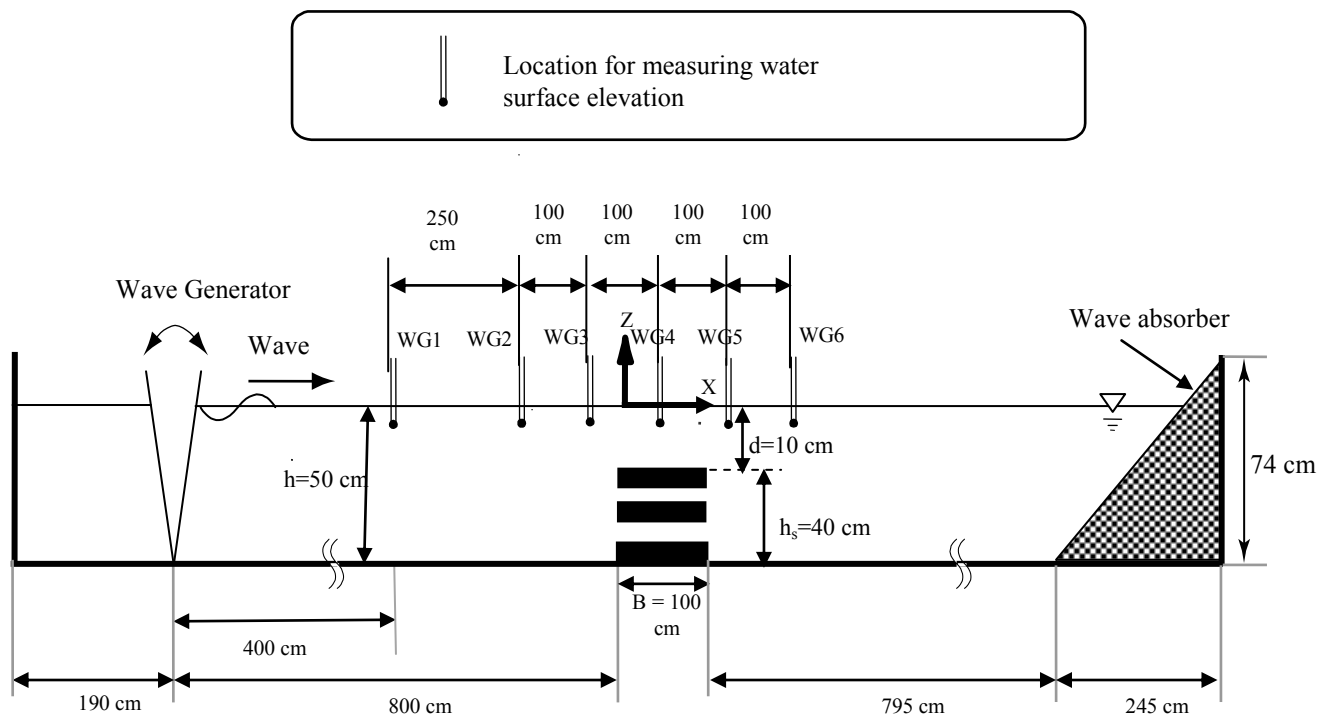


Figure 3.6: Detail of the experimental setup

Three locations are in front of the fixed submerged breakwater to investigate the incident wave properties. The fourth position of data collection is set over the breakwater. Then the last two positions are chosen behind the breakwater to observe the effect of breakwater installation in reduction of wave height.

The first position of data collection is at 400 cm in front of the breakwater. The other positions are at equidistance of 100 cm from each other. Then finally at the end of the flume a wave absorber of 245 cm length is installed. The detail of experimental setup is shown in Figure 3.6.

### 3.3 Measurement Techniques and Test Scenarios

Regular waves of four different wave periods ( $T=1.6$  sec, 1.7 sec, 1.8 sec and 2.0 sec) were generated in the wave flume. At first the water depth was fixed at 50 cm in the

wave flume. Then for the four different wave periods the wave generator was fixed-up with necessary adjustment. Here, for each case the angular rotation  $\omega$ , dimensionless parameters  $\left(\frac{f+e}{f}\right)$  were calculated for wave generator set-up (Figure 3.7). The dimensionless parameters stated earlier are related with the water depth as well as the wave period. Hence, the following table (Table 3.1) was formulated for conducting the experiment to produce desired periodic wave in the laboratory flume by using the laboratory wave generator.

Table 3.1: Wave generator setup for experimental runs

h (cm)	T (sec)	$\omega = \frac{2\pi}{T}$	$\frac{\omega^2 h}{g}$	From Figure 3.7(b)		$\frac{f+e}{f}$	From Laboratory		
				f	e		f	e+f	$\frac{f+e}{f}$
50	1.6	3.927	0.786	0.73	0.5	1.69	15	25	1.67
	1.7	3.696	0.696	0.81	0.46	1.57	25	16	1.56
	1.8	3.491	0.621	0.92	0.44	1.48	16.5	24.5	1.484
	2.0	3.142	0.503	1.1	0.4	1.36	17.5	24	1.37

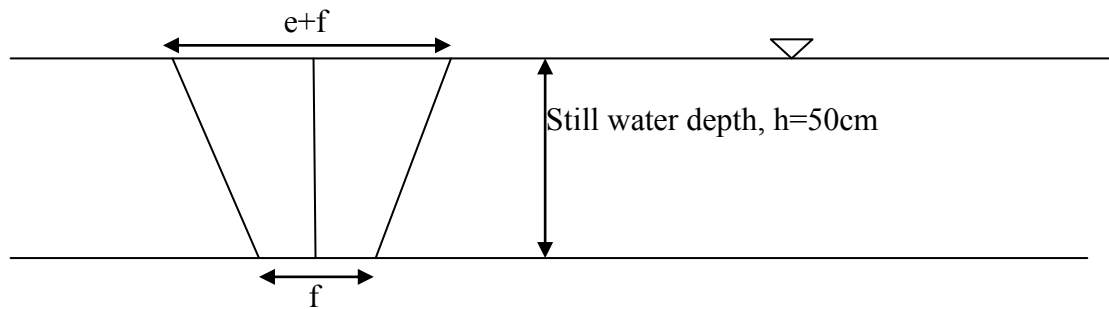


Figure 3.7(a): Measurement of wave paddle of wave generator

The experimental run was carried out after completing all those necessary adjustments for desired wave generation. After setting the frequency of the wave paddle of the wave generator, it is seen that the wave generator can generate waves with wave periods deviating very negligible amount (maximum  $\pm 0.1\%$ ) from the desired wave period, which results slight difference in experimentally generated wavelength than that of actual one. When the actual wave period was seen quite close to the designated wave period by some minor adjustment in the wave generator, then the experiments was carried out and measurements of water level at six different measuring stations

were taken for different run conditions. Table 3.2 presents the test scenarios. At all the run conditions, the still water depth is constant ( $h=50$  cm).

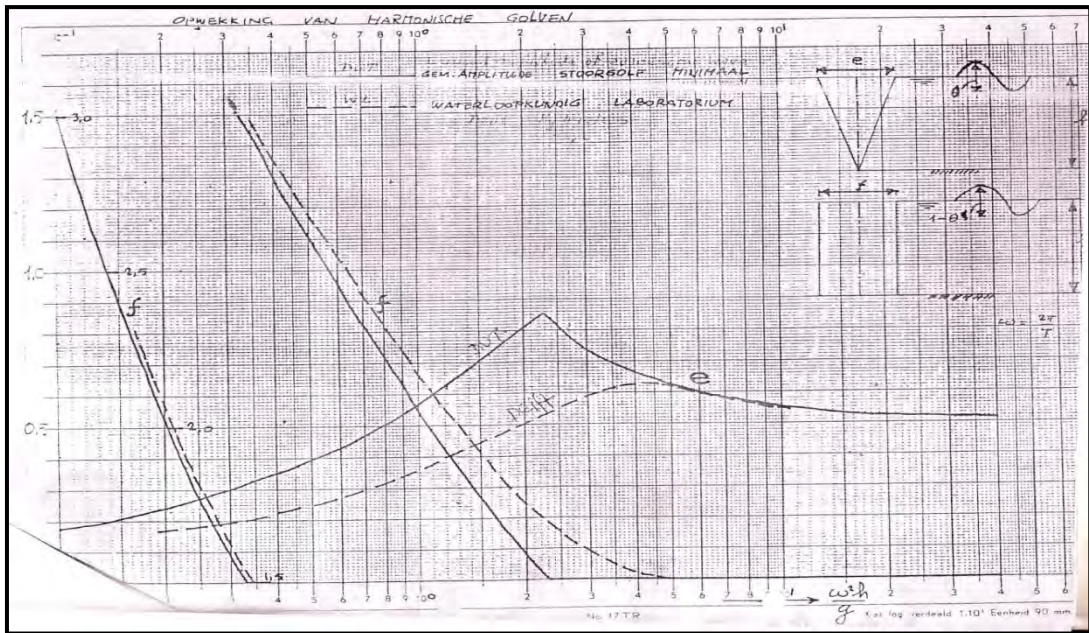


Figure 3.7(b): Nomo gram to obtain the value of  $e$  and  $f$

Table 3.2: Test scenarios

Run No.	Wave properties			Breakwater properties			Still Water Depth, $h$ (cm)
	Wave period, $T$ (sec)	Wave Length $L$ (cm)	Incident Wave Height, $H_i$ (cm)	Porosity (n)	Breakwater Width, $B$ (cm)	Break water Height $h_s$ (cm)	
1	1.6	307	14	0.4	100	40	50
2	1.7	332	14.5				
3	1.8	357	16				
4	2.0	406	17				
5	1.6	307	12.5	0.5			
6	1.7	332	13				
7	1.8	357	13.75				
8	2.0	406	14.5				
9	1.6	307	9.5	0.6			
10	1.7	332	11.5				
11	1.8	357	13				
12	2.0	406	14				

### 3.4 Data Acquisition

To understand the interaction between the wave and the fixed submerged breakwater, data of water surface elevation has been collected at six locations as shown in Figure 3.6. Data of water surface has been collected manually by providing a vertical scale on the flume side made of glass (Figure 3.8(a))

At each position data of water surface have been collected for one minute duration at five seconds interval. To draw the water surface profile at any particular time, it is necessary to start the collection of data at each position simultaneously. This is done by starting the data acquisition at every position when the incident wave reaches the trough. Also the breaking position of wave in each run is measured.

Still photographs and video recordings are taken during each run. Some photographs taken during the experimental runs are given in Figure 3.8(b) to Figure 3.8(f). These are categorized as three different types as the incident waves approaching the breakwater;



*Figure 3.8 (a): Data collection of water surface elevation*



the breaking of waves over the middle of the breakwater, at the onshore end of the breakwater and just behind the breakwater; and the transmitted wave after passing the breakwater.



*Figure 3.8 (b): Wave approaching the breakwater*



*Figure 3.8 (c): Wave breaking over the breakwater*



*Figure 3.8 (d): Wave breaking near the onshore end of the breakwater*



*Figure 3.8 (e): Wave breaking just behind the breakwater*



*Figure 3.8 (f): Transmitted wave after passing the breakwater*

### **3.5 Experimental Results**

When a structure is installed in a marine environment, the presence of that structure will alter the flow pattern in its immediate neighborhoods, resulting in one or more of the phenomena such as formation of lee-wake vortices behind the structure, generation of turbulence, occurrence of reflection and diffraction of waves or occurrence of wave breaking. These phenomena results in dissipating the wave energy, in addition to the dissipation caused by the breakwater itself. The measured data in the laboratory under this study are analyzed and presented in the section below.

#### **3.5.1 Water surface profile**

Figure 3.9 shows the variation of water surface with time (t). The high energy of incident wave is reduced because of installing submerged porous breakwater, which is greater for lower porous structure ( $n=0.4$ ). This is evident in all figures from 3.9(i) to 3.9(xii) as the incident wave height reduces after passing the breakwater.

Among the three different porosities, wave height reduction is greater for  $n=0.4$  than the other two porosities (0.5 and 0.6) at the same wave period. From figure 3.9(i) to 3.9(iii) it is observed that for the interaction of the wave period  $T=1.6$  sec with less porous breakwater of ( $n=0.4$ ) the incident wave height of 9.5 cm reduces to 5 cm at the onshore side of the structure. For  $n=0.5$ , the incident wave height of 12.5 cm is reduced to 7 cm and for  $n=0.6$  porosity 14 cm of incident wave height is reduced to 9 cm. Thus for  $T=1.6$  sec breakwater having  $n=0.4$  reduces 47.4% incident wave height, whereas breakwater having  $n=0.5$  and 0.6 reduce incident wave height up to 44% and 35.71% respectively.

For  $T=1.7$  sec (Figure 3.9(iv) to 3.9(vi)), breakwater having porosity  $n=0.6$  reduces 34.5% incident wave height, whereas  $n=0.5$  porosity of the submerged breakwater reduces wave height up to 34.6 % and maximum wave height reduction of 39.1% is caused by breakwater having  $n=0.4$  porosity for the same wave period.

For  $T=1.8$  sec (Figure 3.9(vii) to 3.9(ix)), maximum reduction wave height is up to 38.5 % which is caused by breakwater of  $n=0.4$  porosity. For the same wave period  $n=0.5$  porous breakwater decreases incident wave height to 34.5%, whereas  $n=0.6$  porous breakwater

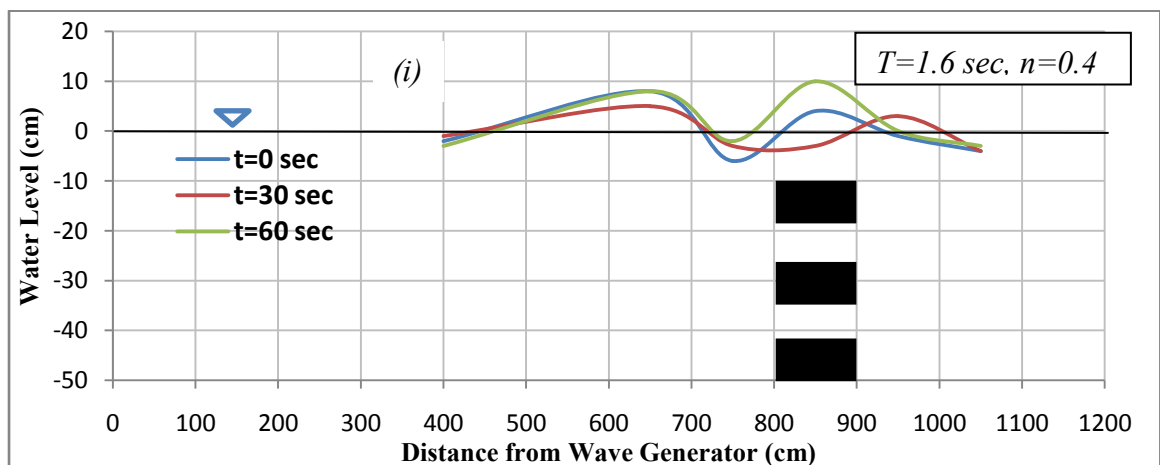
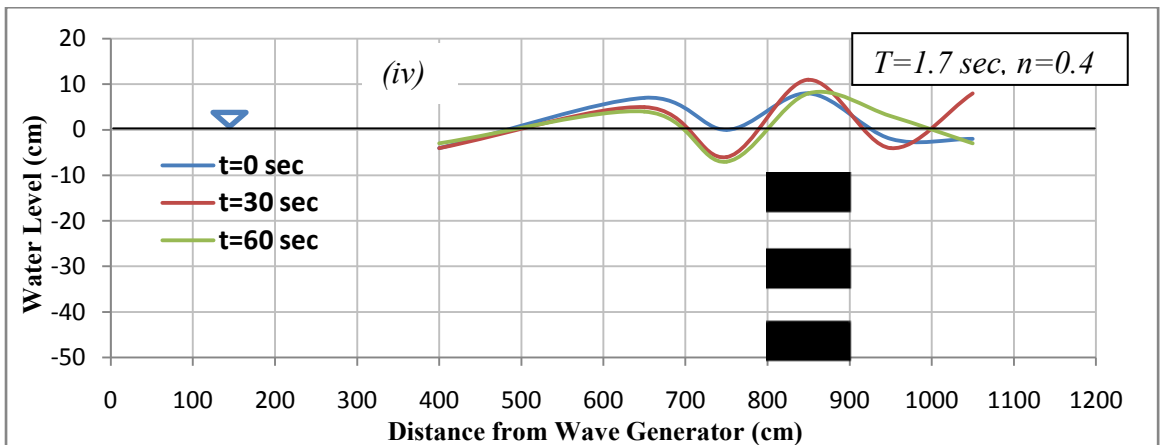
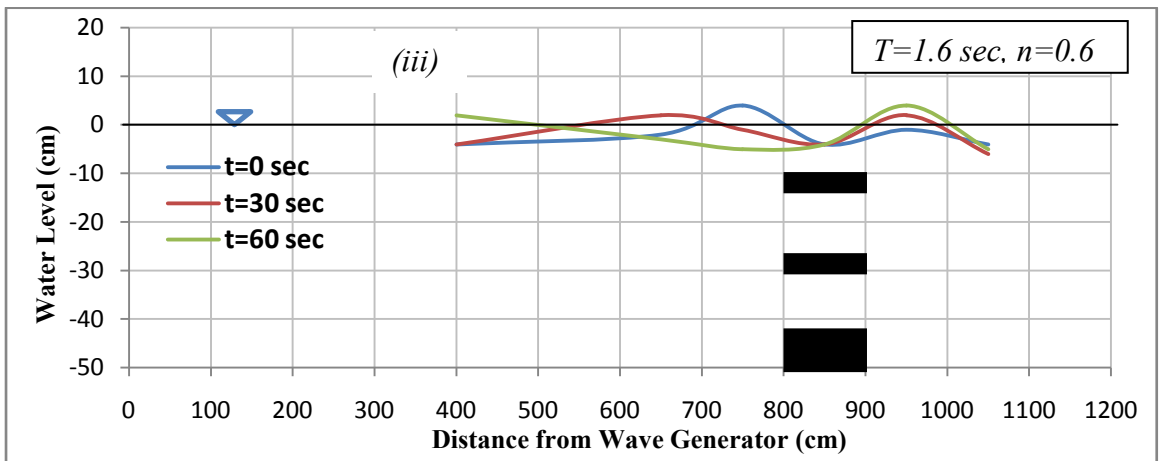
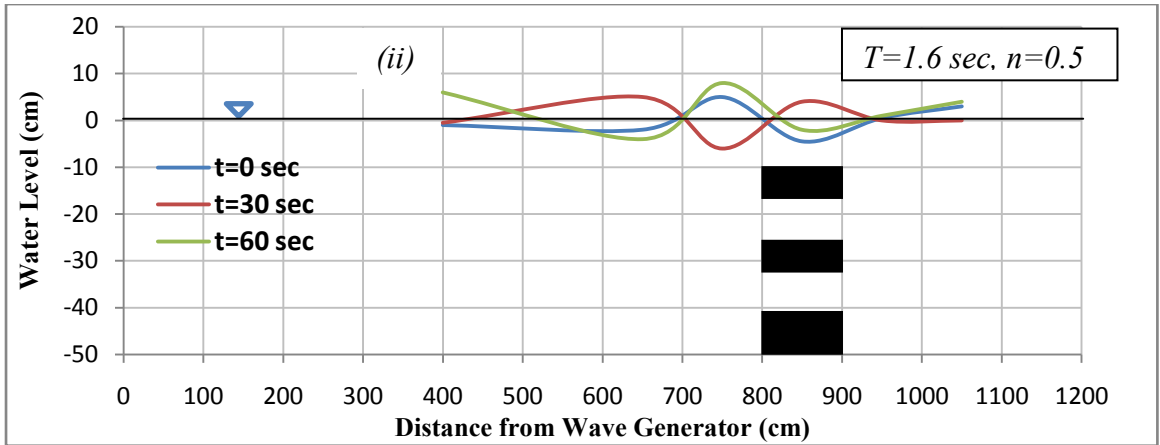
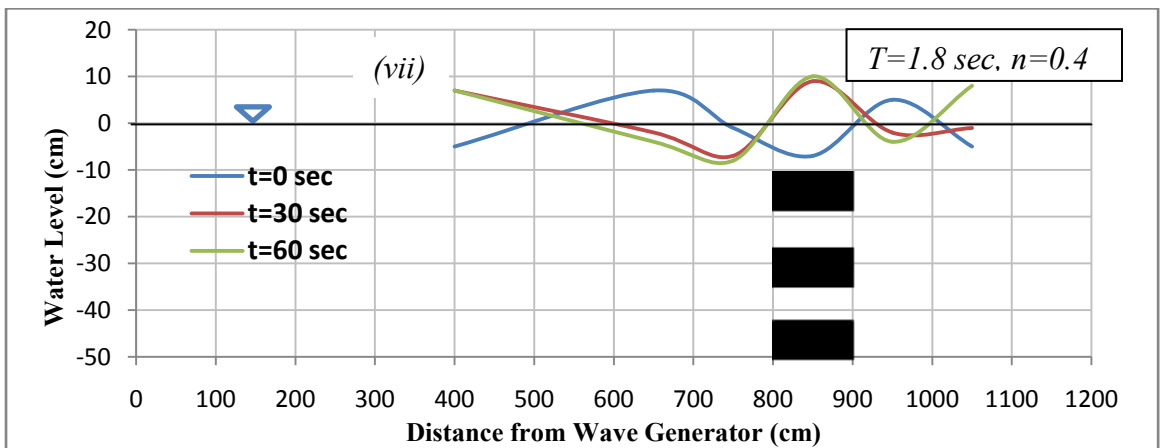
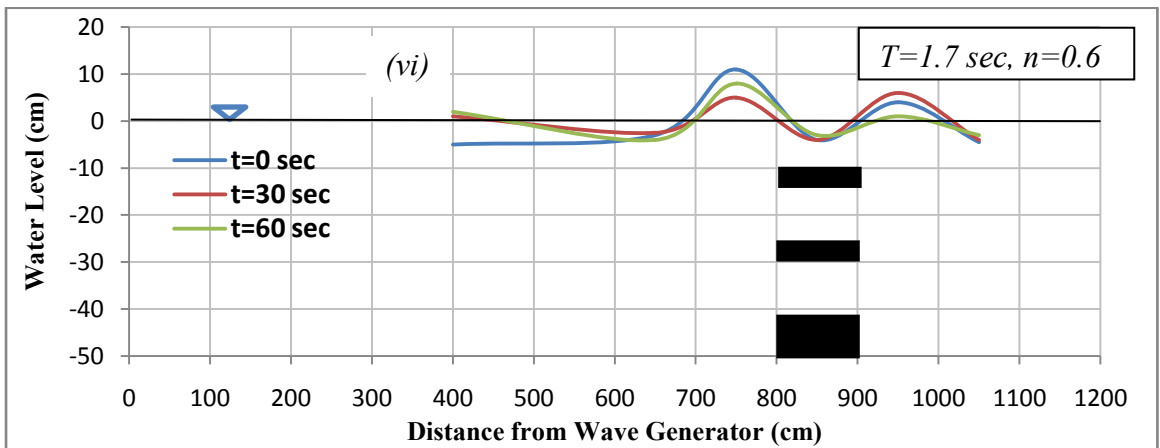
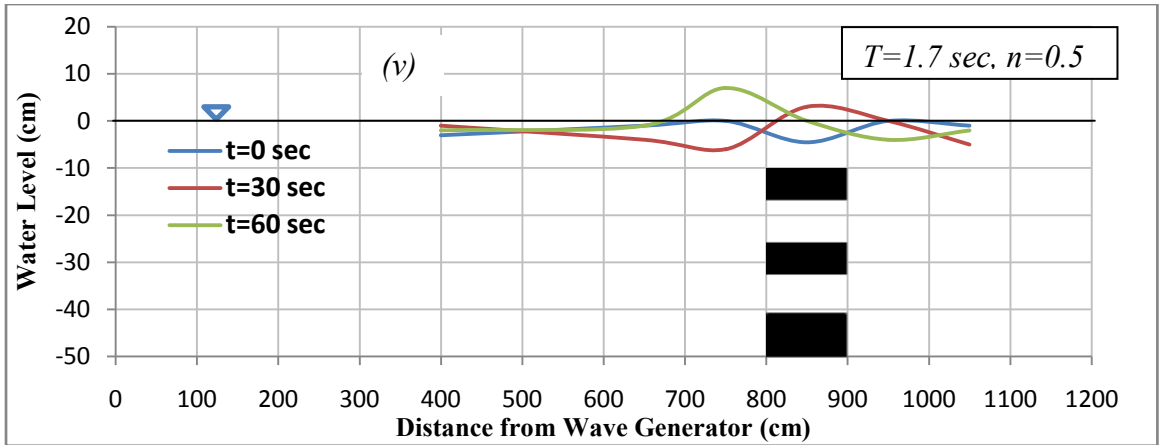


Figure 3.9: Water surface profile for different wave periods and porosities

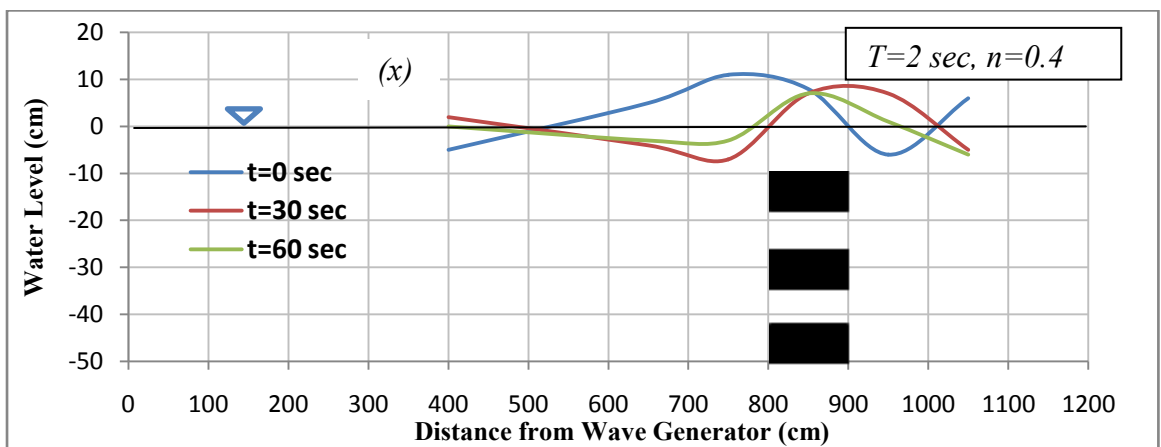
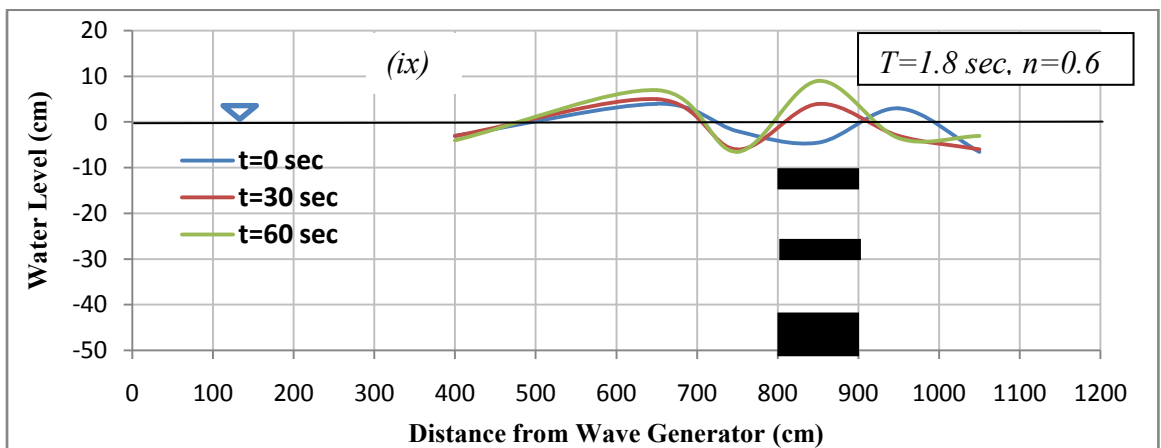
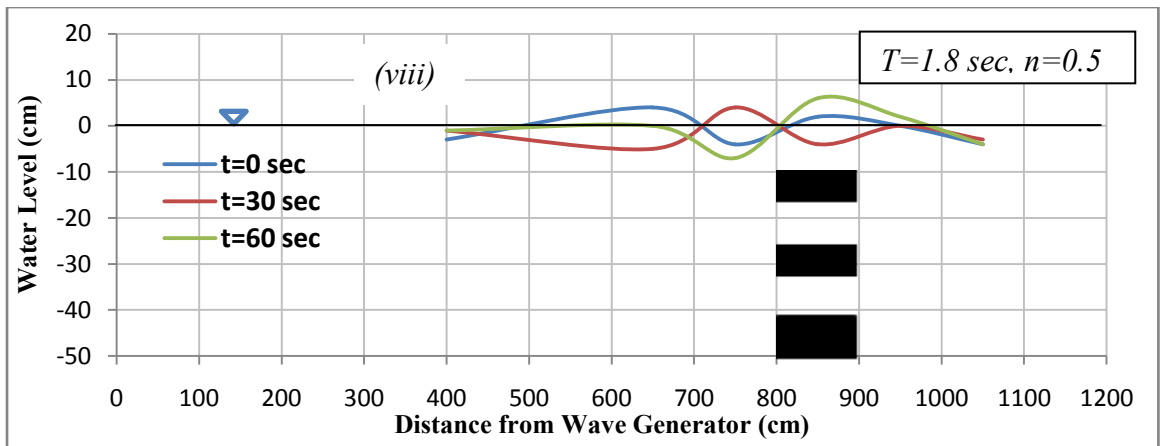




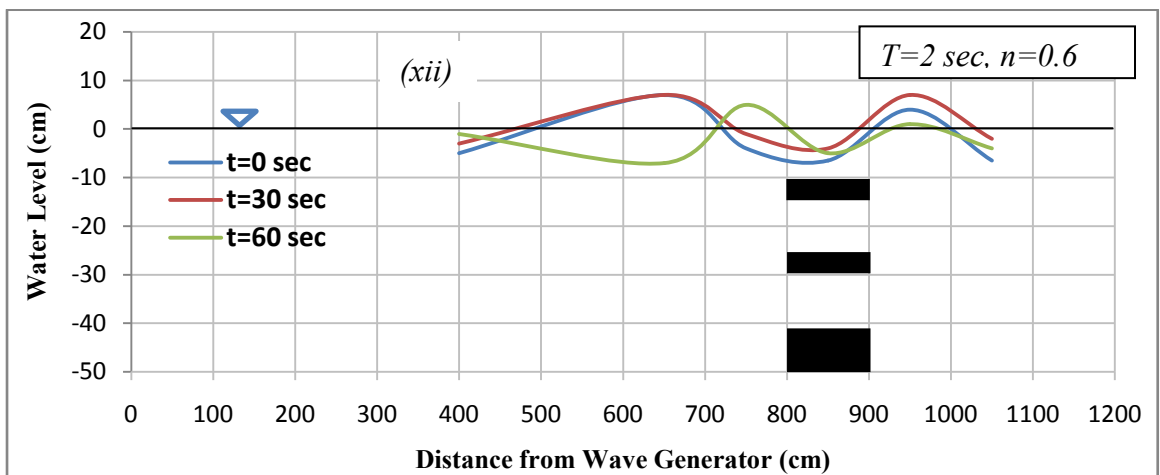
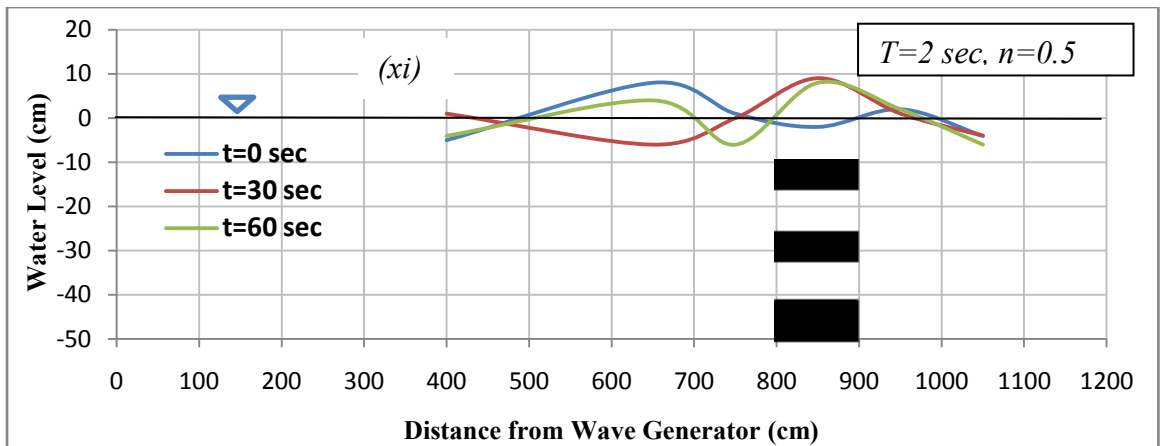
Contd... Figure 3.9: Water surface profile for different wave periods and porosities



Contd... Figure 3.9: Water surface profile for different wave periods and porosities



Contd... Figure 3.9: Water surface profile for different wave periods and porosities



Contd... Figure 3.9: Water surface profile for different wave periods and porosities

reduces 31.25% of incident wave height. Thus for  $T=1.8$  sec  $n=0.4$  porous breakwater is the most effective in reducing wave height among the breakwaters of three different porosities in 50 cm deep water.

For  $T=2$  sec (Figure 3.9(vii) to 3.9(ix)), again the breakwater having  $n=0.4$  causes maximum reduction of incident wave height as 35.7%, whereas  $n=0.5$  porous breakwater can reduce 24.1% and  $n=0.6$  porous breakwater causes 17.64% reduction of incident wave height when installed in a still water depth of 50 cm.

So it is evident from Figure 3.9 that for any wave period among 1.6 sec, 1.7 sec, 1.8 sec and 2 sec maximum reduction of incident wave height is caused by wave breaking over or behind less porous breakwater ( $n=0.4$ ) in a still water depth of 50 cm which is

47.4%. At the same depth of water for the same wave period, breakwater having porosities  $n=0.5$  and  $n=0.6$  can reduce incident wave height up to 44% and 35.71%.

### 3.5.2 Variation of $\eta/H_i$ with $t/T$

Variation of water surface ( $\eta$ ) of transmitted wave (measured at location WG6 behind the breakwater) with time ( $t$ ) is shown in the non-dimensional form as variation of  $\eta/H_i$  with  $t/T$  in Figure 3.10. In Figure 3.10(i), for wave period  $T=1.6$  sec, the incident wave height  $H_i=9.5$  cm is reduced after breaking due to breakwater installation. When the breakwater porosity is  $n=0.4$ , the incident wave height is 47.4% reduced. For installation of breakwater of  $n=0.5$  porosity, the wave height is reduced to 44% of the incident wave height. When the breakwater porosity is  $n=0.6$ , 35.71% wave height is reduced due to wave breaking. For the same wave period, previous studies done by Rahman and Womera (2013) in the same wave flume in case of solid breakwater ( $n=0$ ) of 40 cm height, wave height reduces up to 59% which is shown in the Figure 3.10.

In Figure 3.10(ii), for wave period of 1.7 sec, the maximum reduction of incident wave height is 39.1% for breakwater having  $n=0.4$ . For  $n=0.5$  porosity of the breakwater, the reduction of incident wave height is 34.6% and for  $n=0.6$ , it is up to 34.5%. In case of solid breakwater the incident wave height reduces to 60% (Rahman and Womera, 2013).

In Figure 3.10(iii), for  $T=1.8$  sec, porous breakwater of  $n=0.4$ , reduces incident wave height up to 38.5%, whereas  $n=0.5$  porosity of the breakwater reduces wave height up to 34.5% and breakwater having  $n=0.6$  causes 31.25% reduction of incident wave height. Whereas in case of solid breakwater, for the same wave period of 1.8 sec and 40 cm height the wave height reduction is up to 58% (Rahman and Womera, 2013).

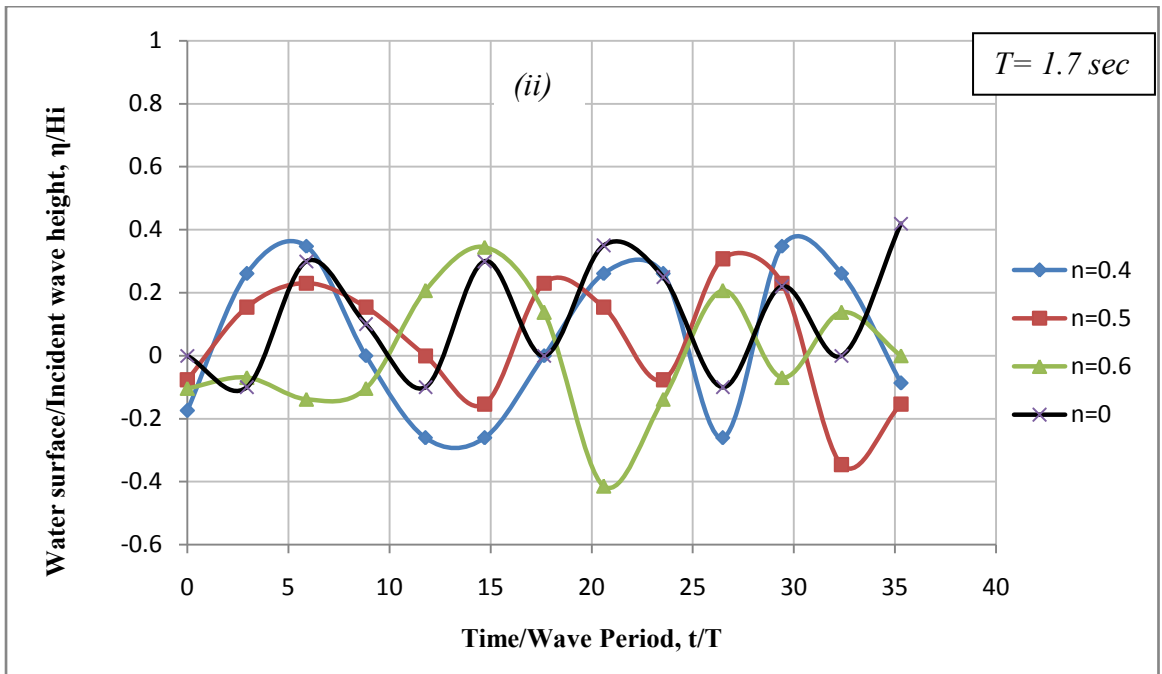
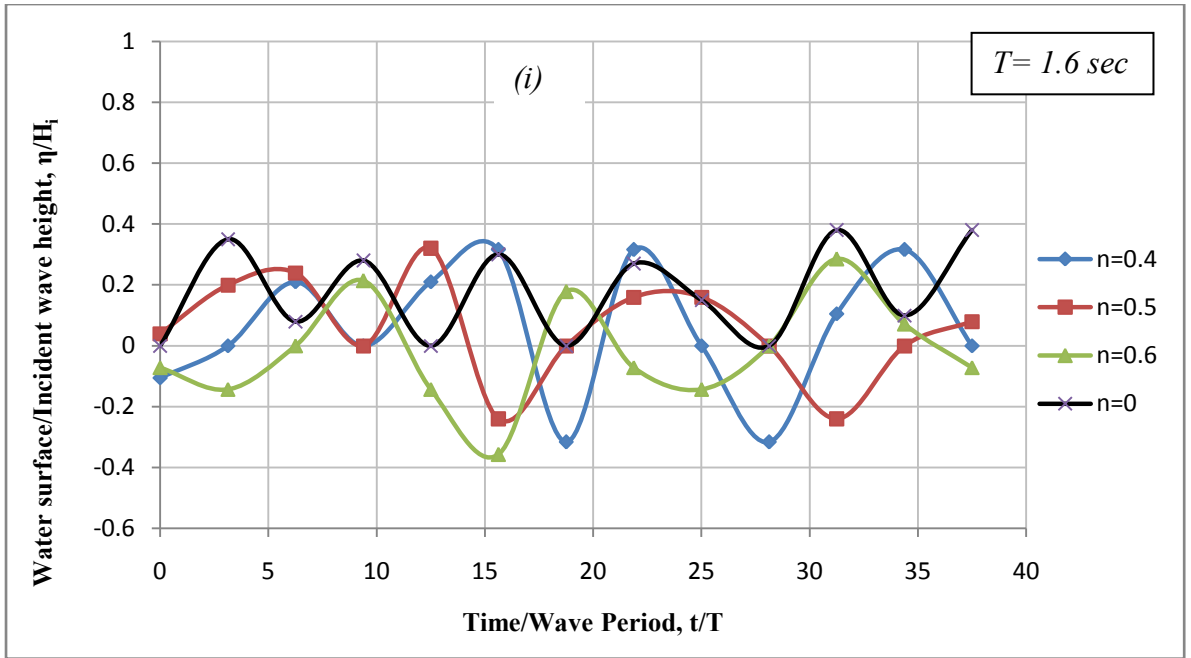
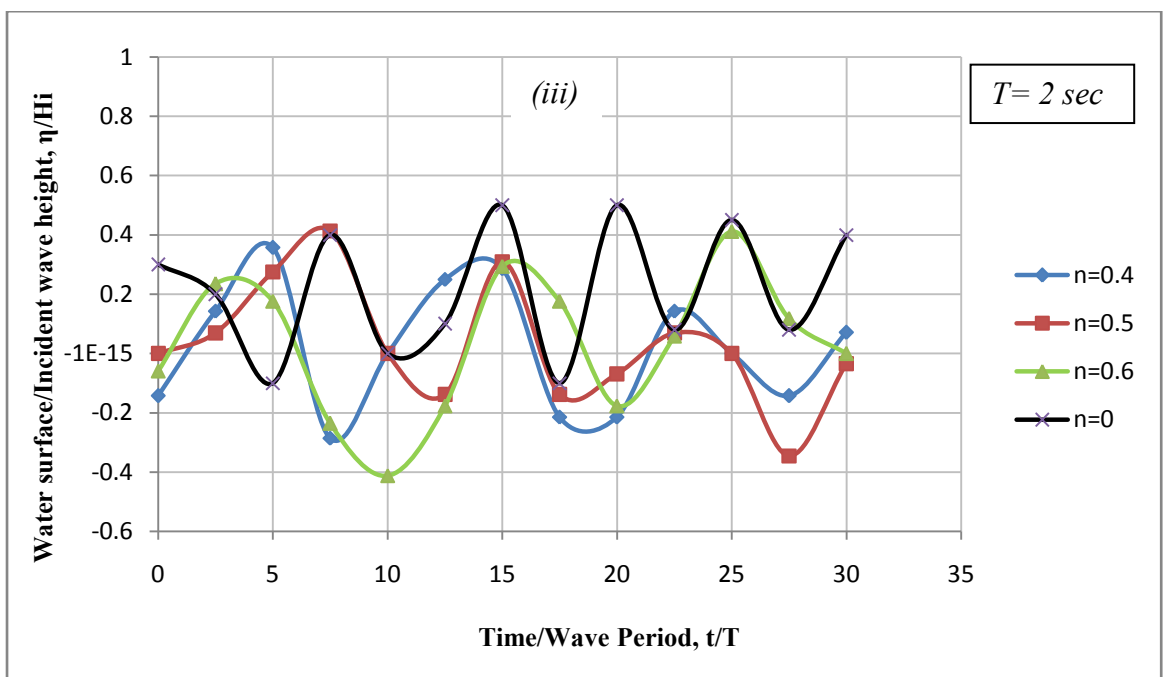
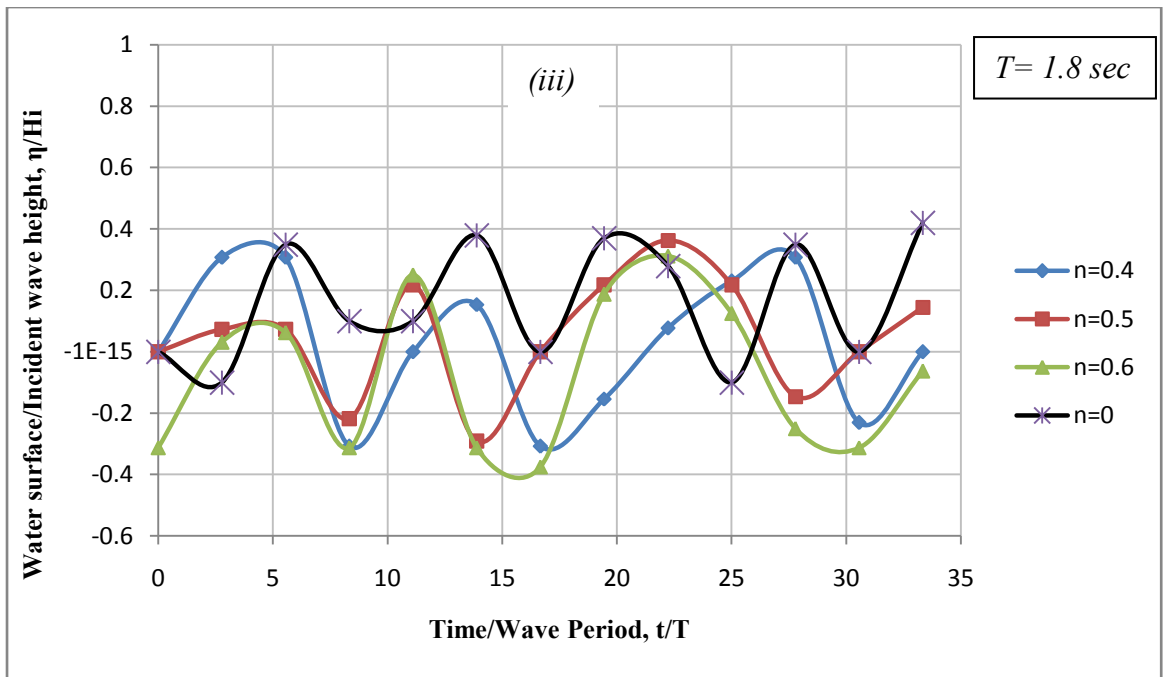


Figure 3.10: Variation of  $\eta/H_i$  with  $t/T$  for different wave periods



Contd... Figure 3.10: Variation of  $\eta/H_i$  with  $t/T$  for different wave periods

Again in Figure 3.10(iv) it is seen that for wave period of 2 sec, reduction of incident wave height because of breaking by  $n=0.4$  porosity of the breakwater is 35.7%, by porous breakwater of  $n=0.5$ , it is 24.1% and by porous breakwater of  $n=0.6$ , reduction of incident wave height occurs up to 17.64%. Now in case of solid breakwater the

wave height reduction is up to 55% of the incident wave height (Rahman and Womera, 2013).

So this is clear from the analysis that, due to the porosity waves transmit through the structure. But in case of solid structure most of the waves are reflected and some are transmitted. So the wave height reduction is greater in solid structure rather than porous structure.

### 3.5.3 Variation of $\eta/H_i$ with $x/L$

Figure 3.11(i) to Figure 3.11 (xii) show the variation of water surface/ incident wave height ( $\eta/H_i$ ) with respect to distance from breakwater/ wave length ( $x/L$ ). These represent the non-dimensional water surface profiles for installing breakwater of three different porosities of  $n=0.4$ , 0.5 and 0.6 in a still water depth of 50 cm at four different wave periods of 1.6sec, 1.7sec, 1.8sec and 2.0 sec respectively.

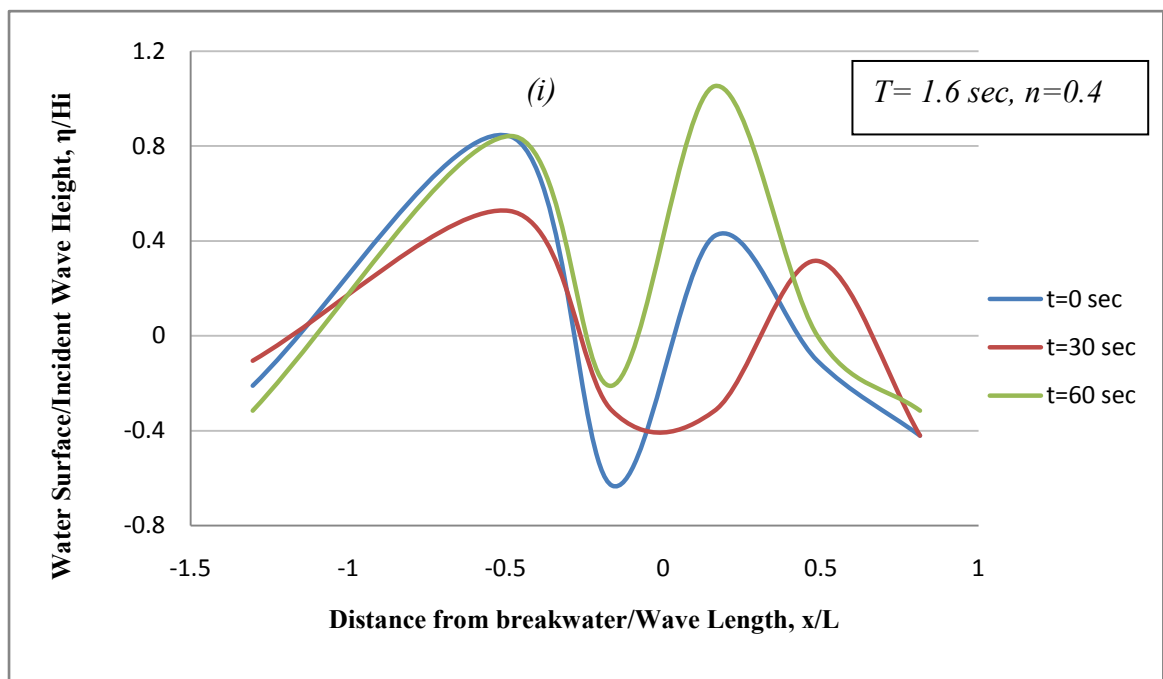
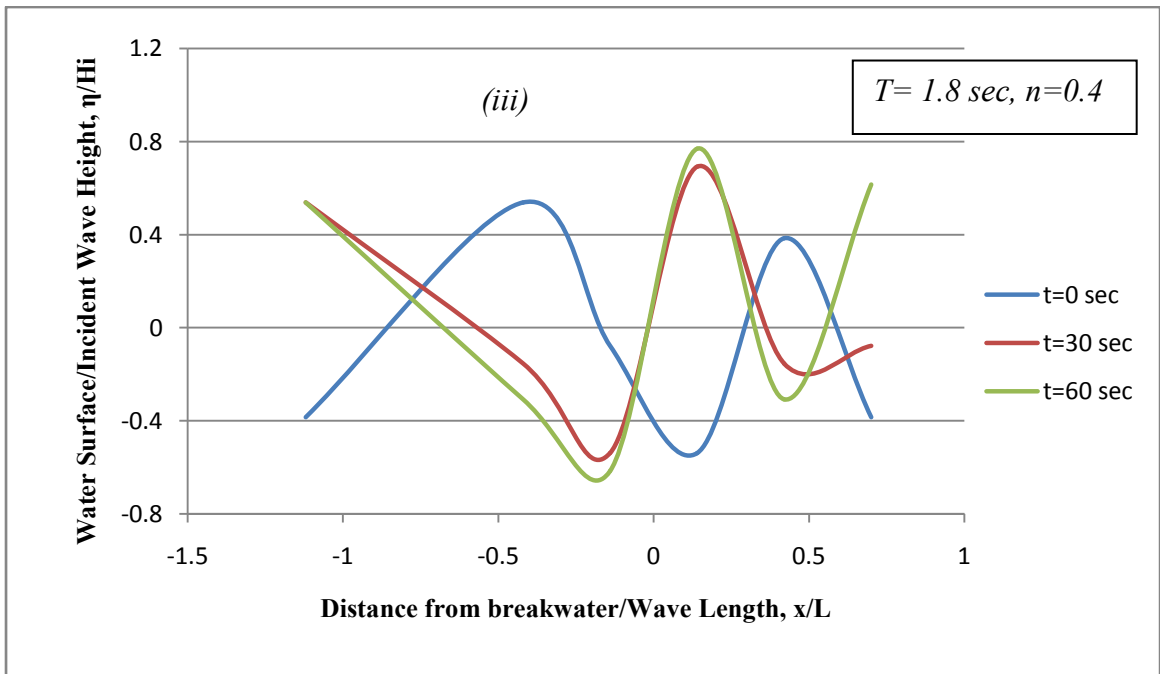
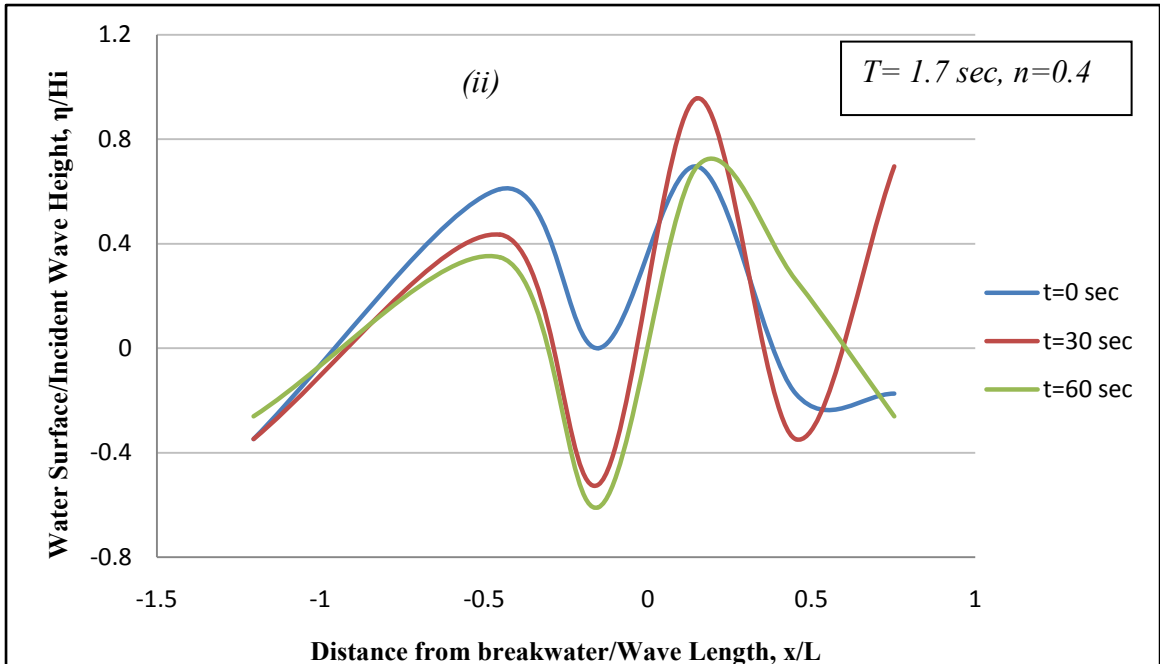
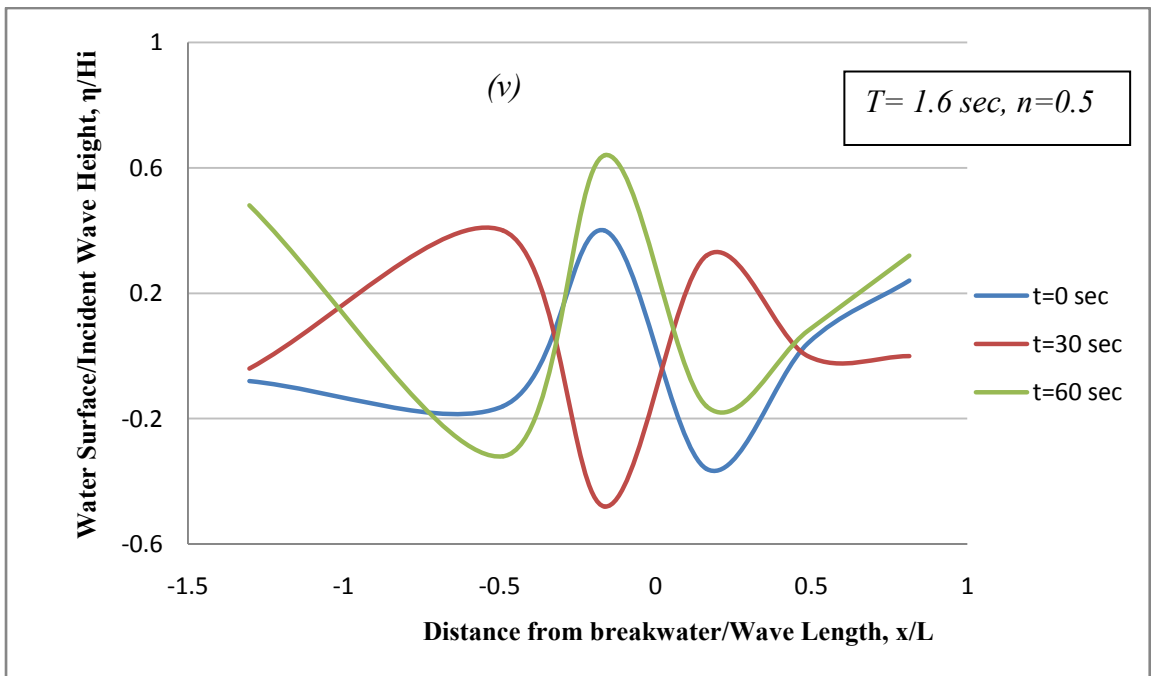
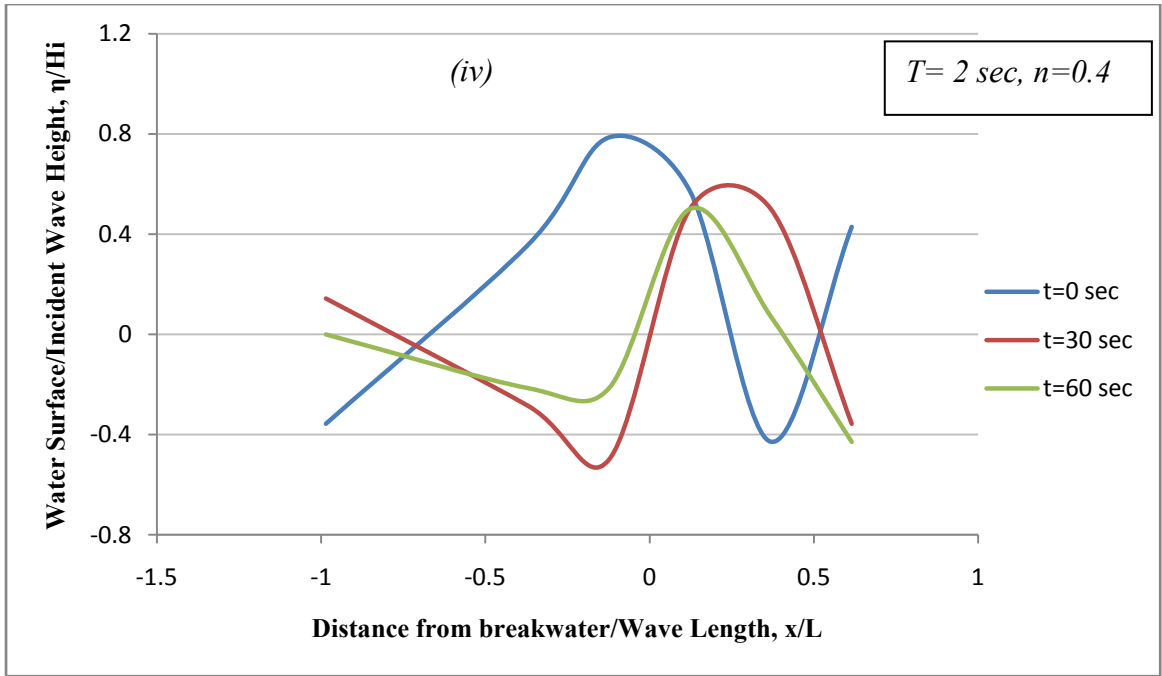


Figure 3.11: Variation of  $\eta/H_i$  with  $x/L$  for different wave periods and porosities

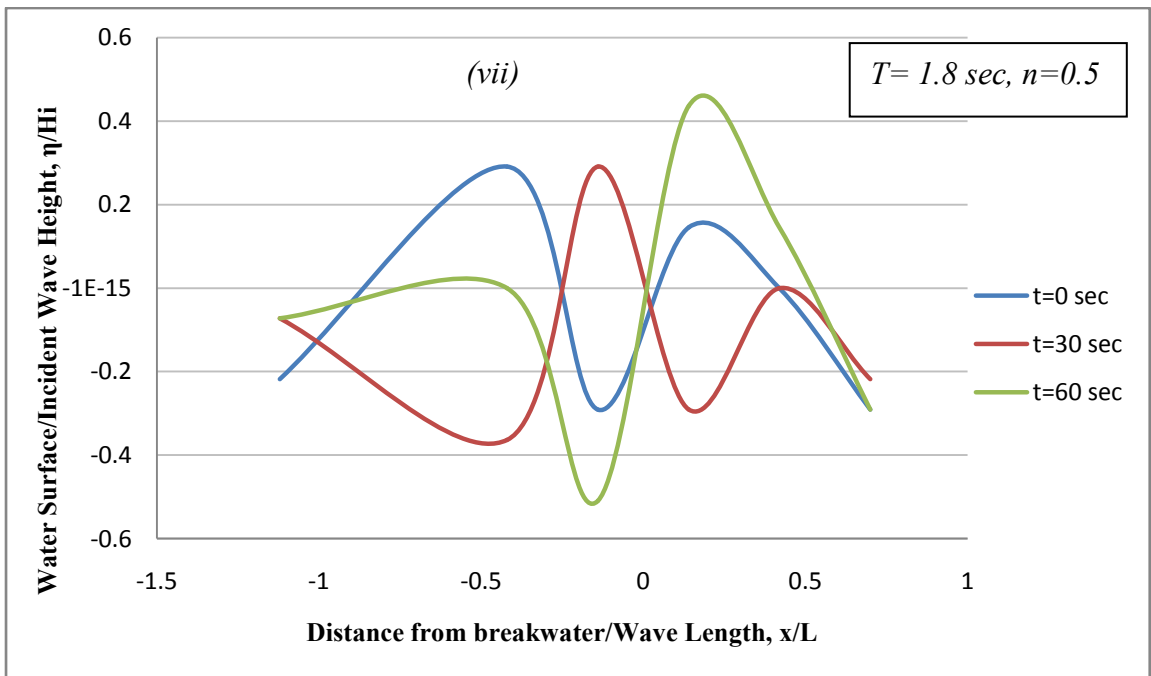
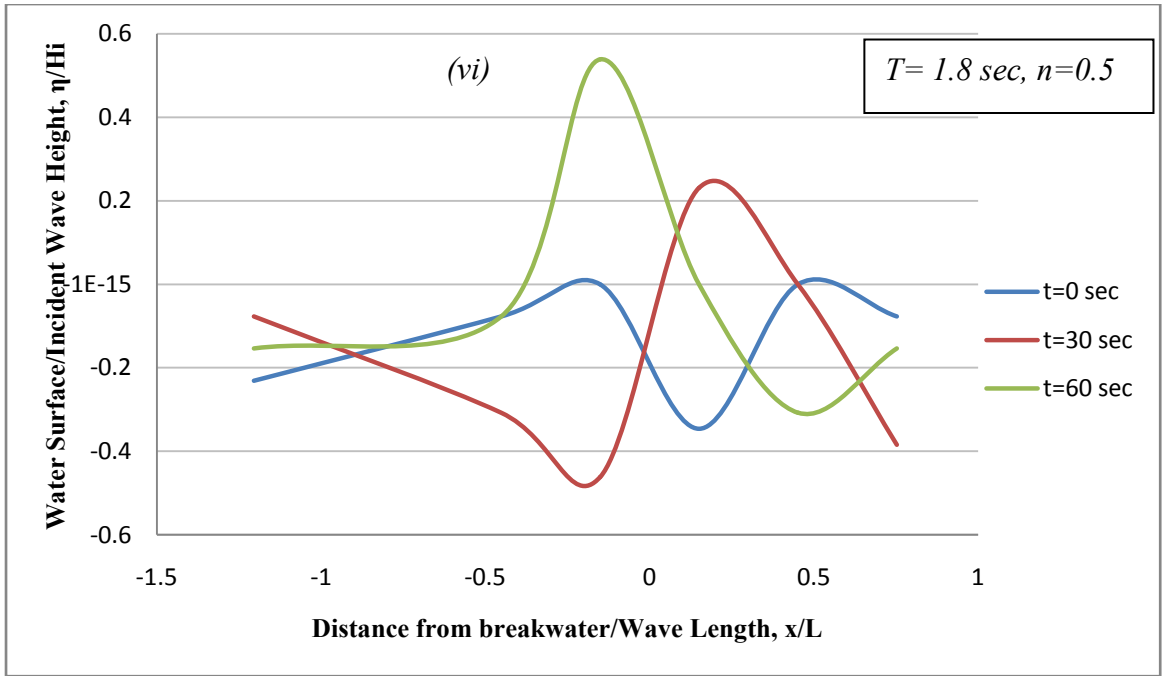




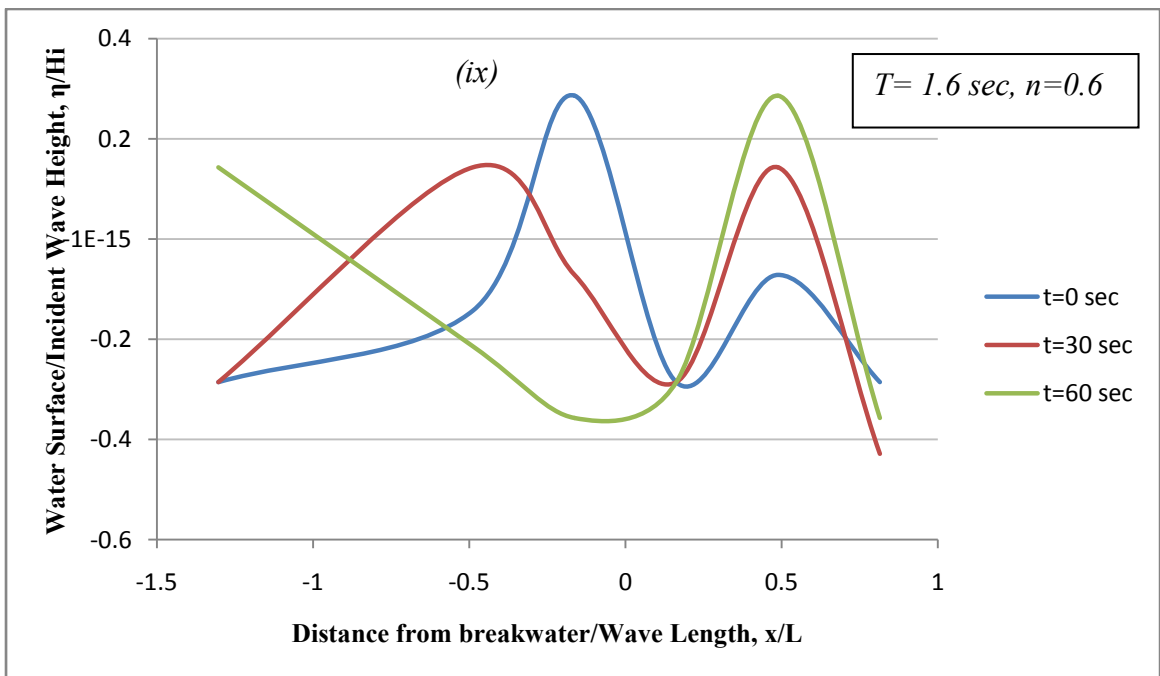
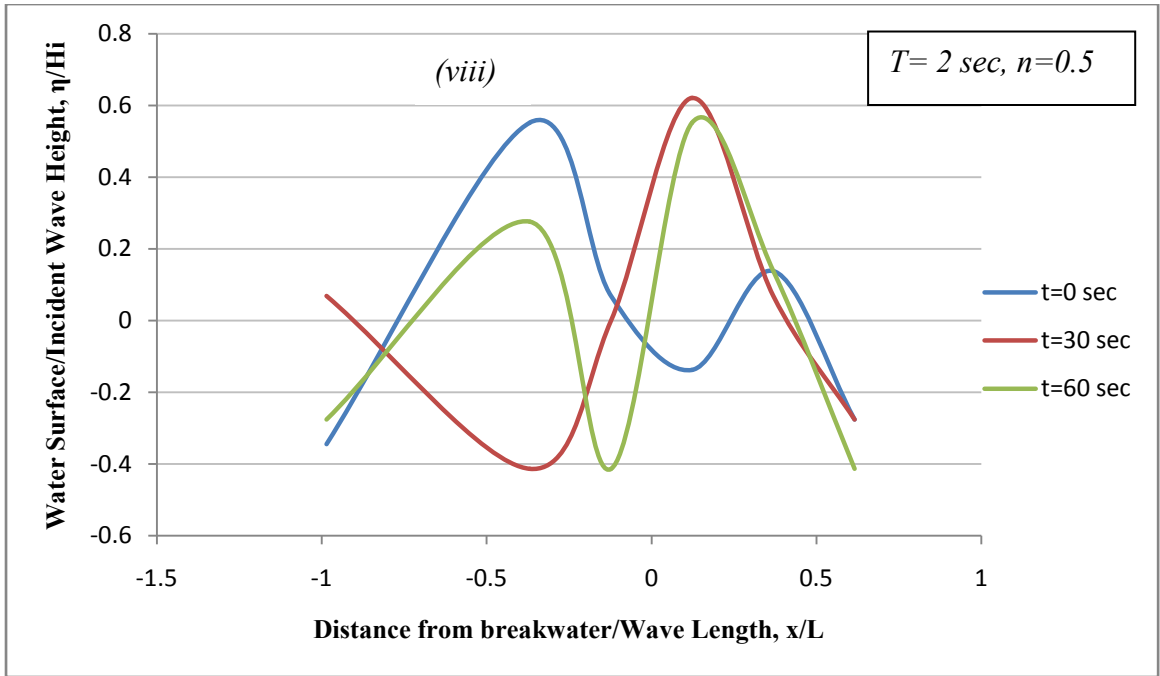
Contd... Figure 3.11: Variation of  $\eta/H_i$  with  $x/L$  for different wave periods and porosities



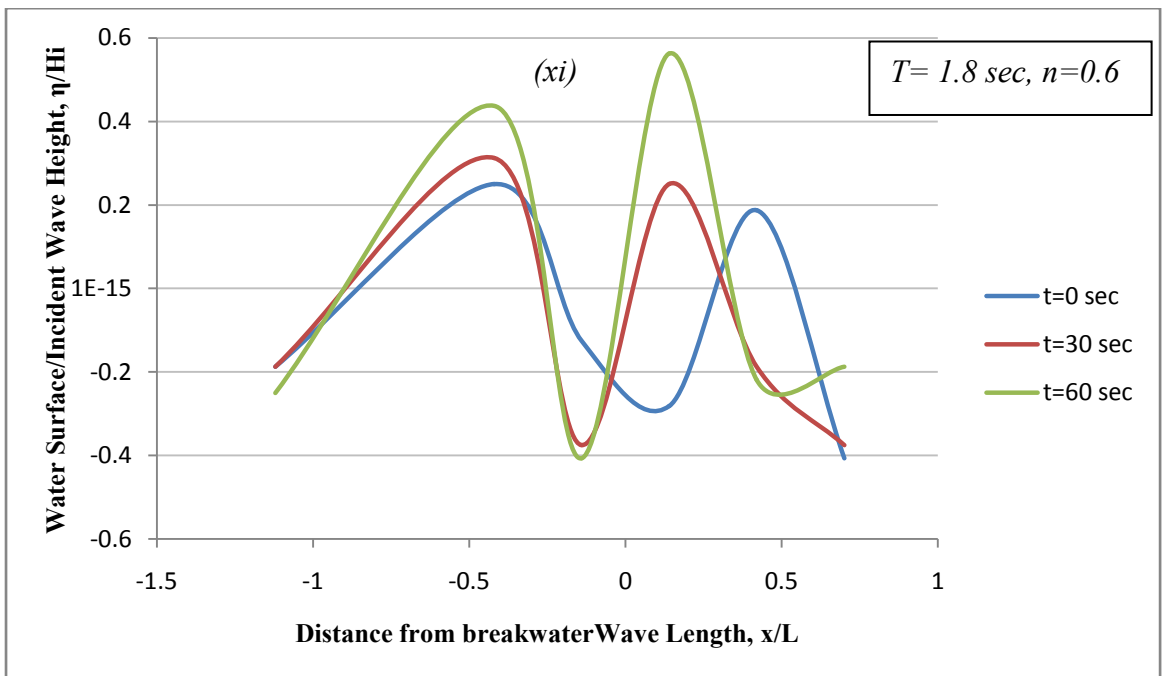
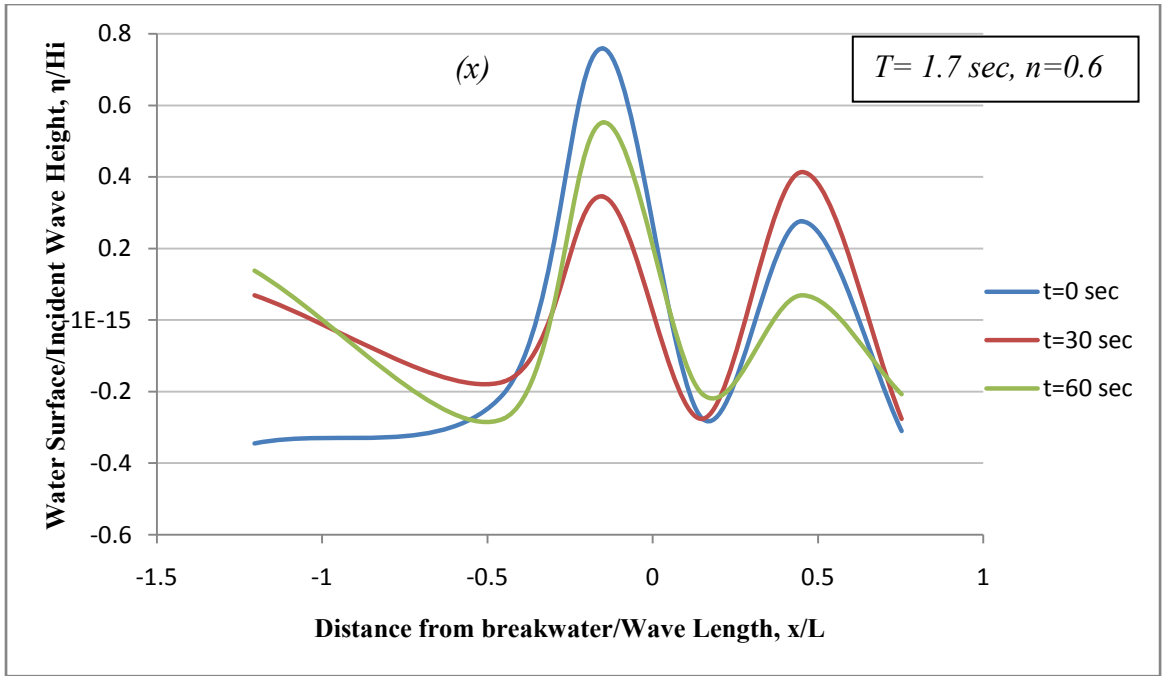
Contd... Figure 3.11: Variation of  $\eta/H_i$  with  $x/L$  for different wave periods and porosities



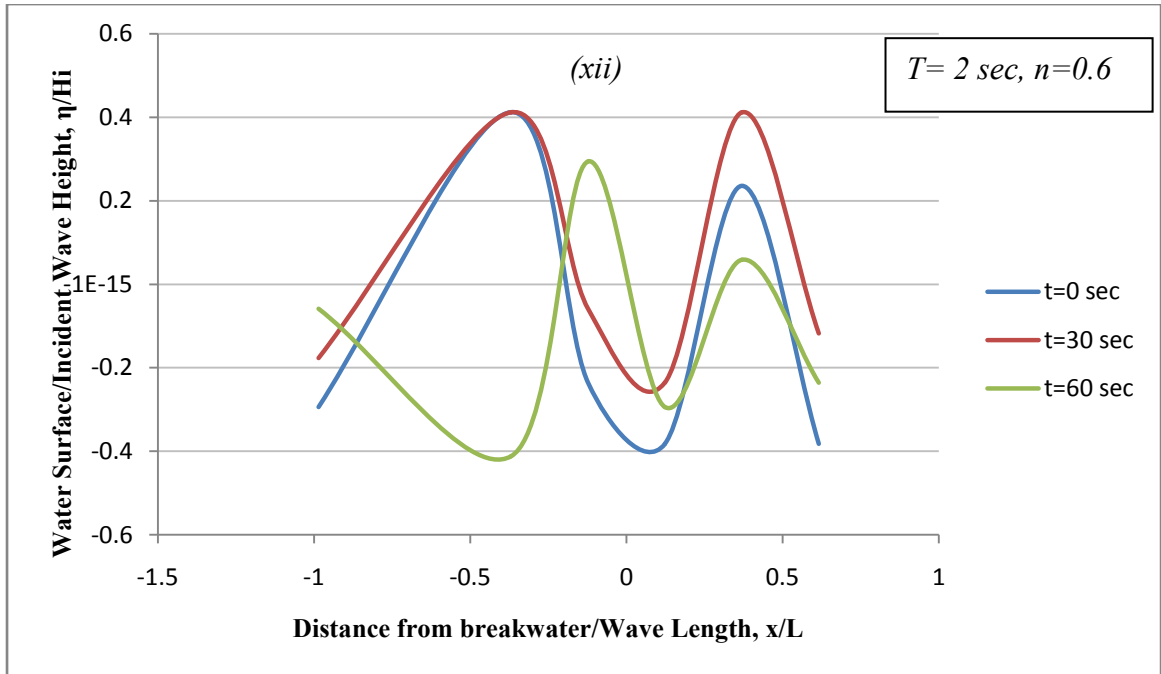
Contd... Figure 3.11: Variation of  $\eta/H_i$  with  $x/L$  for different wave periods and porosities



Contd... Figure 3.11: Variation of  $\eta/H_i$  with  $x/L$  for different wave periods and porosities



Contd... Figure 3.11: Variation of  $\eta/H_i$  with  $x/L$  for different wave periods and porosities



Contd... Figure 3.11: Variation of  $\eta/H_i$  with  $x/L$  for different wave periods and porosities

### 3.5.4 Determination of hydrodynamic co-efficient

In design of porous breakwaters, the usual practice of assessing their functional efficiency is by the measure of wave reflection, transmission, and wave energy loss coefficient. In practical designs, these coefficients are obtained either by conducting physical model tests or by using appropriate theoretical, empirical or numerical models.

The maximum and the minimum wave heights ( $H_{\max}$ . and  $H_{\min}$ .) at the wave generator side, upstream the breakwater, and the transmitted wave heights ( $H_t$ ) at the wave absorber side, downstream the breakwater, were measured to estimate the reflection and the transmission coefficients ( $K_r$  and  $K_t$ ) as follows:

$$H_t = (H_{\max} + H_{\min}) / 2$$

$$H_r = (H_{\max} - H_{\min}) / 2$$

where,

$H_{\max}$  = maximum wave height, measured at antinode

$H_{\min}$  = minimum wave height, measured at nodes.

Then;

$$K_r = H_r / H_i$$

$$K_t = H_t / H_i$$

Where,

$H_i$  = Incident wave height

$H_r$  = Reflected wave height

$H_t$  = Transmitted wave height

Based on energy conservation, the energy-loss coefficient,  $K_L$  can be calculated from the following relation (Thornton and Calhoun 1972):

$$K_r^2 + K_t^2 + K_L^2 = 1$$

So the wave energy loss,  $E_L$  (or  $K_L$  as used herein) can be determined from:

$$E_L = K_L = (1 - K_r^2 - K_t^2)^{1/2}$$

The conventional method as used by Dean and Dalrymple (1991) has been adopted to separate the measured wave train into its incident and reflected wave components. For measuring maximum and minimum wave heights, two wave gauges were placed at fixed distances of  $L/4$  and  $L/2$  from the breakwater, where  $L$  is the wave length. At each position (antinode,  $L/4$  and node,  $L/2$ ) data of water surface have been collected for one minute duration at five seconds interval. Then maximum or minimum wave heights ( $H_{max}$  or  $H_{min}$ ) in cm can be calculated by taking difference between the maximum and minimum water surface reading at antinode and node respectively.

Wavelength  $L$  is measured for four different wave periods ( $T=1.6, 1.7, 1.8$  and  $2$  sec) by using the equation

$$L = gT^2 / 2\pi \times \text{coefficient for transitional wave length.}$$

### 3.5.5 Effect of porosity on the wave reflection coefficient ( $K_r$ )

Figure 3.12 presents the relationship between the wave reflection coefficient ( $K_r$ ) and the relative breakwater width ( $k.B=2B\pi/L$ ), for  $n= 0.4, 0.5$  and  $0.6$ , where  $k$  is the wave number ( $2\pi/L$ ),  $B$  is the breakwater width and  $L$  is the wave length.

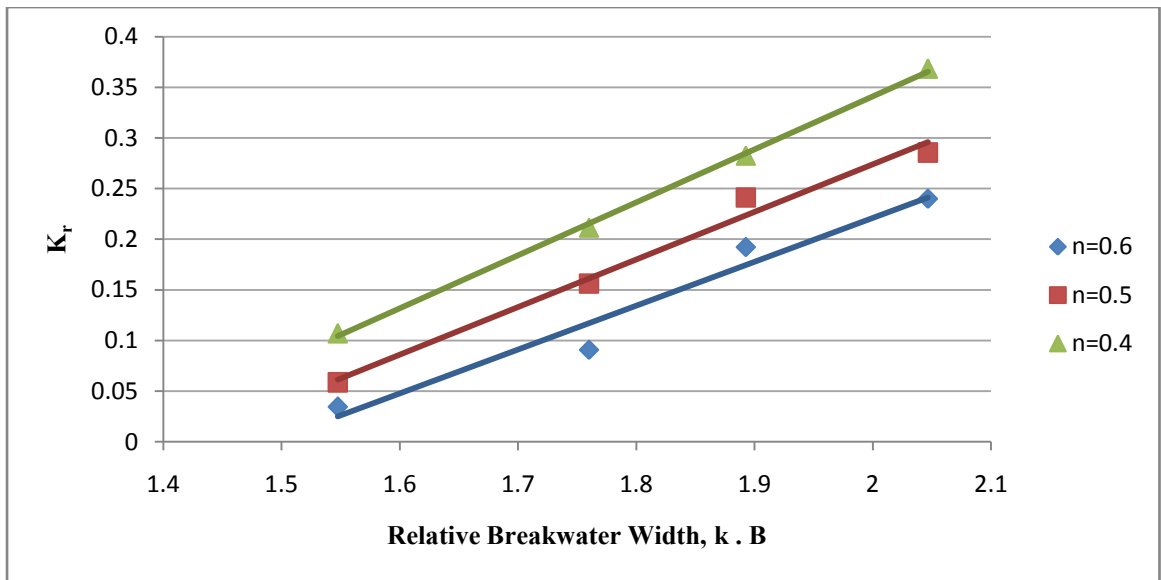


*Figure 3.12: Effect of breakwater porosity on the reflection coefficient*

The figure shows that,  $K_r$  increases as relative breakwater width  $k.B$  increases. This may be attributed to the increase of the wave energy loss as the width of the porous media increases. Also, the reflection coefficient ( $K_r$ ) decreases as porosity increases.

Reflection coefficient ( $K_r$ ) decreased from 0.368 to 0.107 as  $k.B$  increases from 1.55 to 2.05 when structure porosity was  $n=0.4$ , decreased from 0.286 to 0.059 when structure porosity was  $n=0.5$ , and decreased from 0.24 to 0.034 when structure porosity was  $n=0.6$ , which are shown in Figure 3.12.

So it is evident from the figure that, when  $n=0.6$  porosity of the breakwater was used, the reflection coefficient shows very low value, as most of the wave energy passes through the breakwater.

### **3.5.6 Effect of Porosity on the wave transmission coefficient ( $K_t$ )**

Figure 3.13 presents the relationship between the transmission coefficient ( $K_t$ ) and the relative breakwater width  $k.B$ . The figure shows that, the transmission coefficient ( $K_t$ ) decreases as  $k.B$  increases. This means that, the wide breakwater reduces the transmitted waves more as compared to narrow breakwater.



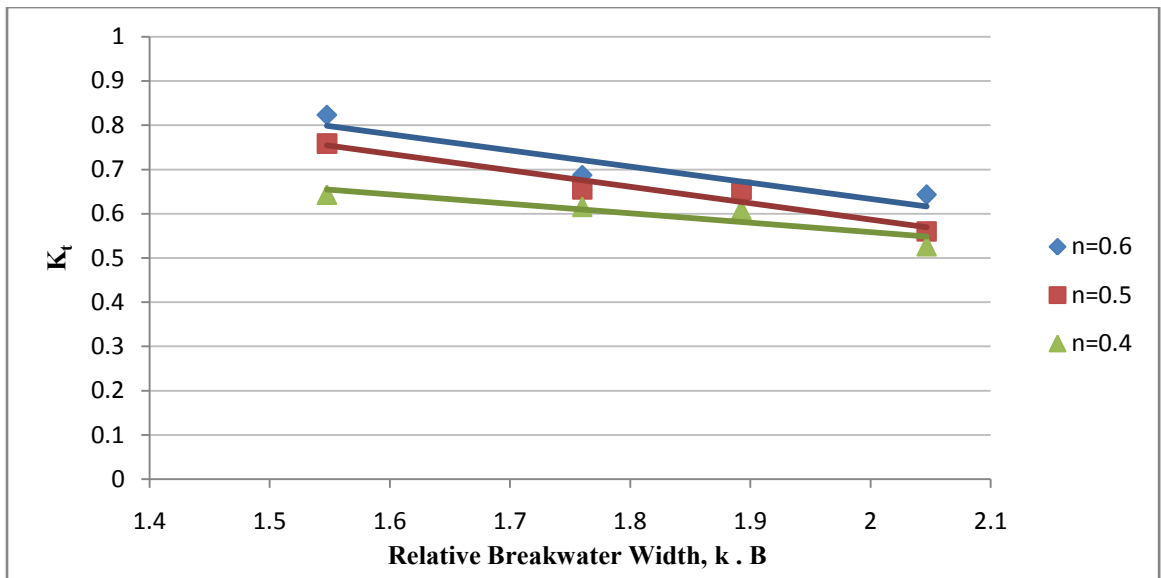


*Figure 3.13: Effect of breakwater porosity on the transmission coefficient*

The above mentioned behavior could be attributed to two reasons. First, the increase of the breakwater width causes the increase of the friction between the breakwater surface and the transmitted waves, causing more loss of wave energy. Second, as the wave becomes short, the water particle velocity and acceleration face changes and the turbulence caused due to these changes cause dissipation in the wave energy.

In Figure 3.13, when porosity is  $n=0.4$ , the transmission coefficient ( $K_t$ ) decreased from 0.64 to 0.53 for  $k.B$  increasing from 1.55 to 2.05. When porosity increased to  $n=0.5$ , transmission coefficient ( $K_t$ ) decreased from 0.76 to 0.56, and when the porosity is  $n=0.6$ ,  $K_t$  decreased from 0.82 to 0.64 with increasing  $k.B$  from 1.55 to 2.05.

### **3.5.7 Effect of Porosity on the wave energy loss coefficient ( $K_L$ )**

Figure 3.14 presents the relationship between the wave energy loss coefficient ( $K_L$ ) and the relative breakwater width  $k.B$  for  $n= 0.4, 0.5$  and  $0.6$ . These figures show that,  $K_L$  increases as  $k.B$  increases. Also the wave energy loss coefficient ( $K_L$ ) increases as the porosity decreases.

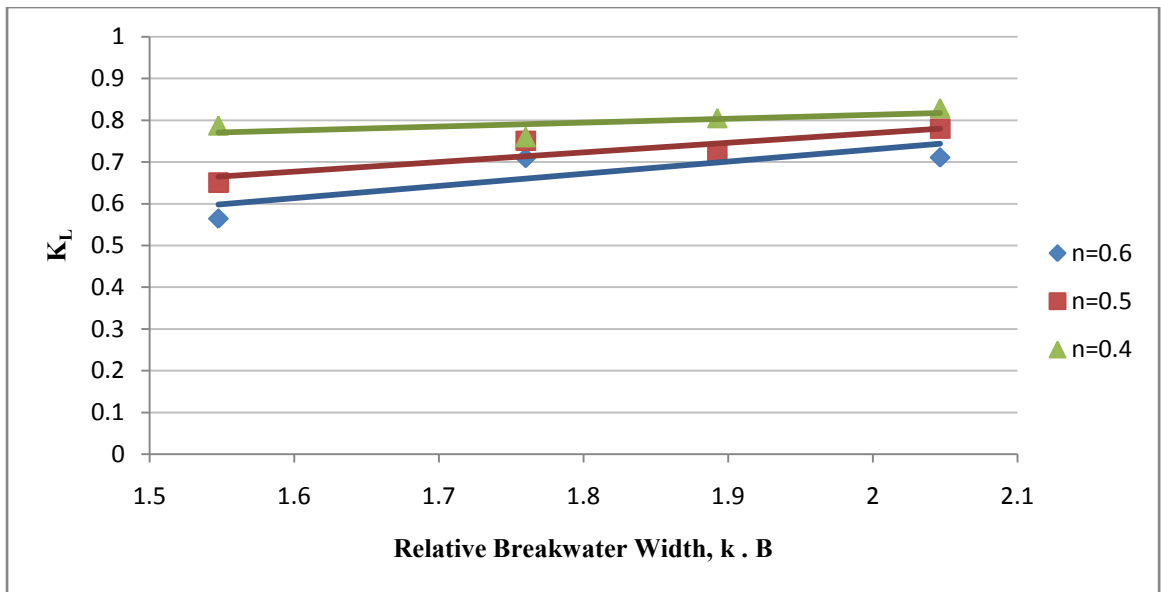


*Figure 3.14: Effect of breakwater porosity on the wave energy loss coefficient*

In Figure 3.14, when porosity is  $n=0.4$ , the wave energy loss coefficient ( $K_L$ ) increased from 0.61 to 0.68 for  $k.B$  increasing from 1.55 to 2.05. For porosity  $n=0.5$ ,  $K_L$  increased from 0.56 to 0.63, and for  $n=0.6$  structure porosity,  $K_L$  increased from 0.47 to 0.55 with increasing  $k.B$  from 1.55 to 2.05.

Hence it can be said from the above results that, wave energy loss coefficient is higher for less porous structure. This is due to the fact that most of the wave energy can be transmitted through the highly porous structure. That's why the wave transmission coefficient is greater for this kind of structure.

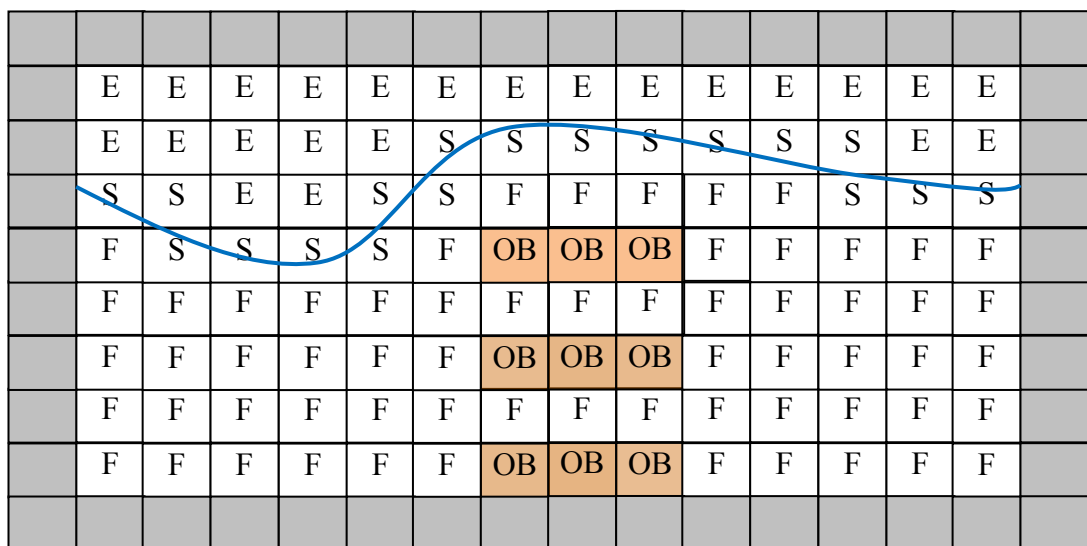
# CHAPTER 4

## NUMERICAL MODELING

### 4.1 General

The numerical analysis of submerged porous structures plays an obvious role in the fields of coastal engineering. This chapter contains the numerical analysis of the wave interaction with the horizontal slotted submerged porous breakwater. Modification of SOLA-VOF model for horizontal slotted breakwater and numerical run conditions are described here. The results of numerical simulation are verified by the experimentally measured values. From the developed two-dimensional numerical model water surface profile, velocity components and magnitude of pressure along the computational domain and the value of F (VOF function) that represents fraction of volume occupied by fluid at any time are obtained. The detail results of numerical analyses are presented here.

### 4.2 Modification of SOLA-VOF for Horizontal Slotted Submerged Breakwater



E = Empty cell, S = Surface cell, F = Fluid cell, OB= Obstacle cell

*Figure 4.1: Free surface geometric model of VOF method for porous breakwater*

In this study, the two-dimensional model of wave interaction with fixed submerged breakwater developed by Rahman and Womera (2013) is updated to adapt it for simulating wave interaction with horizontal slotted submerged porous breakwater. To adapt the model for horizontal slotted submerged breakwater, the boundary condition at the obstacle location is changed. The width of the obstacle is kept fixed and in vertical direction obstacle cells are declared keeping gaps for the fluid cells to flow between the obstacle cells as all the cells in the computational domain were declared as fluid cells earlier which is displayed in Figure 4.1. And in the obstacle faces no slip condition is applied.

### 4.3 Numerical Model Run Conditions

At first, the developed numerical model is run for incident wave period,  $T= 1.6$  sec, incident wave height,  $H_i=12$  cm and  $h=50$  cm without any breakwater in the computational domain. The model simulated water surface profiles are compared with the waves generated from Stokes 3<sup>rd</sup> order wave theory. Then the model is run for different wave periods ranging from 1.6 sec to 2.0 sec for breakwaters of three different porosities as  $n=0.4, 0.5$  and  $0.6$  to simulate water surface profile, velocity profile, VOF function  $F$  and pressure along the computational domain. Table 4.1 shows typical inputs in the numerical model and Table 4.2 shows the incident wave property for different run conditions

*Table 4.1: Typical inputs in the numerical model*

X axis length		800 cm
Z axis length		74 cm
Structure position (from source)		400 cm
Still water depth		50 cm
Structure dimension	Width along wave direction	100 cm
	Length normal to wave direction	76 cm
	Height	40 cm

Table 4.2: Incident wave property for different run conditions

Run No.	Incident Wave Height	Incident Wave Period	Porosity
Run 1	12	1.6	0.4
Run 2	13	1.7	0.4
Run 3	14	1.8	0.4
Run 4	15	2.0	0.4
Run 5	12	1.6	0.5
Run 6	13	1.7	0.5
Run 7	14	1.8	0.5
Run 8	15	2.0	0.5
Run 9	12	1.6	0.6
Run 10	13	1.7	0.6
Run 11	14	1.8	0.6
Run 12	15	2.0	0.6

The typical orientation of the cells in the two-dimensional grid of the numerical model is shown in Figure 4.2.

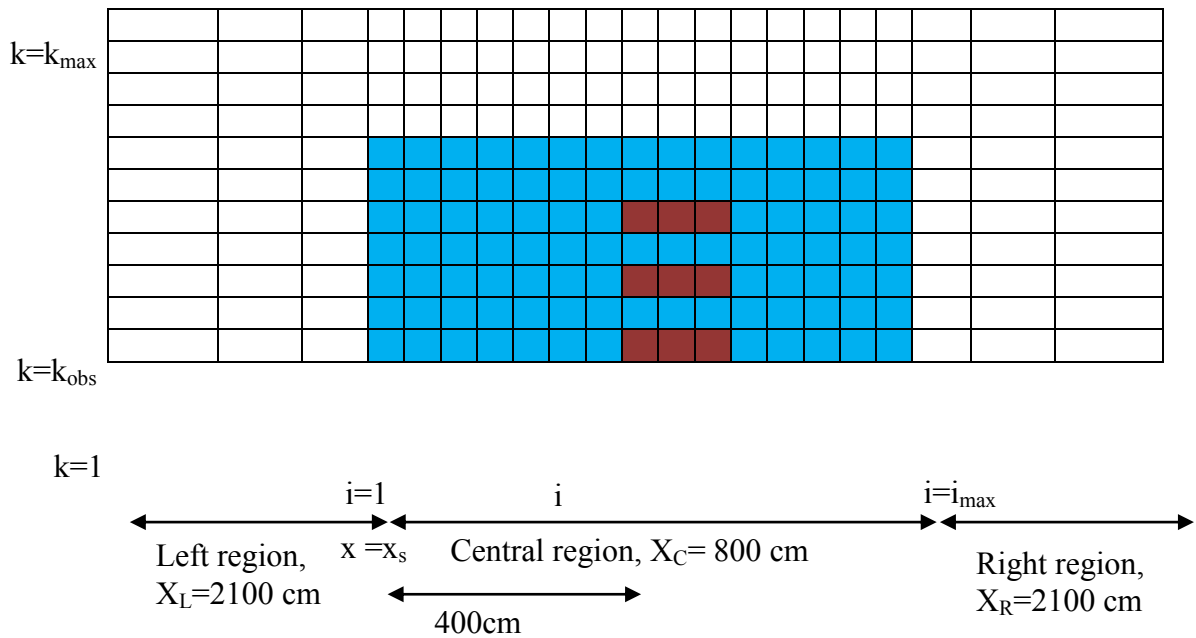


Figure 4.2: Typical orientation of cells set in numerical model

- Left region: Open boundary of added dissipation zone; Changeable Ratio of  $\Delta x = 1.03$ ; Number of Cell,  $\text{IMAXL} = 120$

- Central region: Main computational grid; Fixed cell width  $\Delta x = 2$  cm; Number of Cell,  $IMAXC = 400$ .
- Right region: Open boundary of added dissipation zone; Changeable Ratio of  $\Delta x = 1.03$ ; Number of Cell,  $IMAXR = 120$
- Z axis: Constant cell width,  $\Delta z = 1$  cm. Number of Cell,  $KMAX = 74$

Referring to the Figure 4.2, Table 4.3 shows input boundary conditions of the velocity as below.

*Table 4.3: Input boundary conditions for velocity*

Position	Velocity
Boundary cell faces	$u(1,k) = u(2,k)$ $w(1,k) = w(2,k)$ $u(i_{max}, k) = u(i_{max}-1, k)$ $w(i, k_{max}) = w(i, k_{max}-1)$
Position	Velocity
Obstacle cell faces	$u(i-1, k) = 0 \quad [k = 1, k_{obs}]$ $w(i-1, k) = 0 \quad [k = 1, k_{obs}]$ $u(i', k) = 0 \quad [k = 1, k_{obs}]$ $w(i', k) = 0 \quad [k = 1, k_{obs}]$

#### 4.4 Verification of the Modified Numerical Model

The numerical model is based on SOLA-VOF scheme. The method used for calculating water surface using SOLA-VOF scheme is represented in chapter 2 (article 2.4). Stokes 3<sup>rd</sup> order wave theory uses the following equation for water surface calculation.

$$\eta^{(3)} = -\frac{3}{8}(\alpha^4 - 3\alpha^2 + 3)a^3k^2 \cos \theta + \frac{3}{64}(8\alpha^6 + (\alpha^2 - 1)^2)a^3k^2 \cos 3\theta$$

where,  $a =$  amplitude of wave  $= 0.5 H$ ,

$\theta =$  phase angle

$$\alpha = \coth kh, \quad k = \frac{2\pi}{L}$$

Here,  $h =$  still water depth,  $H =$  wave height and  $L =$  wave length

Wave generated by the developed model show good agreement with the wave generated by Stokes 3<sup>rd</sup> order wave theory which is displayed in Figure 4.3.

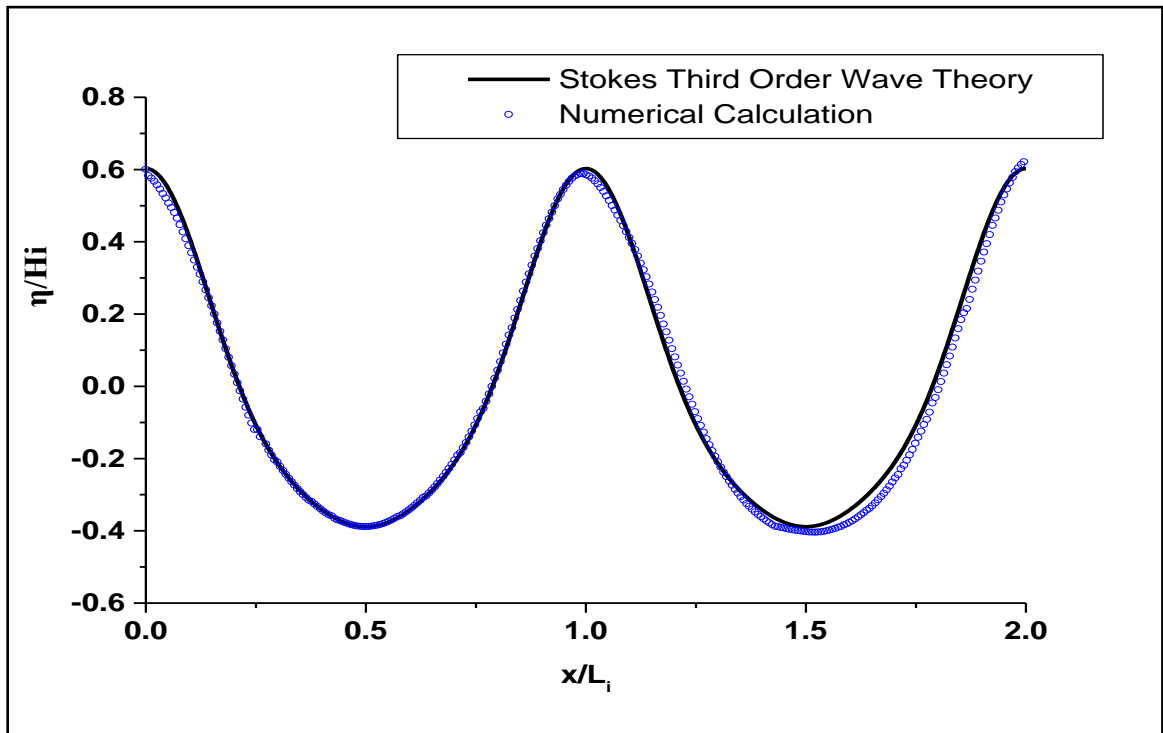


Figure 4.3: Comparison of dimensionless water surface profiles by numerical computation and 3<sup>rd</sup>-order Stokes wave theory ( $H_i=12\text{cm}$ ,  $T=1.6\text{ sec}$ ,  $h=50\text{ cm}$ )

#### 4.5 Comparison between Numerical and Experimental Results

The performance of the developed two-dimensional numerical model has been verified by comparing the model simulated results with experimentally measured data. The model simulated water surface profiles for all 12 laboratory run conditions are compared with the experimentally measured data for the respective run condition and are shown in Figure 4.7. In the figure, the experimentally measured data of water surface profile show good agreement with the water surface profiles generated by the developed numerical model. The data collected from the experimental investigations shows the maximum of  $\pm 20\%$  variations with the numerical results.

Wave breaking positions measured by the laboratory experiments are also presented in this figure. The measured breaking positions in the laboratory experiments show small differences from the locations of breaking indicated by the numerical model

simulation. In the model simulated water surface profiles the breaking position is considered at the point where the waves collapse.

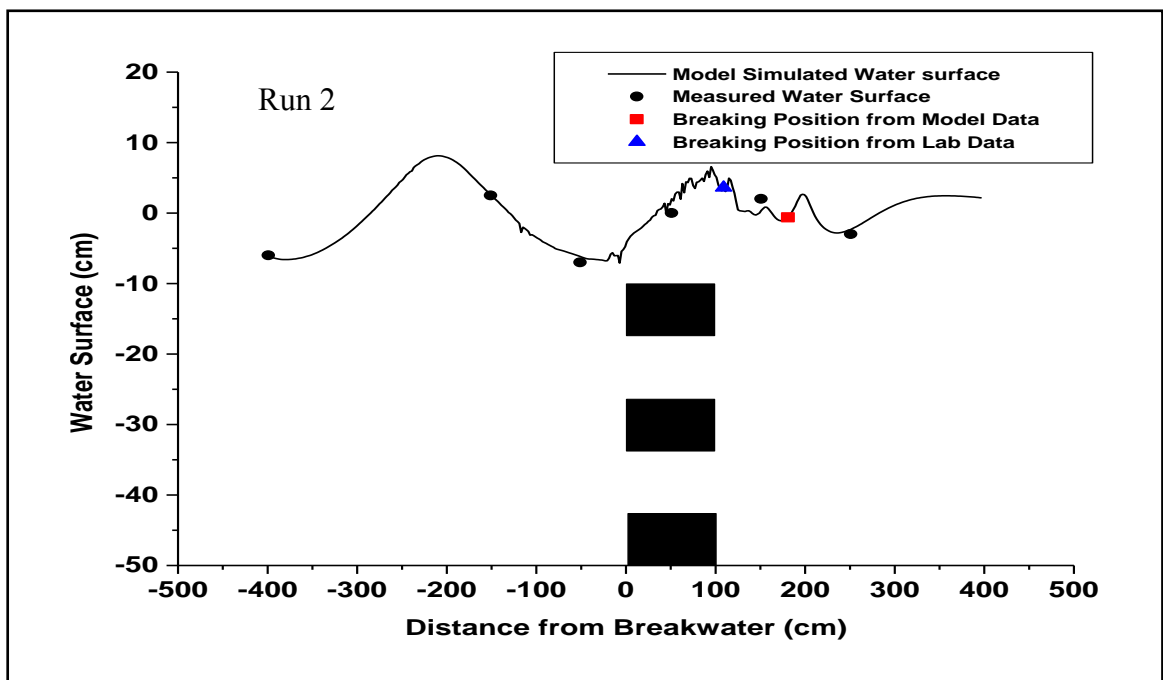
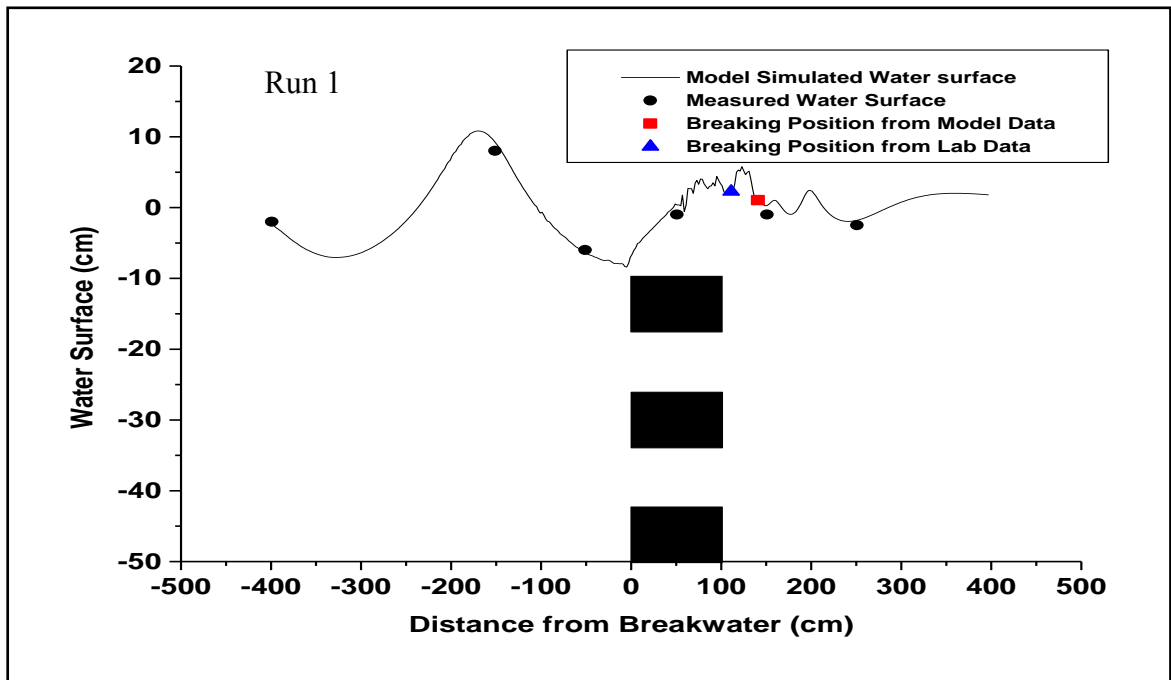
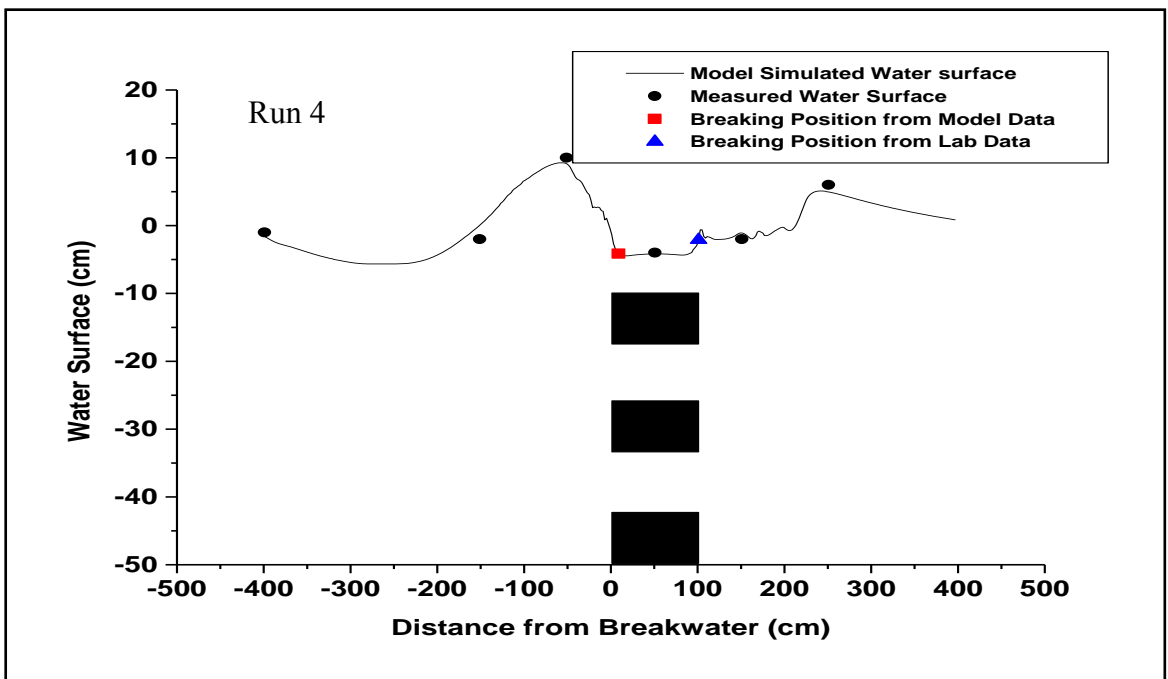
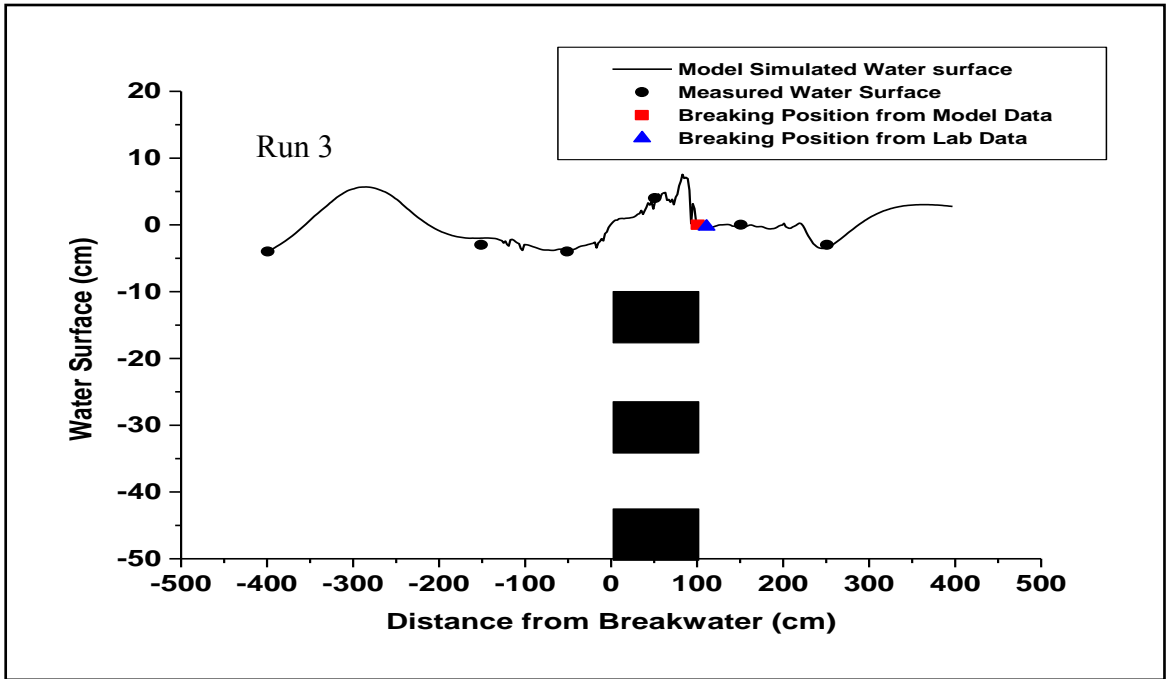
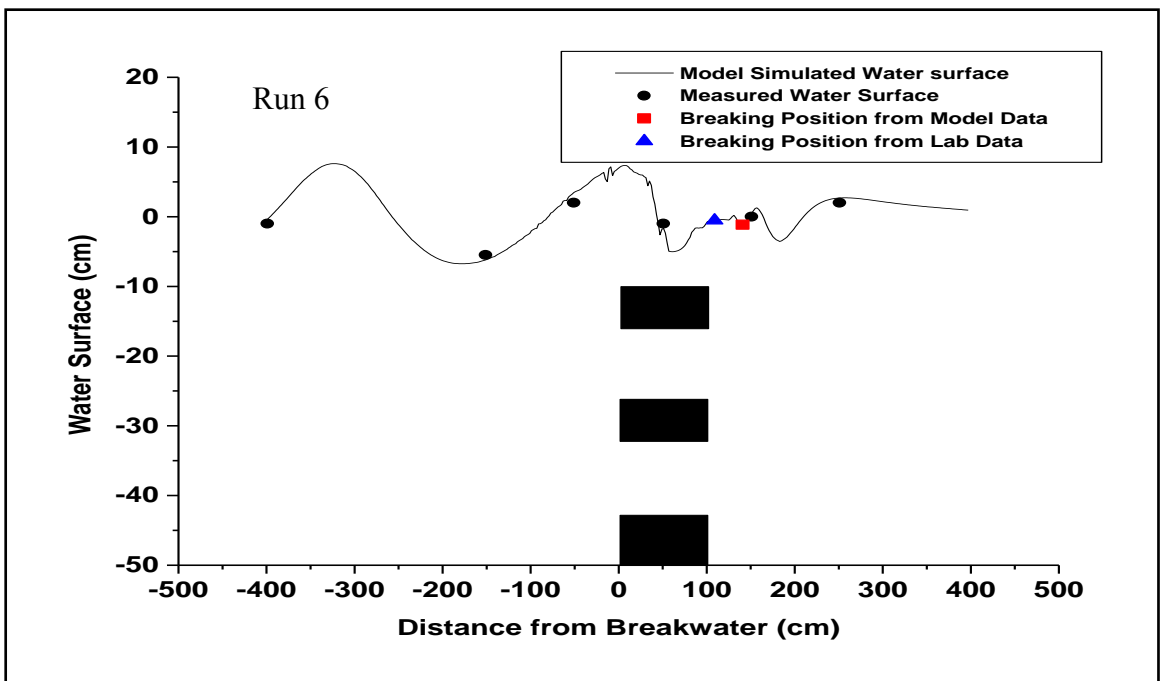
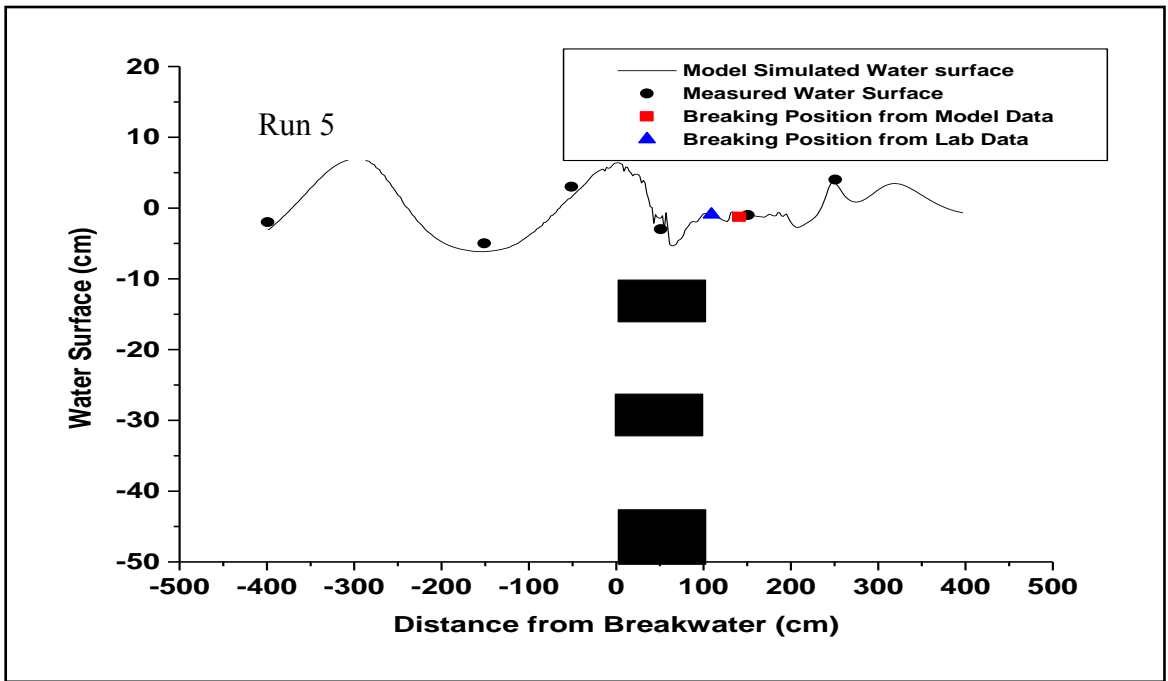


Figure 4.4: Comparisons between numerical and experimental results of water surface profile and wave breaking position for different Run conditions

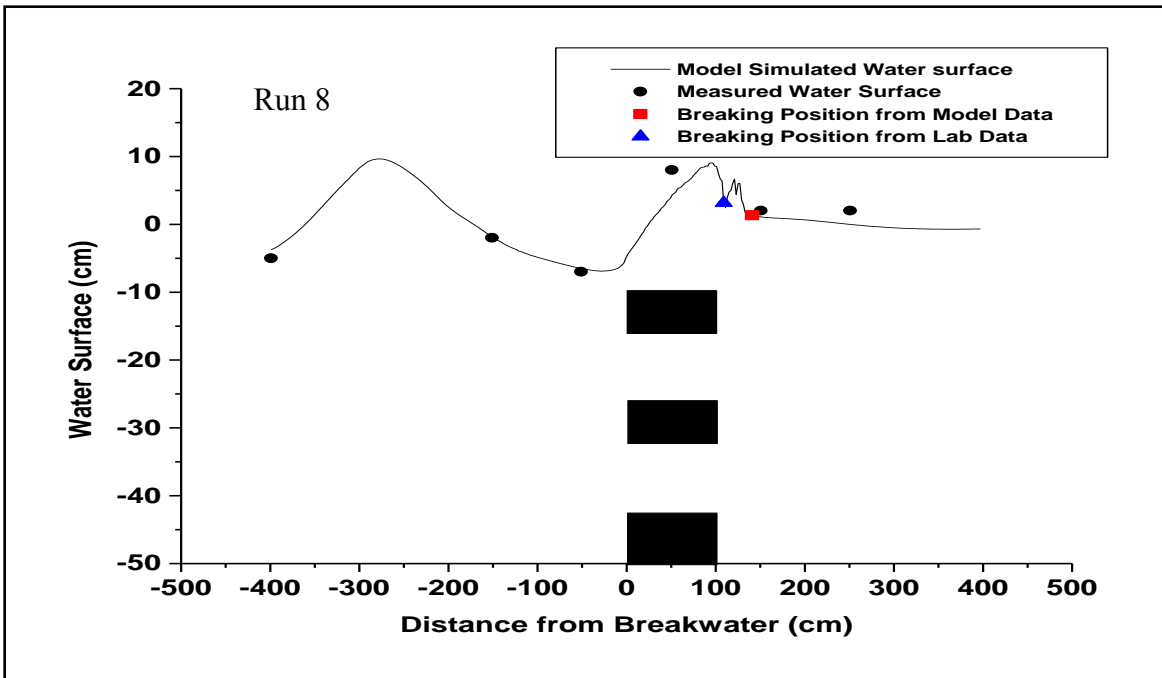
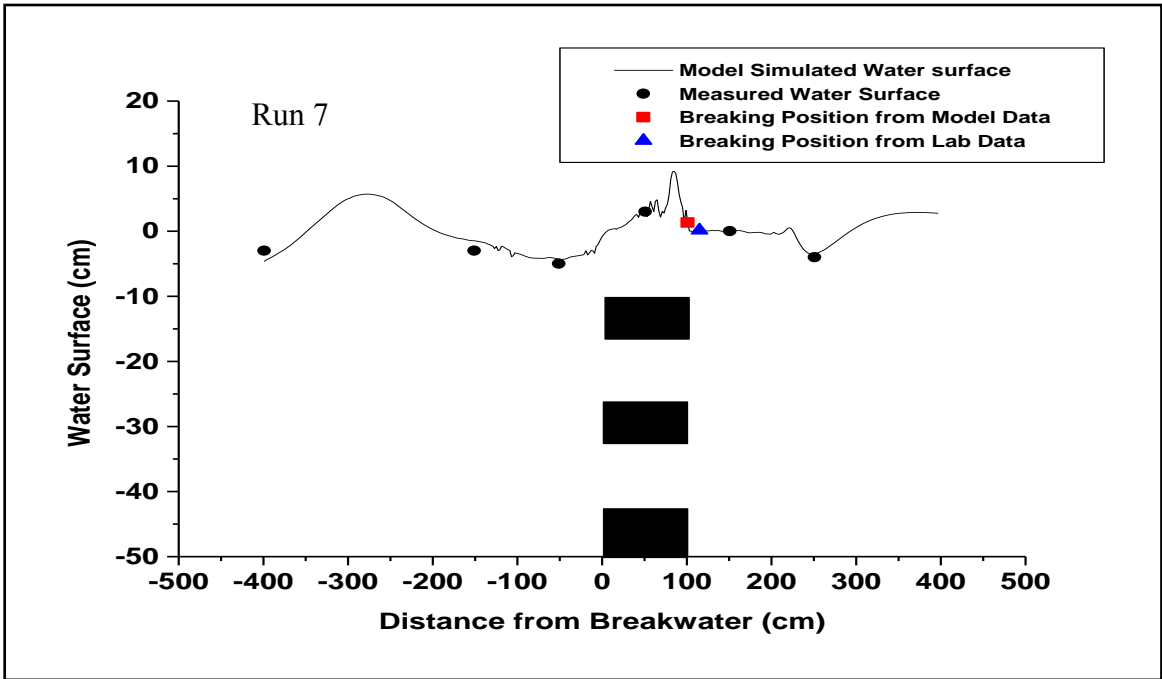




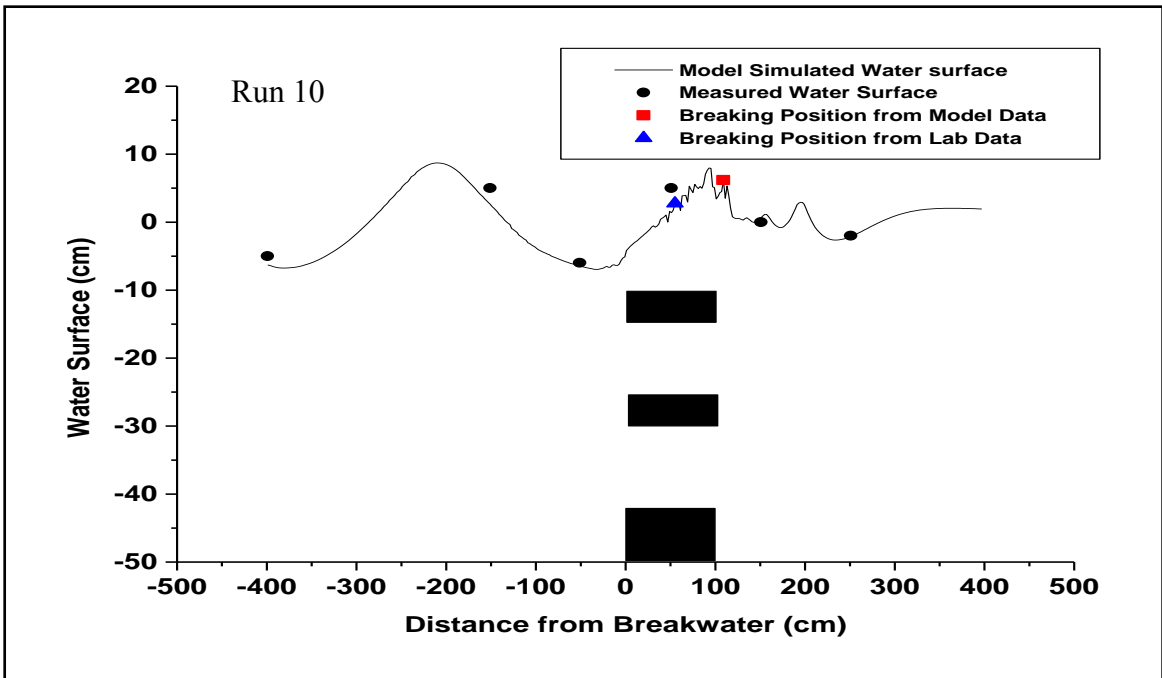
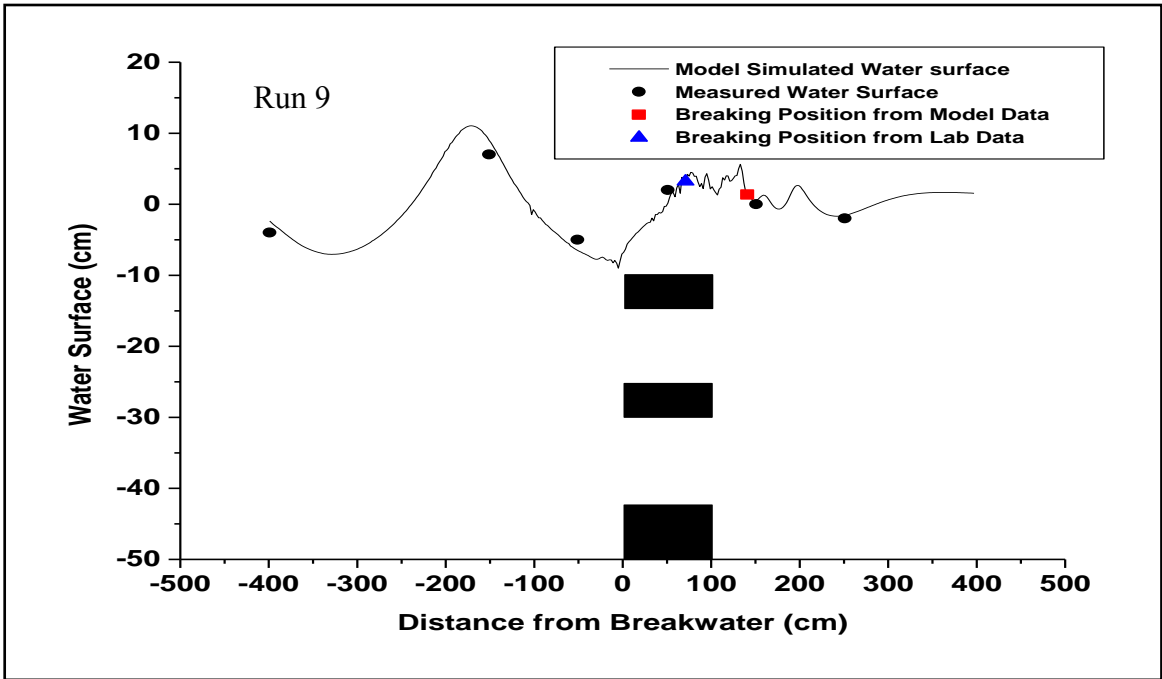
*Contd... Figure 4.4: Comparisons between numerical and experimental results of water surface profile and wave breaking position for different Run conditions*



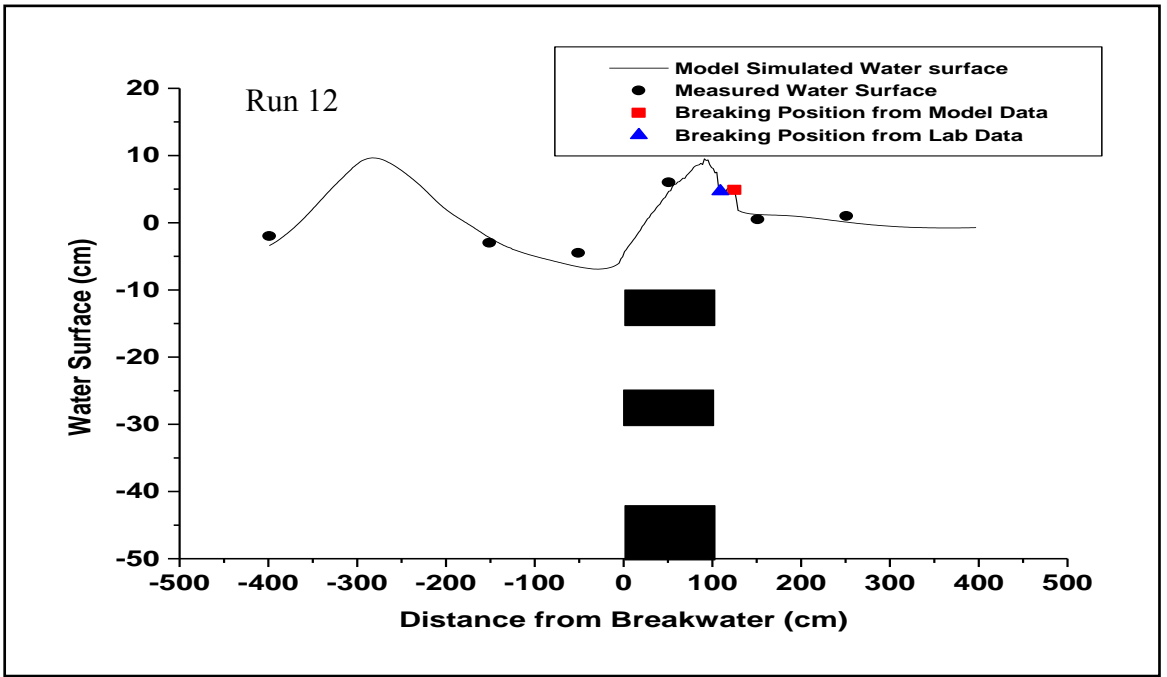
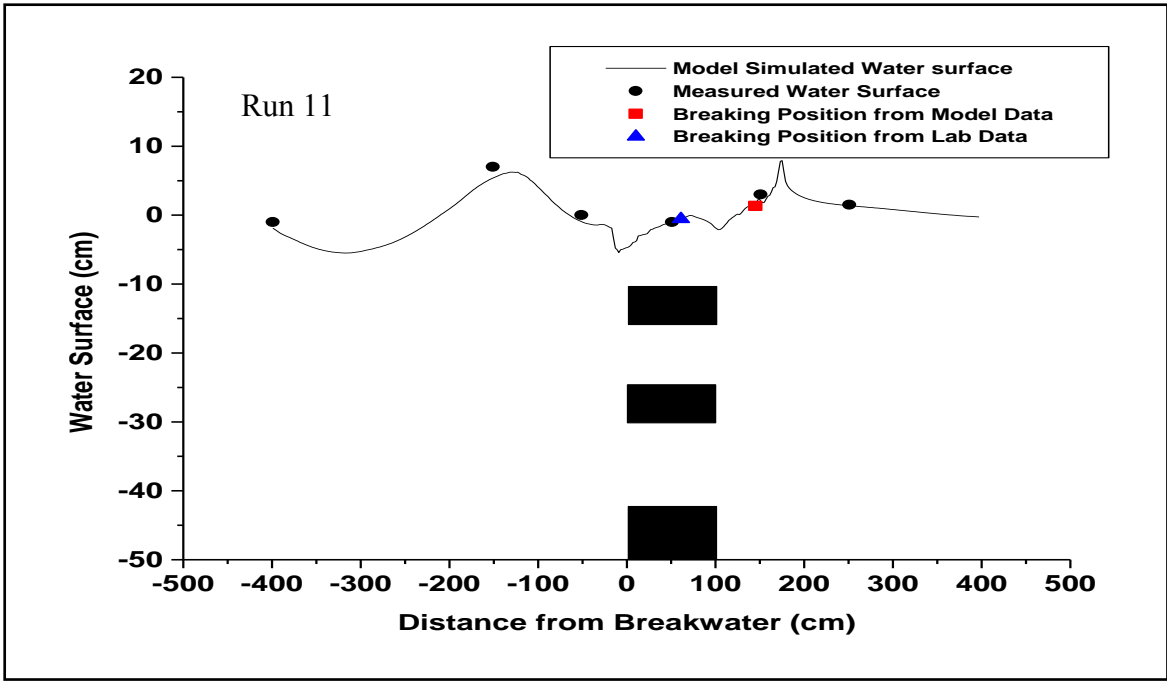
Contd... Figure 4.4: Comparisons between numerical and experimental results of water surface profile and wave breaking position for different Run conditions



Contd... Figure 4.4: Comparisons between numerical and experimental results of water surface profile and wave breaking position for different Run conditions



Contd... Figure 4.4: Comparisons between numerical and experimental results of water surface profile and wave breaking position for different Run conditions



*Contd... Figure 4.4: Comparisons between numerical and experimental results of water surface profile and wave breaking position for different Run conditions*

#### 4.6 Numerical Model Simulation of Time Series Water Surface Profiles

Figure 4.5 shows the numerical simulation of water surface profiles along the flume length for different stages of a wave cycle. The wave height, the wave period and the water depth are considered as 12 cm, 1.6 seconds and 50 cm respectively. The depth and width of the submerged body are 40 cm and 100 cm respectively. The water surface profiles at different moments of a full wave period (T) are shown in the figure. The overtopping of the water surface over the submerged body is seen in the figure. The irregular water surface profiles just behind the breakwater indicate the wave breaking and after breaking it is seen that the wave height reduces. Since the model is able to express the overtopping, the model can calculate the wave deformation around the structure due to nonlinear effects.

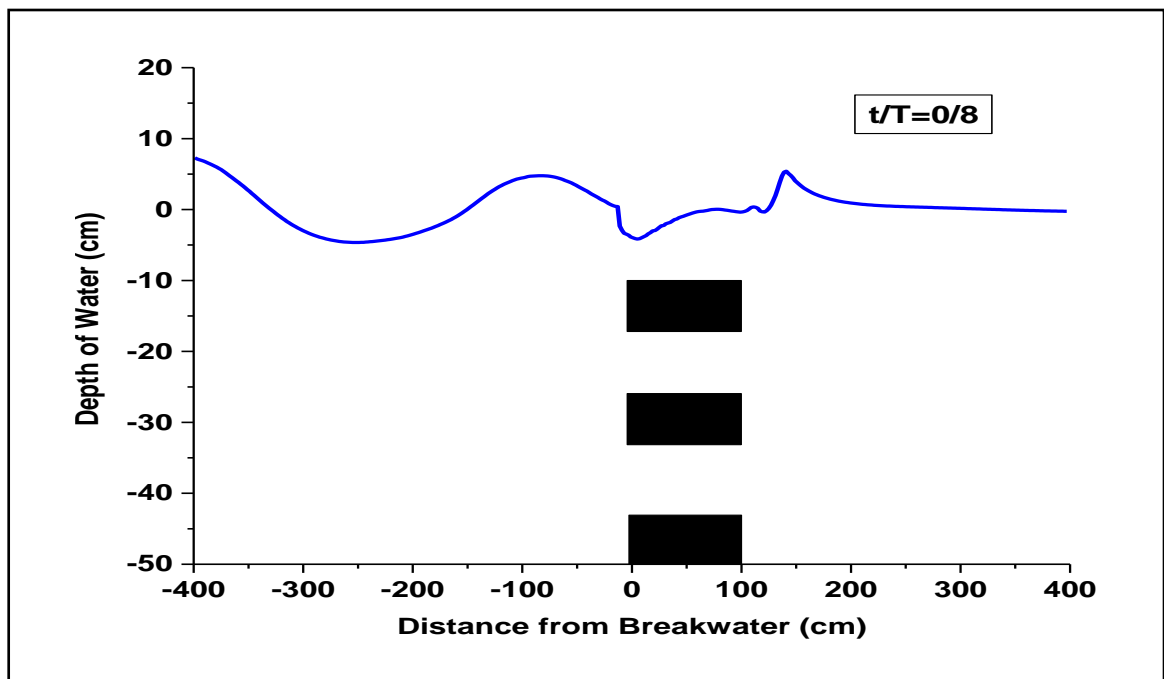
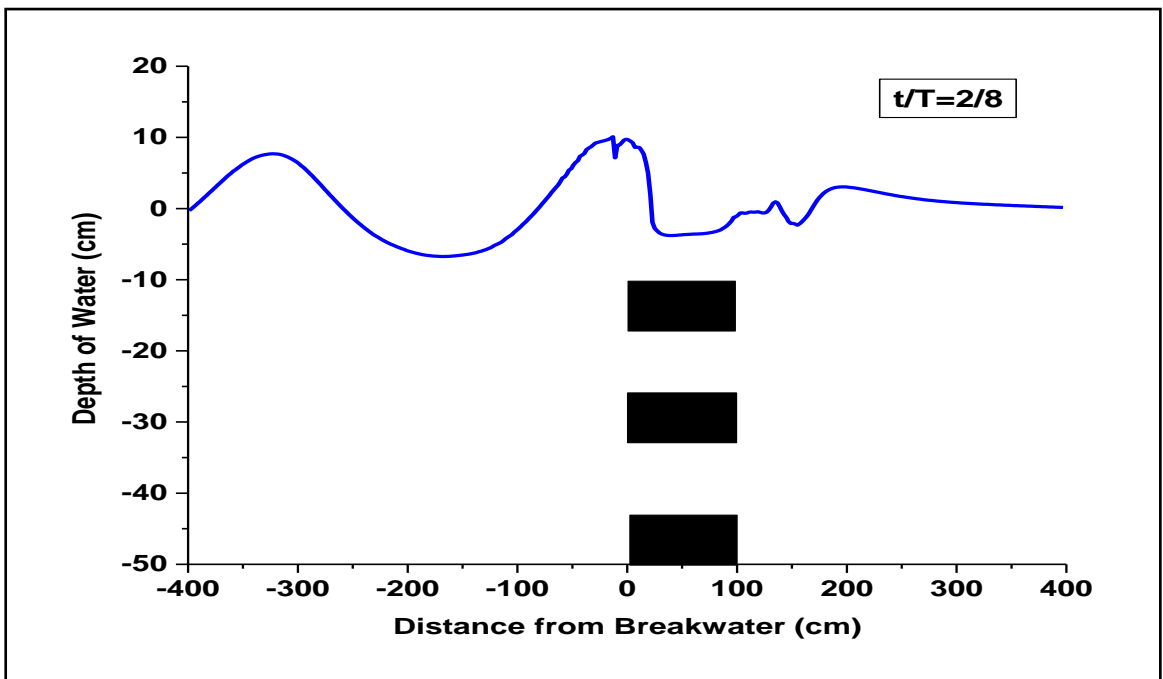
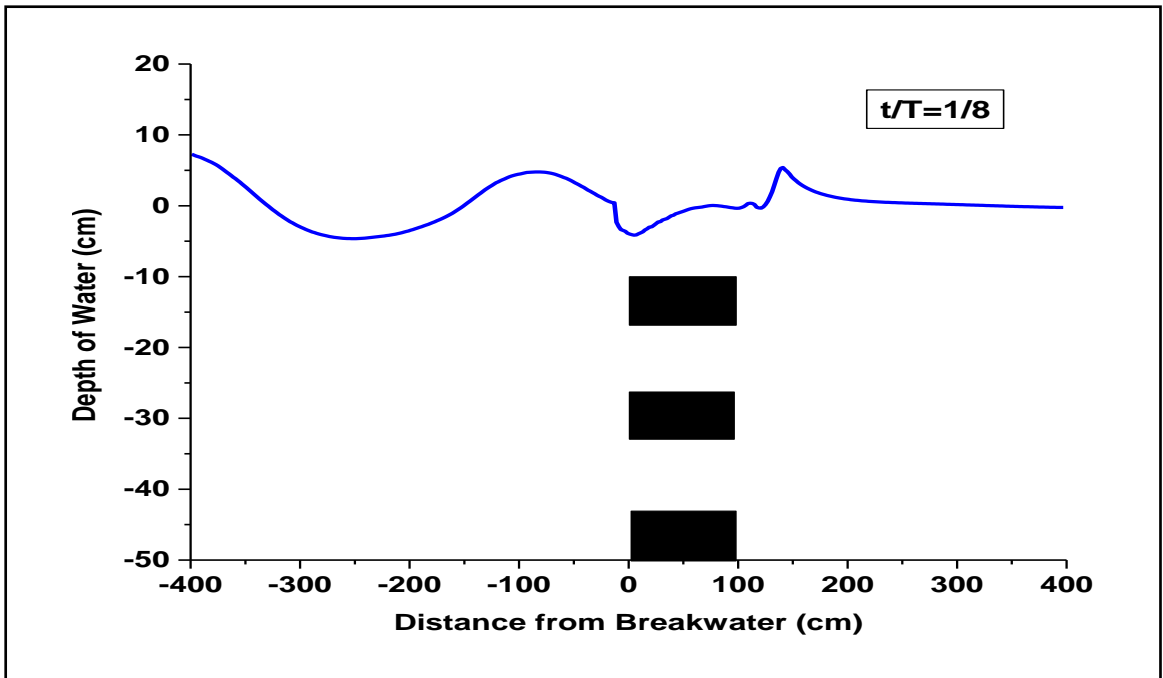
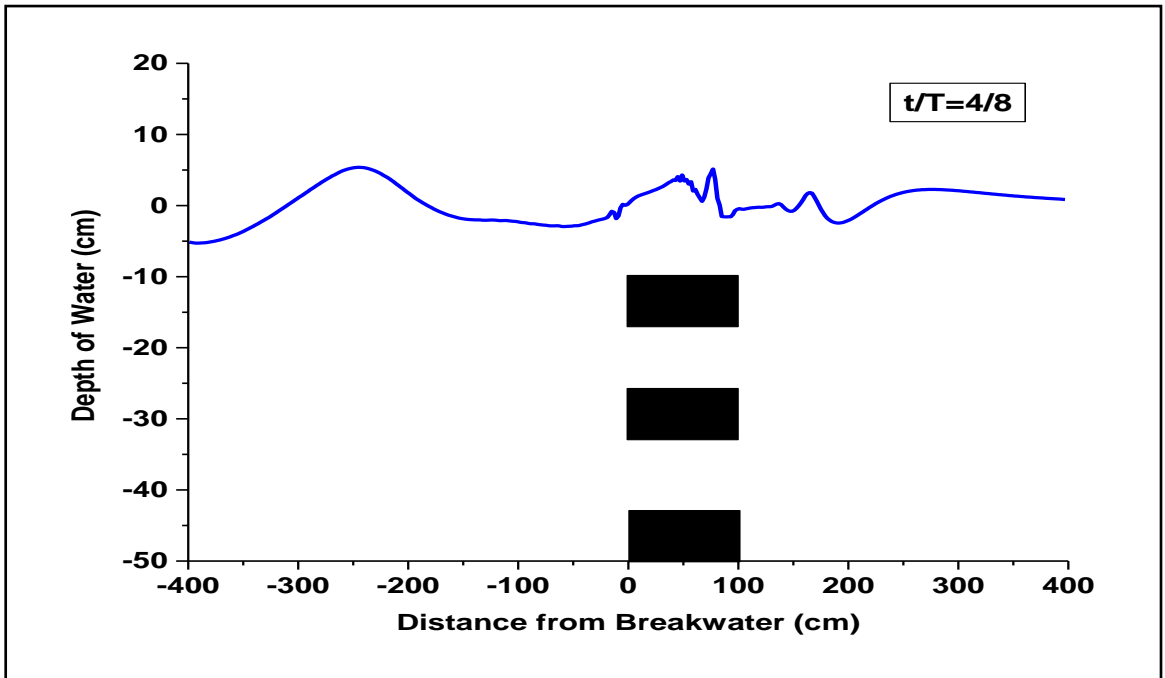
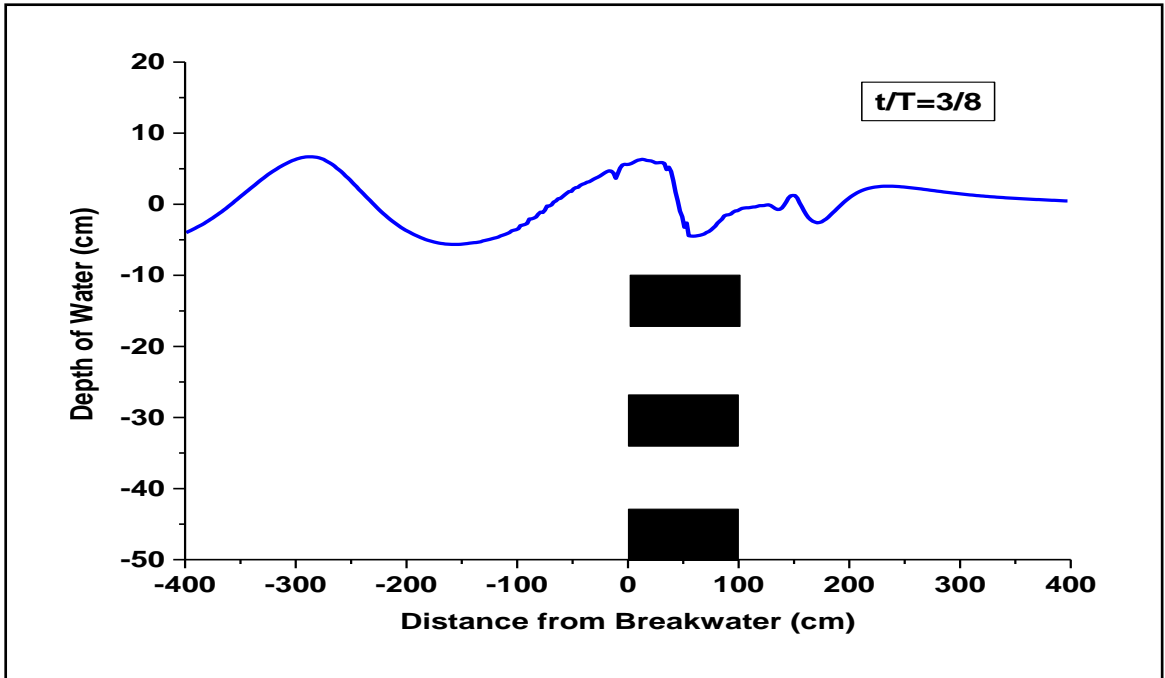


Figure 4.5: Numerical model simulation of time series water surface profile for run 1

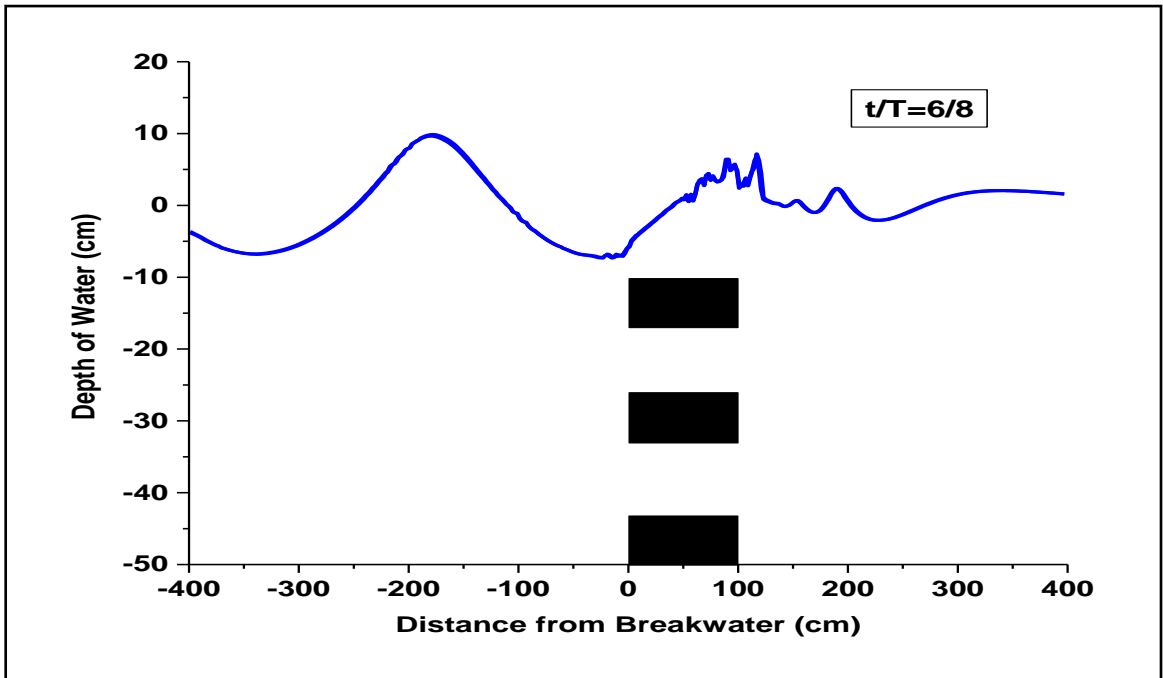
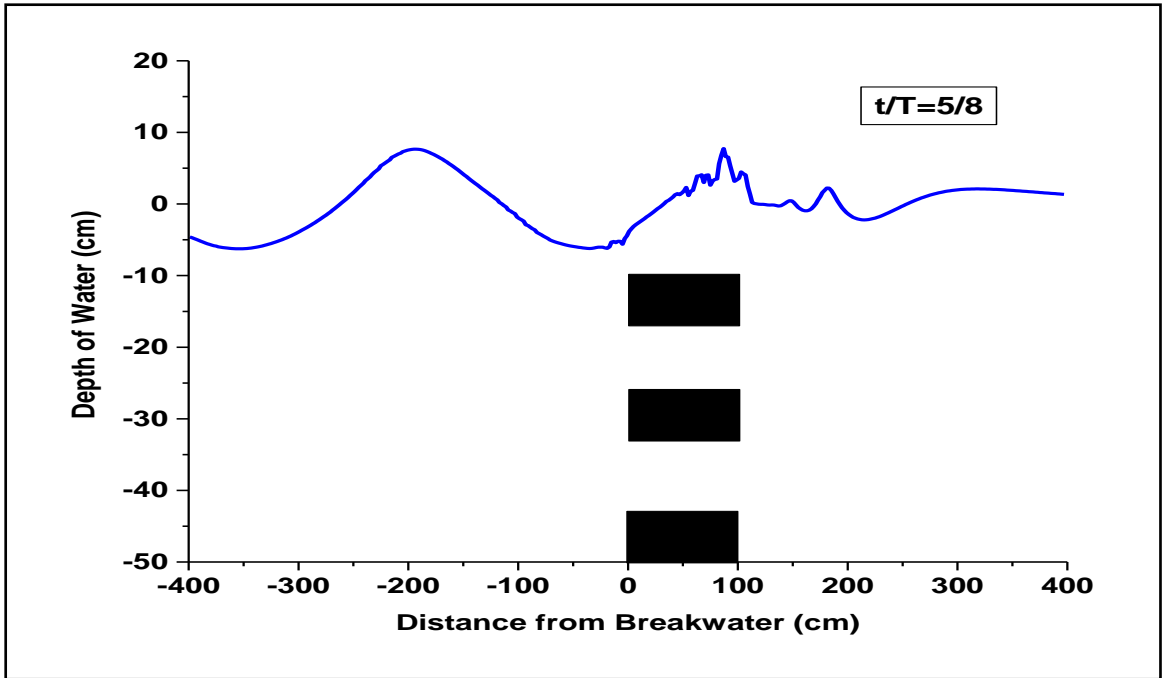


*Contd... Figure 4.5: Numerical model simulation of time series water surface profile for run 1*

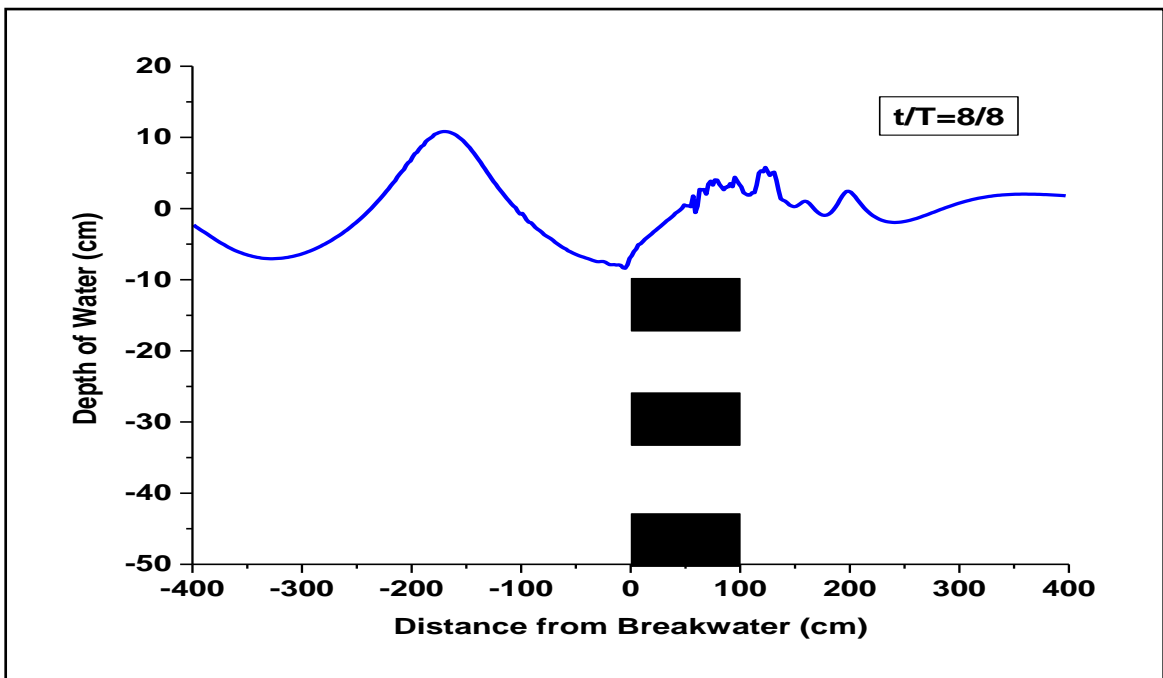
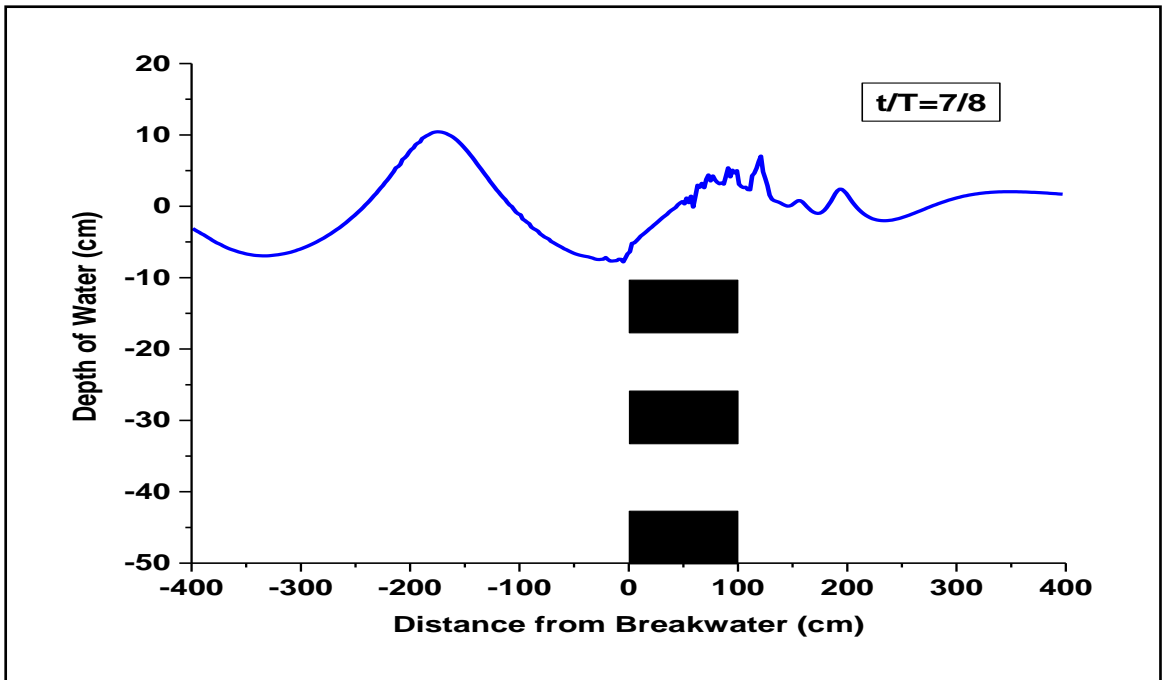


Contd... Figure 4.5: Numerical model simulation of time series water surface profile for run 1





Contd... Figure 4.5: Numerical model simulation of time series water surface profile for run 1



Contd... Figure 4.5: Numerical model simulation of time series water surface profile for run 1

#### 4.7 Numerical Model Simulation of Point Velocity around the Horizontal Slotted Submerged Breakwater

The water particle velocity field around the breakwater at the moment of  $t=5.0$  second after starting the simulation is shown in Figure 4.4. The wave height, the wave period and the water depth are considered as 12 cm, 1.6 seconds and 50 cm respectively. The details of numerical simulation of the water particle velocity field around the breakwater for different stages of a wave cycle are shown. The breaking of wave over or just behind the breakwater is clearly understood from the figure.

From the Figure 4.6, it is seen that the vortexes are generating behind the breakwater and the wave passing over the breakwater breaks with an overturning wave front. The arrow of the vector represents the direction and the length of arrow represents the magnitude of the velocity. Furthermore, this figure illustrates that the higher magnitude of the water particle velocity in the offshore side of the breakwater

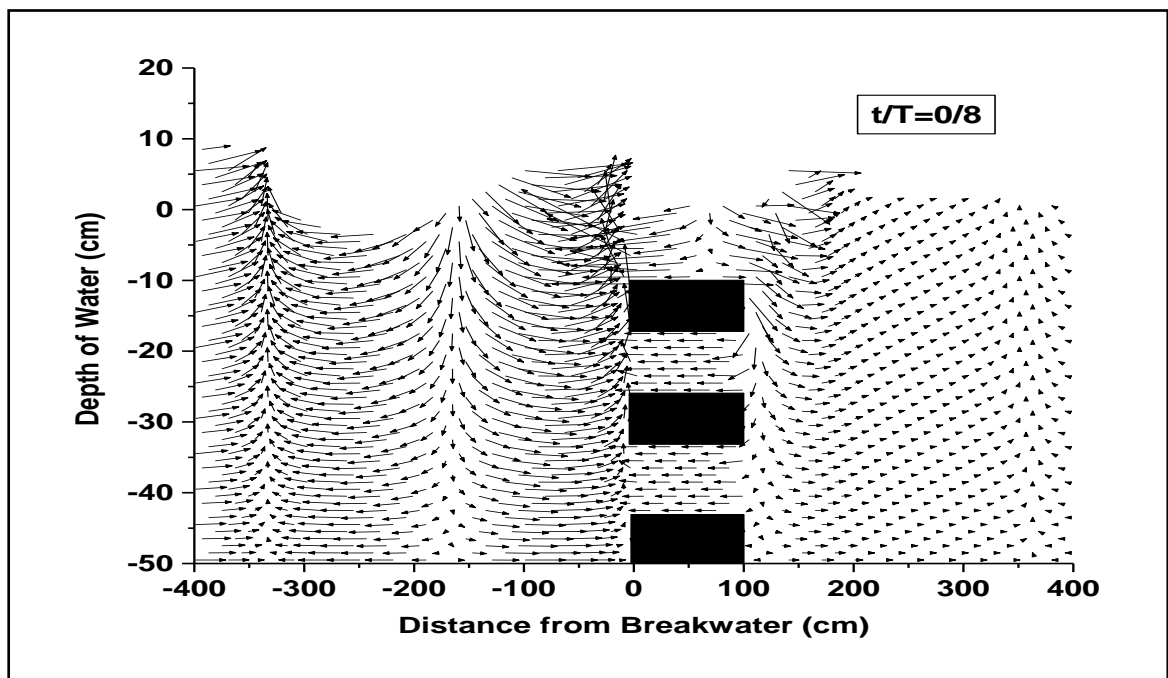
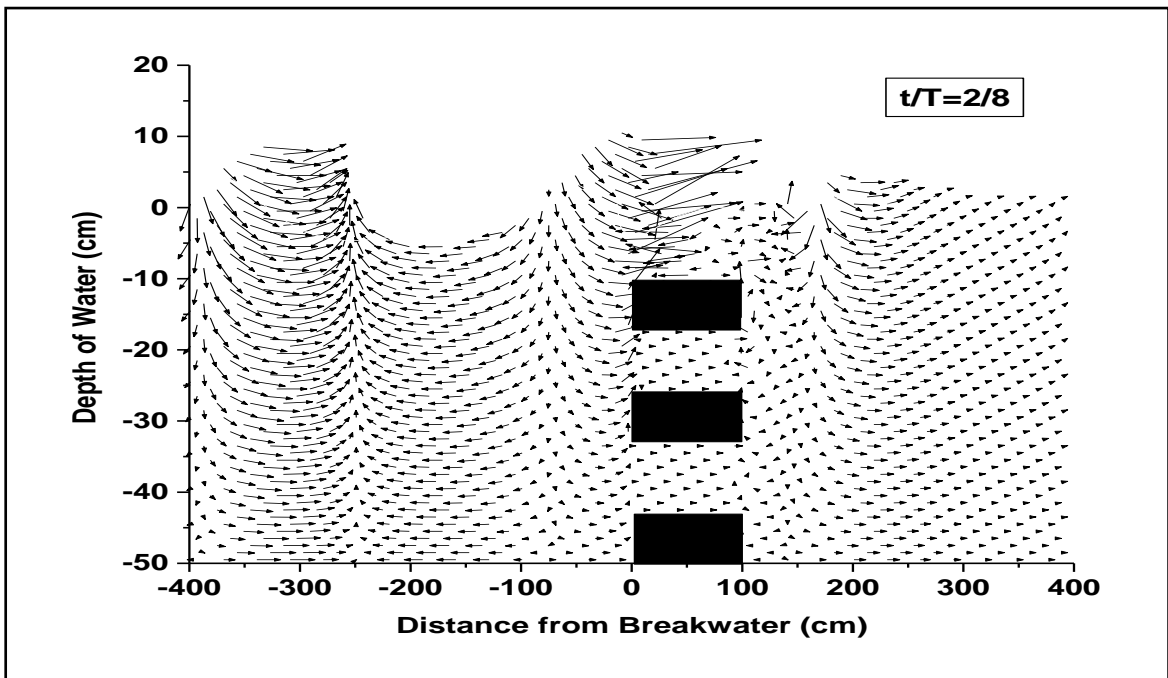
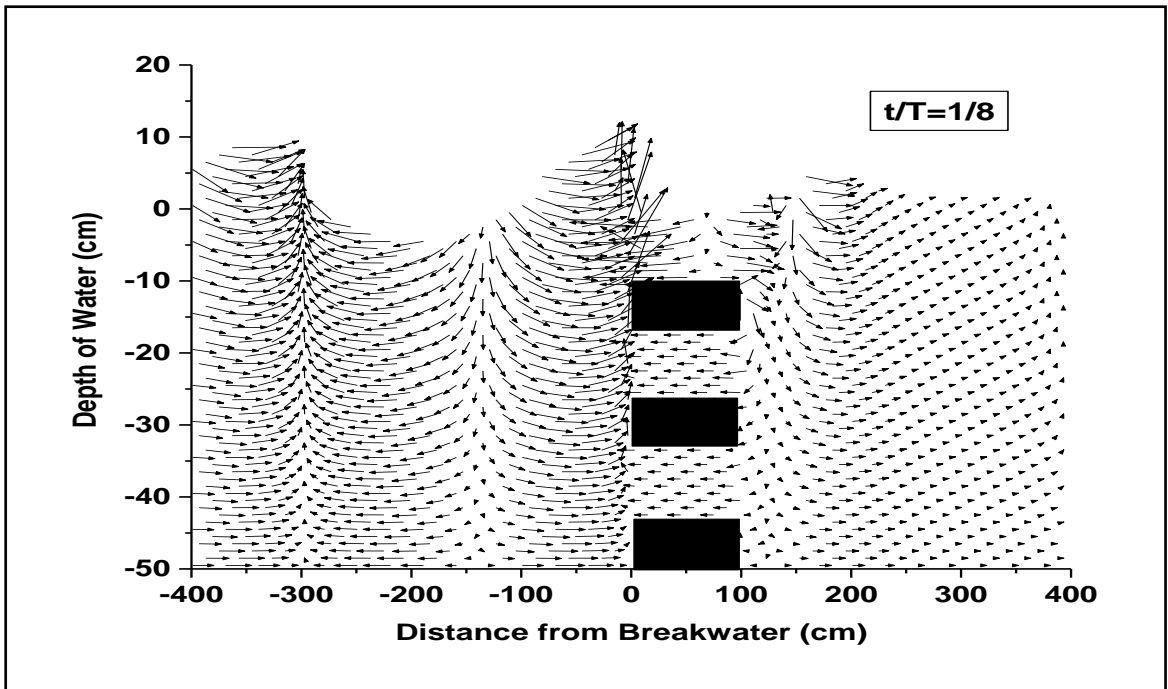
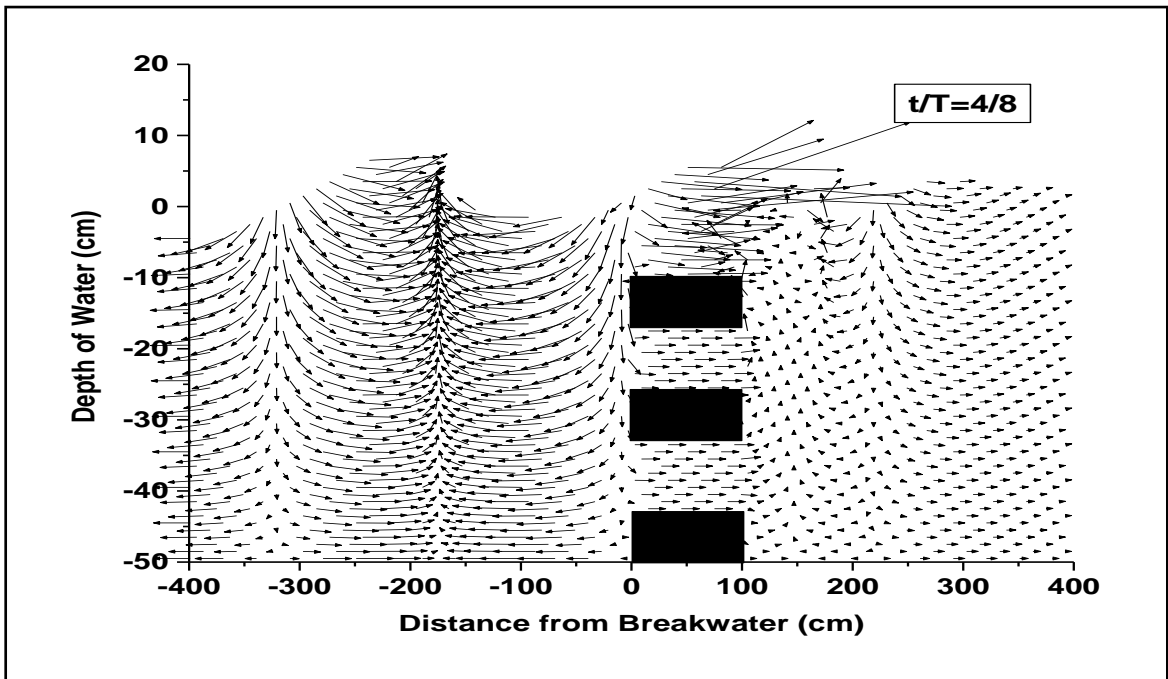
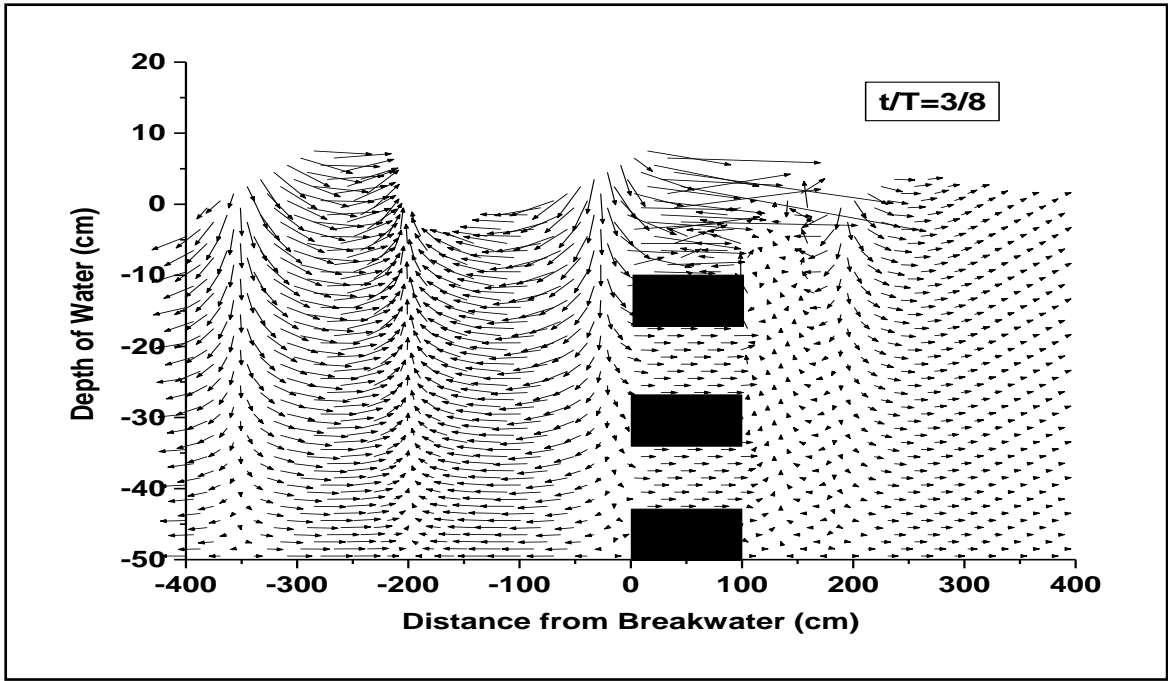


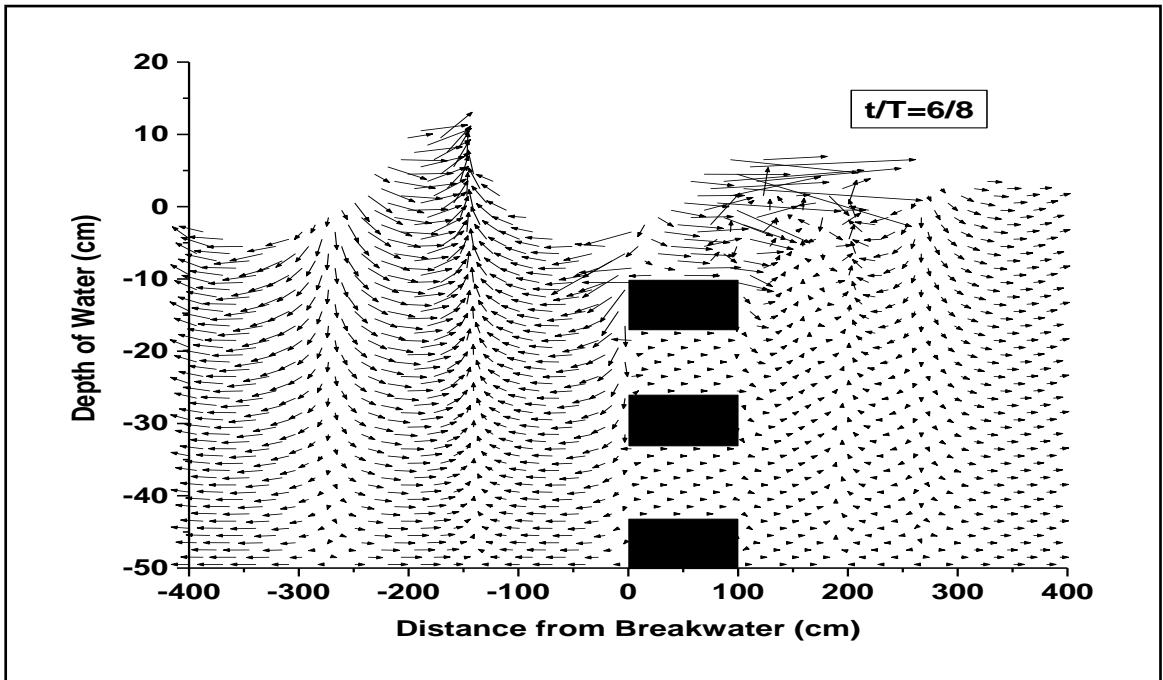
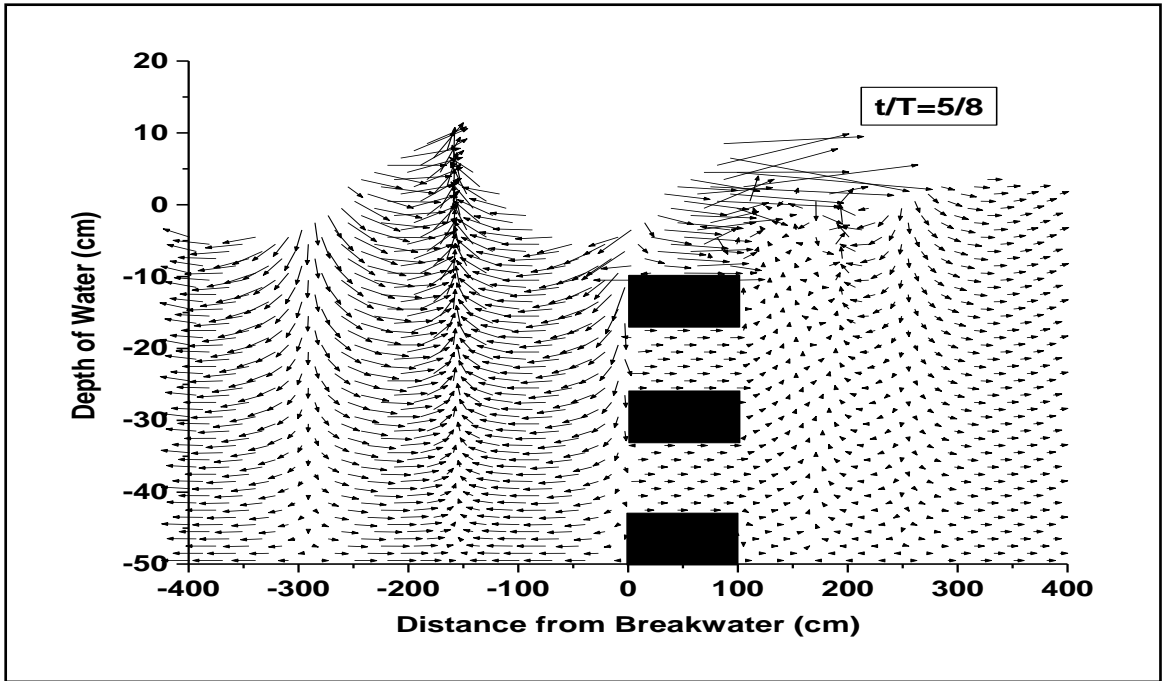
Figure 4.6: Numerical model simulation of time series water particle velocity around the horizontal slotted submerged breakwater for run 1



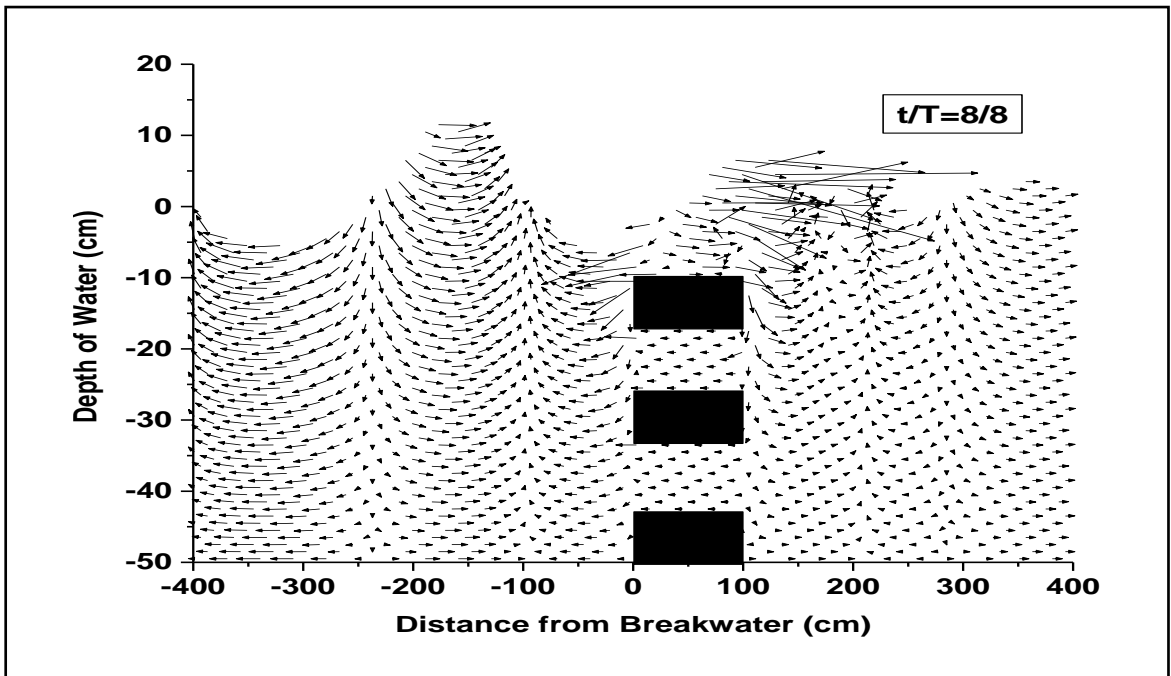
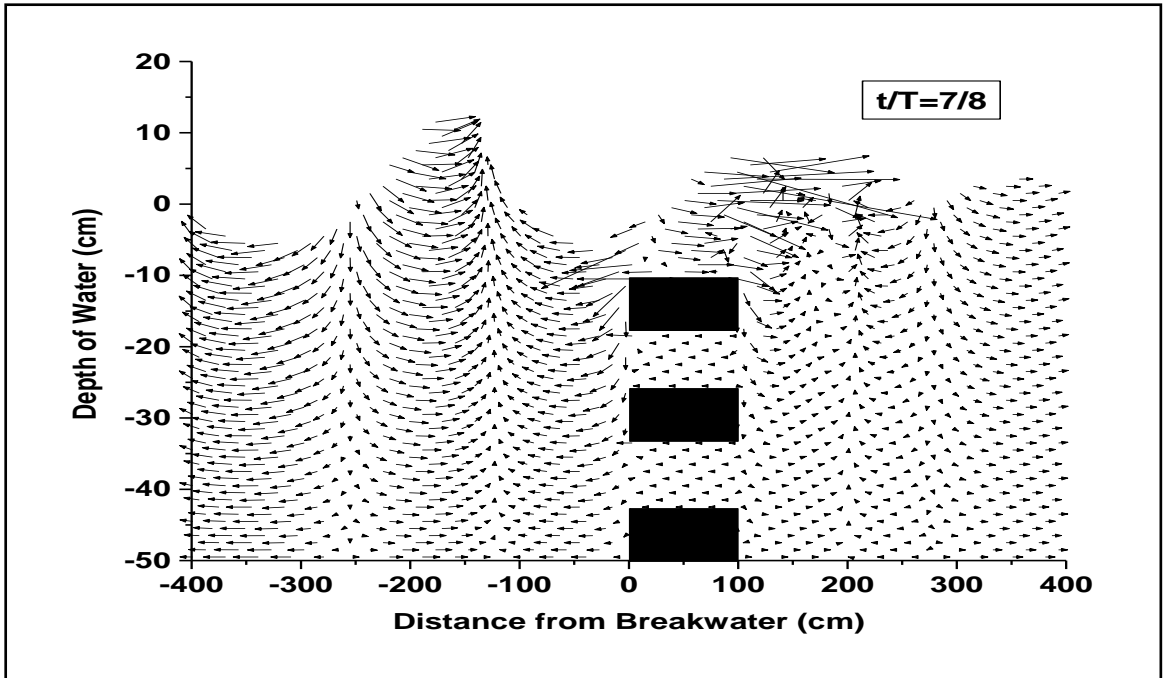
Contd... Figure 4.6: Numerical model simulation of time series water particle velocity around the horizontal slotted submerged breakwater for run 1



Contd... Figure 4.6: Numerical model simulation of time series water particle velocity around the horizontal slotted submerged breakwater for run 1



Contd... Figure 4.6: Numerical model simulation of time series water particle velocity around the horizontal slotted submerged breakwater for run 1



Contd... Figure 4.6: Numerical model simulation of time series water particle velocity around the horizontal slotted submerged breakwater for run 1

decreases in the onshore side due to the wave energy dissipation through wave breaking by the breakwater. Also the greater length of arrows over or just behind the breakwater shows breaking of waves in that zone.

#### 4.8 VOF Function F around the Breakwater

From the experimental video clips, it is seen that most of the wave breaking occurs when the wave front passes over the top surface of the breakwater and its immediate onshore side. Figure 4.5 shows the numerical simulation of the contour map of the VOF function  $F$ , which ranges from 0 to 1 at the moment of  $t = 6$  sec after starting the simulation. The wave height, the wave period and the water depth are considered as 13 cm, 1.7 seconds and 50 cm respectively.

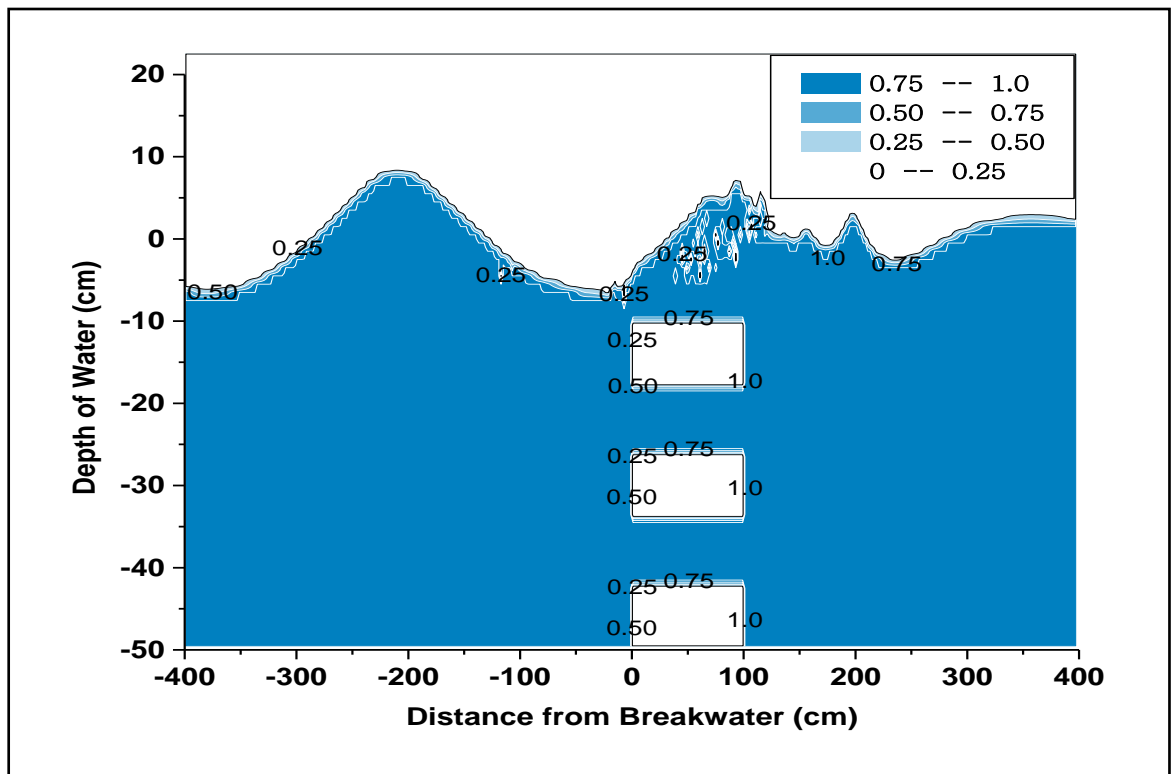
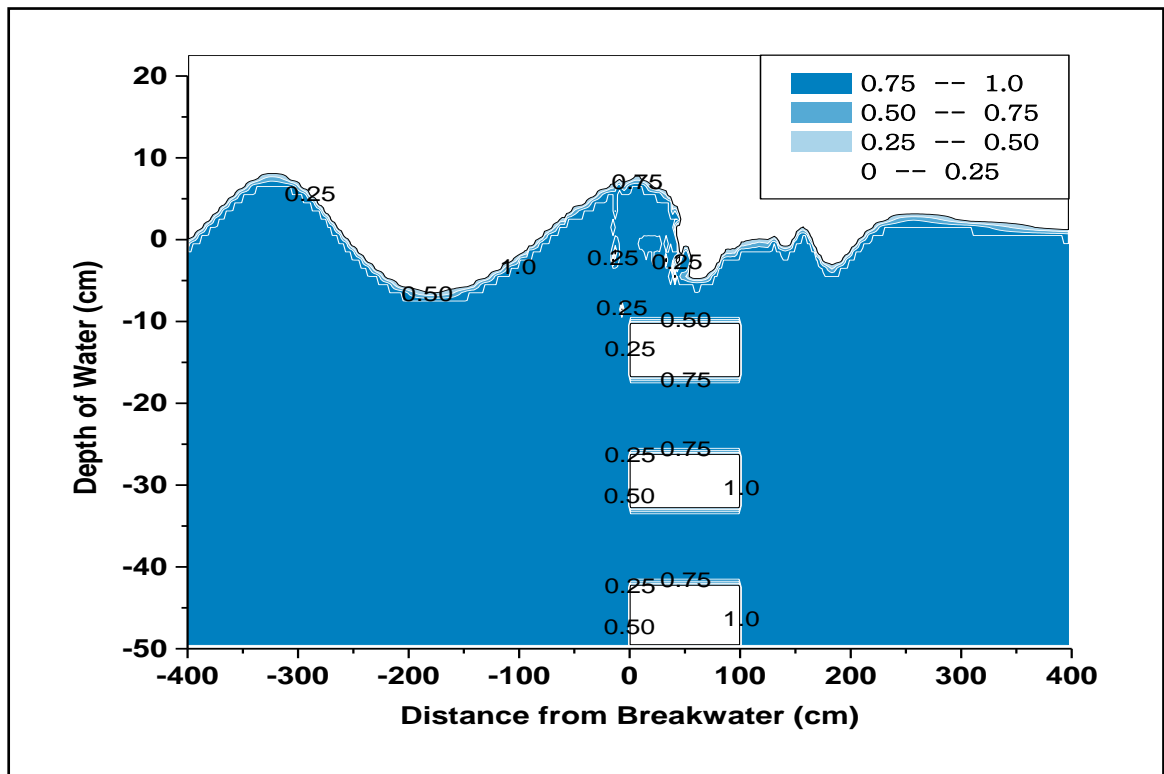


Figure 4.7: Numerical model results of VOF function value  $F$  around the breakwater for run 2

In Figure 4.7, the  $F$  value of the top surface of the water surface profile is seen less than 1 ( $F < 1$ ), that represents the surface cells. It shows that the breaking of wave occurs here and the air-bubble entrained in the corresponding numerical mesh cells due to wave breaking reduces the water volume less than the full volume of a fluid cell. For this reason the numerical model calculates  $F$  value of these cells less than 1. Also, the cells having  $F < 1$  are seen in offshore side of the breakwater. This may happen due to the reason that the higher water particle velocity in vertically



downward direction at the offshore face of the breakwater may cause partial void at some cells near the offshore face bottom corner forming vortex in this zone, which can also be seen in Figure 4.8 and 4.9.



*Figure 4.8: Numerical model results of VOF function value  $F$  around the breakwater for run 6*

At a distance from the breakwater the value of  $F$  is 1 at deep water zone because in these regions the computational cells are completely filled by the fluid. The  $F$  value is less than 1 in the surface cells partially occupied by water and partially filled by air. Again just at the offshore end of the breakwater, over the breakwater and at the onshore end of the breakwater the value of  $F$  is less than 1 because of the presence of bubble and eddies in these cells some air is entrapped there. Figure 4.8 shows the effect of installing a porous submerged breakwater having  $n=0.5$  in 50 cm depth of water. In this case the variation in the value of  $F$  is almost similar. In Figure 4.9, changes in the value of  $F$  as a result of breaking of wave by submerged porous breakwater of  $n=0.6$  are shown. Here as the waves break overtopping the breakwater, the variation in the value of  $F$  can be clearly understood.

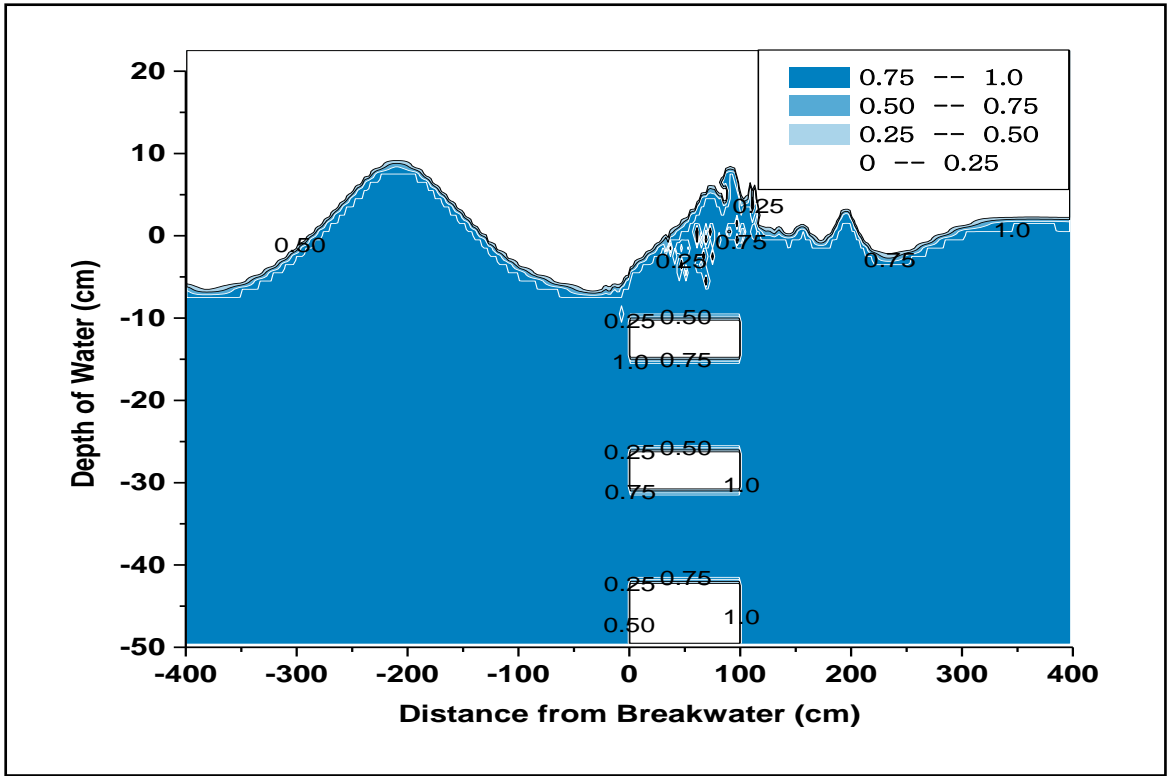


Figure 4.9: Numerical model results of VOF function value  $F$  around the breakwater for run 10

#### 4.9 Pressure Distribution around the Breakwater

Figure 4.10 to Figure 4.12 show the numerical simulation of the water pressure distribution at the moment of  $t = 6$  sec after starting the simulation in  $\text{dyne/cm}^2$  unit. The wave height, the wave period and the water depth are considered as 12 cm, 1.6 seconds and 50 cm respectively. The solid portion in the middle of this figure represents the breakwater. The changes in the pressure distribution around the breakwater are presented here.

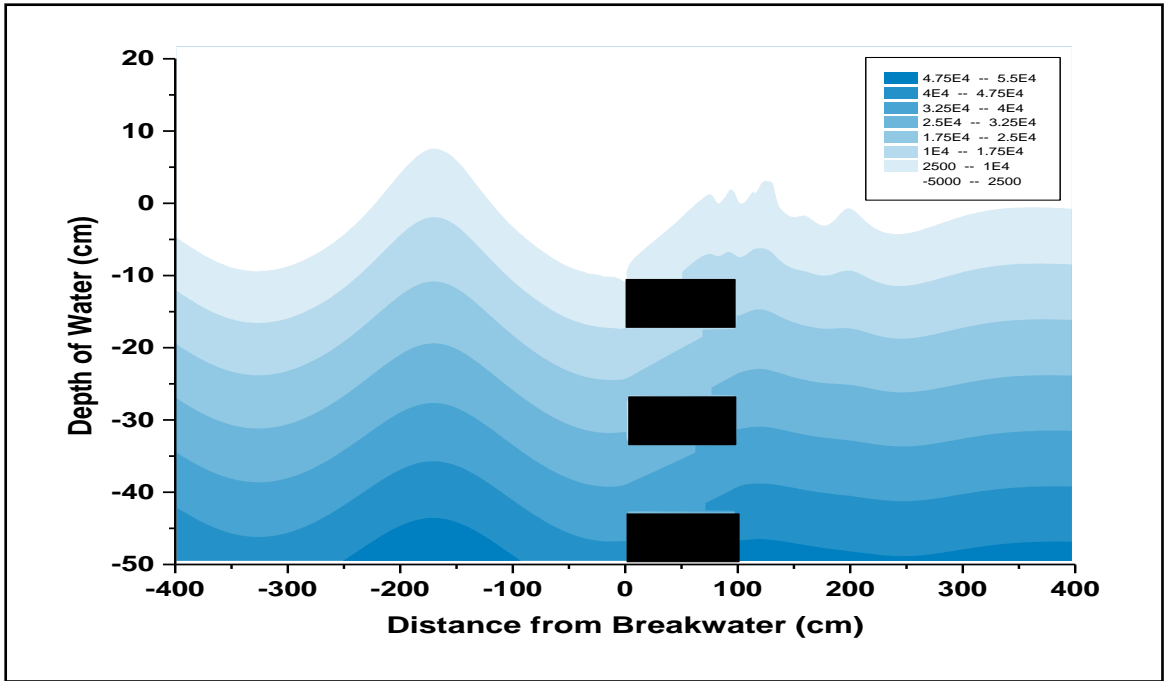


Figure 4.10: Numerical model results of pressure distribution around the breakwater for run 1

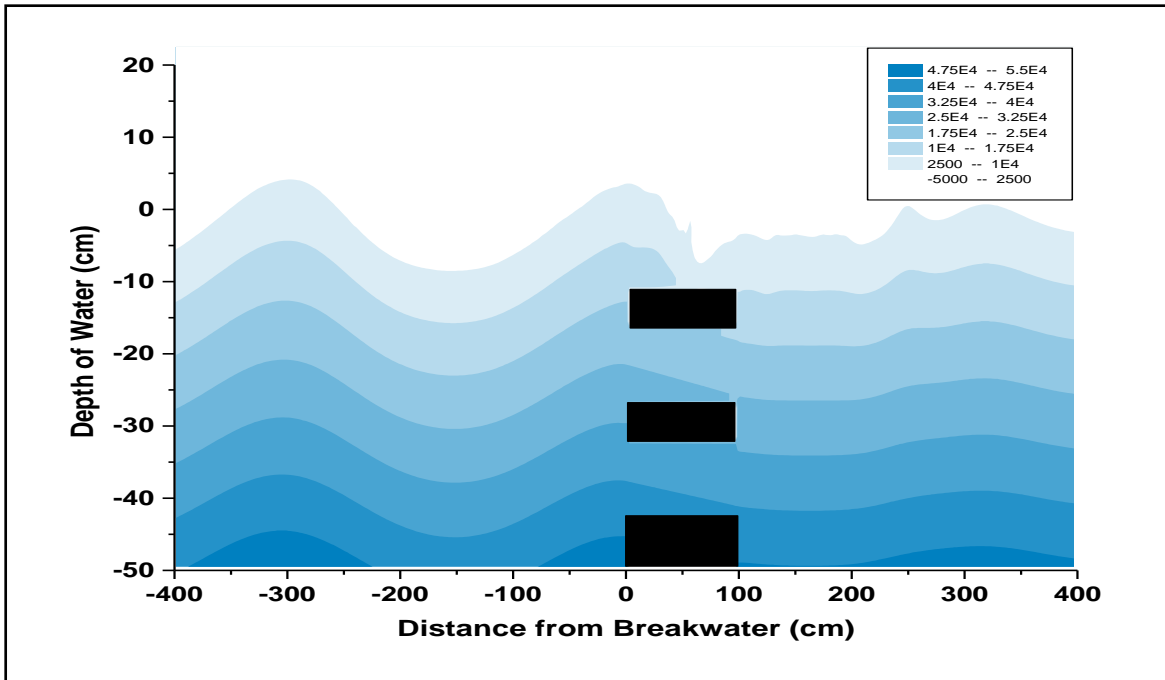


Figure 4.11: Numerical model results of pressure distribution around the breakwater for run 5

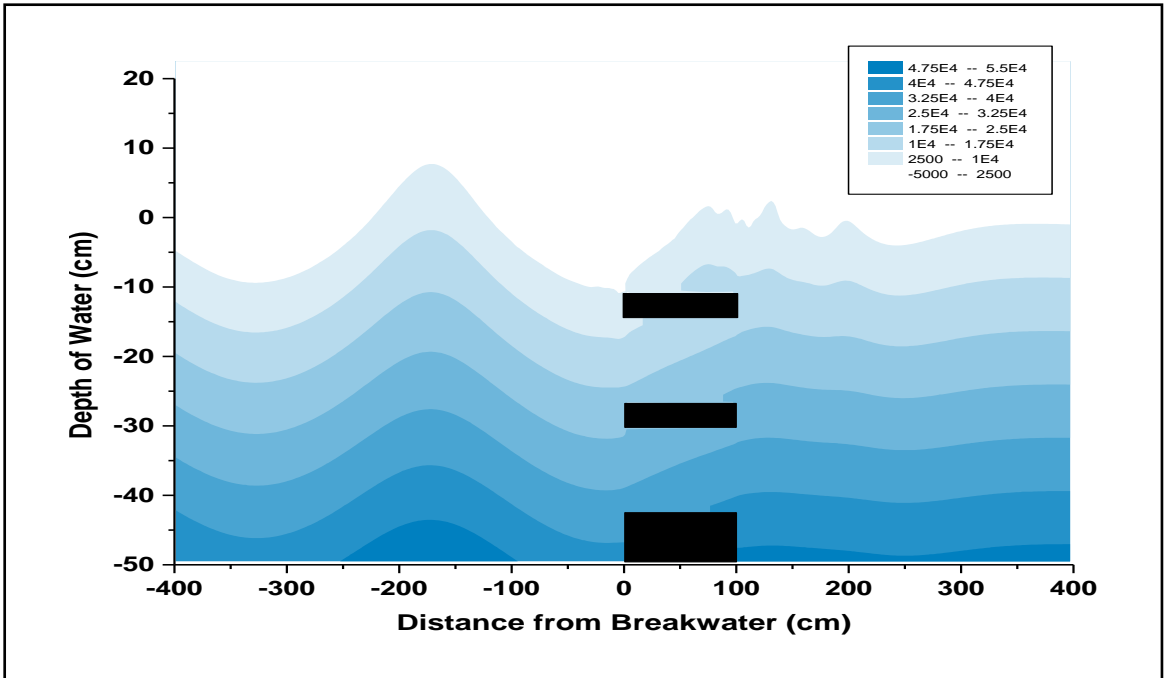


Figure 4.12: Numerical model results of pressure distribution around the breakwater for run 9

# CHAPTER 5

## CONCLUSIONS AND RECOMMENDATIONS

### 5.1 Conclusions

Horizontal slotted submerged porous breakwater is able to enhance water circulation and exchange of water between the open sea and sheltered areas. Because of the submergence of the breakwater, its application of protecting coastal areas attracts more attention due to environmental concerns. In this study, the interaction between wave and horizontal slotted submerged breakwater has been investigated both experimentally and numerically to find out the effective size and porosity of this protection structure for the reduction of incoming wave energy. In a two-dimensional wave flume, twelve experimental runs have been conducted with horizontal slotted submerged body of three different porosities ( $n=0.4, 0.5$  and  $0.6$ ) in constant water depth of  $h=50$  cm for regular waves of four different periods as  $T= 1.6$  sec,  $1.7$  sec,  $1.8$  sec and  $2.0$  sec respectively. Moreover, a two-dimensional numerical model of wave interaction with submerged solid breakwater developed by Rahman and Womera (2013) is adapted in this study to simulate the wave interaction with horizontal slotted submerged breakwater. The adapted model can simulate water surface profile, velocity profile, water pressure all through the flume length including wave breaking over and around the breakwater. Finally the experimentally measured water surface profiles and wave breaking positions for each of the twelve run conditions are compared with the simulated results. From this study the following conclusions can be derived:

(a) The functional efficiency of horizontal slotted submerged porous breakwater is measured by wave reflection, transmission and wave energy loss co-efficient. From the experimental data analysis it can be concluded that:

(i) Wave reflection coefficient ( $K_r$ ) increases as relative breakwater width ( $k.B$ ) increases ( $k.B=2B\pi/L$ , where  $k$  is the wave number). Also, the reflection coefficient ( $K_r$ ) decreases as porosity ( $n$ ) increases. Reflection coefficient ( $K_r$ ) decreased from  $0.368$  to  $0.107$  with decreasing  $k.B$  from  $2.05$  to  $1.55$  when structure

porosity was  $n=0.4$ , decreased from 0.286 to 0.059 when structure porosity was  $n=0.5$ , and decreased from 0.24 to 0.034 when structure porosity was  $n=0.6$ .

(ii) The transmission coefficient ( $K_t$ ) decreases as relative breakwater width  $k.B$  increases. This means that, the breakwater reduces the transmitted waves as the breakwater width ( $B$ ) increases or the wave length ( $L$ ) decreases. When porosity is  $n=0.4$ , the transmission coefficient ( $K_t$ ) decreased from 0.64 to 0.53 with increasing  $k.B$  from 1.55 to 2.05. When porosity increased to  $n=0.5$ , transmission coefficient ( $K_t$ ) decreased from 0.76 to 0.56, and when the porosity is  $n=0.6$ ,  $K_t$  decreased from 0.82 to 0.64 with increasing  $k.B$ .

(iii) Wave energy loss coefficient,  $K_L$  increases as relative breakwater width  $k.B$  increases. Also the wave energy loss coefficient ( $K_L$ ) increases as the porosity decreases. When porosity is  $n=0.4$ , the wave energy loss coefficient ( $K_L$ ) increased from 0.61 to 0.68 with increasing  $k.B$  from 1.55 to 2.05. For porosity  $n=0.5$ ,  $K_L$  increased from 0.56 to 0.63, and for  $n=0.6$  structure porosity,  $K_L$  increased from 0.47 to 0.55 with increasing  $k.B$  from 1.55 to 2.05.

(iv) The transmission coefficient ( $K_t$ ) is found minimum for minimum porosity of  $n=0.4$  which is 0.5263 and increased to 0.6428 with the increasing porosity of  $n=0.6$ . Also the wave energy loss coefficient ( $K_L$ ) is found maximum for minimum porosity of  $n=0.4$  which is 0.8288 and decreased to 0.7107 with the increasing porosity of  $n=0.6$ . So in some important coastal areas where full dissipation of wave energy is not required, horizontal slotted submerged porous breakwater of porosity  $n=0.4$  can be used efficiently in those areas, as almost 83% of energy is dissipated by this breakwater. Thus, the submerged porous breakwater would be an excellent option for coastal soft defense structures that are able to enhance water circulation and exchange between open sea and sheltered areas.

(b) The water surface profiles simulated by the numerical model are in good agreement with wave profiles generated from Stokes 3<sup>rd</sup> order wave theory which indicates the satisfactory performance of the adapted model for any type of wave generation.

(c) From the comparison between experimentally measured water surface profiles with that of the model simulated values, it is seen that the measured data agree well with the model results with maximum  $\pm 20\%$  deviation at some points.

(d) The comparison between experimentally measured wave breaking positions also agree well with model simulated wave breaking positions.

(e) The numerical model developed under this study can be used for analyzing wave interaction with horizontal slotted submerged porous breakwater having different porosities. Thus the developed model will help the coastal engineers for optimizing the breakwater dimensions during its design.

## **5.2 Recommendations**

In this study, the effectiveness of a horizontal slotted submerged breakwater exposed to unidirectional regular waves in the reduction of wave height has been investigated both experimentally and numerically. The following recommendations are made for further study:

- i. Interaction between this type of breakwater with irregular waves can be studied.
- ii. A three dimensional wave-structure interaction model can be developed which can be used in investigating problems related to vertical slotted porous breakwater.

## REFERENCES

- [1] Al-Banna, K. and Liu, P. (2007). "Numerical study on the hydraulic performance of submerged porous breakwater under solitary wave attack". *Journal of Coastal Research*, Vol. 50, pp. 201-205.
- [2] Balaji. R (2012). "Performance of Porous Breakwaters: Application of the BOUSS-2D Model", *The Journal of Engineering Research*, Vol. 9(1), pp. 11-20.
- [3] Brorsen, M and Larsen, J. (1987). "Source generation of nonlinear gravity waves with the boundary integral equation method", *Coastal Engineering*, Elsevier, Vol. 11, pp. 93–113.
- [4] Dick, T.M. and Brebner, A. (1968) "Solid and permeable submerged breakwaters" *Proc. 11th. Conf. On Coastal Engineering, ASCE, New York, N.Y., II*, pp.1141-1158.
- [5] Hur D., Mizutani N. (2003). "Numerical estimation of wave forces acting on a three-dimensional body on submerged breakwater", *Coastal Engineering*, Elsevier, Vol. 47, pp. 329-345.
- [6] Hieu, P. D., and Tanimoto, K. (2006). "Verification of a VOF-based two-phase flow model for wave breaking and wave–structure interactions". *Ocean engineering*, Vol. 33(11), pp. 1565-1588.
- [7] Hinatsu, M. (1992). "Numerical simulation of unsteady viscous non-linear waves using moving grid system fitted on a free surface." *J. Kansai Soc. Naval Arch. Japan* Vol. 217, pp. 1-11
- [8] Huang, C. J., Chang, H. H., and Hwung, H. H. (2003). "Structural permeability effects on the interaction of a solitary wave and a submerged breakwater", *Coastal engineering*, Vol. 49(1), pp. 1-24.
- [9] Hsu,T. et al. (2008). "A parabolic equation for wave propagation over porous structure," *Journal of Coastal Engineering*, Vol. 55(12), pp. 1148-1158.
- [10] Jin. W, Qi-hua. Z, Deng-ting. W, Shukrieva. S. (2013). "Solitary Wave Propagation Influenced by Submerged Breakwater", *Chaina Ocean Eng.*, Vol. 27(5), pp. 593-604
- [11] Jhang. J.S, Jeng D.S, Liu. P.L.F. (2011). "Numerical study for waves propagating over a porous seabed around a submerged permeable breakwater: PORO-WSII model", *Ocean Engineering*, Vol. 38, pp. 954-966



- [12] Kawasaki, K., Iwata, K. (2001) "Wave breaking-induced dynamic pressure due to submerged breakwater," Proceedings of the Eleventh (2001) International Offshore and Polar Conference, Stravanger, Norway, Vol. 3., pp. 488-493.
- [13] Kobayashi, N., Meigs, L. E., Ota, T., & Melby, J. A. (2007). "Irregular breaking wave transmission over submerged porous breakwater", *Journal of waterway, port, coastal, and ocean engineering*, Vol. 133(2), pp. 104-116.
- [14] Liao, Y. C., Jiang, J. H., Wu, Y. P., & Lee, C. P. (2013). "Experimental Study of Wave Breaking Criteria and Energy Loss Caused by a Submerged Porous Breakwater on Horizontal Bottom", *Journal of Marine Science and Technology*, Vol. 21(1), pp. 35-41.
- [15] Lee, C. et al. (2003). "Wave field with a submerged porous breakwater", *Journal of the Chinese Institute of Engineers*, Vol. 26(3), pp. 333-342.
- [16] Lee, C., Shen, M. and Huang, C. (2007). "Transformation of irregular waves propagating over a submerged breakwater", *Proceedings of the 12th ISOPE Conference*, pp. 1-6.
- [17] Mendez, J. et al. (2001). "Wave-induced mean magnitudes in permeable submerged breakwaters", *Journal of Waterway, Port, Coastal and Ocean Engineering*, Vol. 127(1), pp. 7-15.
- [18] Ohya, T. and Nadaoka, K. (1991). "Development of a numerical wave tank for analysis of nonlinear and irregular wave field." *Fluid Dynamics Research* Vol. 8, pp. 231-251
- [19] Rageh, O.S. (2009). "Hydrodynamic Efficiency of Vertical Thick Porous Breakwaters", *Thirteenth International Water Technology Conference, IWTC 13*, Hurgada, Egypt, pp. 1659-1671.
- [20] Rahman, M.A., Mizutani, N. and Kawasaki, K. (2006). "Numerical modeling of dynamic responses and mooring forces of submerged floating breakwater", *Coastal Engineering*, Elsevier, Vol. 53, pp.799-815.
- [21] Rahman, M.A. and Akter, A. (2014). "The effect of porosity of submerged and emerged breakwater on wave transmission", *International Journal of Environmental Science and Development*, Vol. 5(5), pp. 473-478
- [22] Rahman, M.A. and Womera, S.A. (2013). "Experimental and Numerical Investigation on Wave Interaction with Submerged Breakwater", *Journal of Water Resources and Ocean Science*, Vol. 2(6), pp. 155-164

- [23] Sakakiyama, T. R. and Kajima, R. (1992). "Numerical simulation of nonlinear wave interacting with permeable breakwaters," *Proc. 22nd Int. Conference on Coastal Engineering, ASCE, Venice*, pp. 1517–1530.
- [24] Sidek, F.J. and Wahab, M. (2007). "The effects of porosity of submerged breakwater structures on non-breaking wave transformation", *Malaysian Journal of Civil Engineering*, Vol. 19(1), pp. 17-25.
- [25] Thornton, E. B., and Calhoun, R. J. (1972) "Spectral resolution of breakwater reflected waves." *Journal of Waterway, Harbor and Coastal Engineering*, ASCE, 98(4), pp.443-460.
- [26] Wu, Y. T., Hsiao, S. C., & Chen, G. S. (2012). "Solitary wave interaction with a submerged permeable breakwater: experiment and numerical modeling", *Coastal Engineering Proceedings*, Vol. 1(33), pp.30.
- [27] Wiryanto, L. H. (2011). "Wave propagation passing over a submerged porous breakwater", *Journal of Engineering Mathematics*, Vol. 70(1-3), pp. 129-136.